

**A Two-Prong Approach for Targeting mRNA Cap-Dependent Translation Initiation:
Small Molecules and Hydrocarbon Stapled Peptides**

by

James Min Chang Song

A dissertation submitted in partial fulfillment
of the requirements for the degree of
Doctor of Philosophy
(Chemical Biology)
in the University of Michigan
2018

Doctoral Committee:

Assistant Professor Amanda L. Garner, Chair
Associate Professor Jolanta Grembecka
Assistant Professor Matthew B. Soellner
Professor Duxin Sun

James M. Song

jmsong@umich.edu

ORCID iD: [0000-0002-1592-8843](https://orcid.org/0000-0002-1592-8843)

© James M. Song 2018

DEDICATION

I would like to dedicate my work to my family. None of this would have been possible without their unwavering support and love.

ACKNOWLEDGEMENTS

I would like to first thank Professor Amanda L. Garner for her unwavering support and guidance throughout my graduate career. I would also like to thank my committee members, Professor Matthew B. Soellner, Professor Duxin Sun, and Professor Jolanta Grembecka for their advice and guidance. Also, I am appreciative for the Cellular Biotechnology Training Program and GAANN for providing graduate fellowships. Last but not least, I am deeply thankful for my fellow Garner group graduate students, postdocs, staff scientists, and all the other brilliant scientists I had the honor of working with.

Table of Contents

Dedication	ii
Acknowledgements.....	iii
List of Tables	viii
List of Figures	ix
Abstract.....	xvi
CHAPTER 1 CAP-DEPENDENT PROTEIN TRANSLATION BIOLOGY AND INHIBITORS	1
1.1 PI3K-AKT-MTOR PATHWAY AND INHIBITORS	2
1.2 EIF4F BIOLOGY AND INHIBITORS	7
1.2.1 EIF4E INHIBITORS	11
1.2.2 EIF4A INHIBITORS	12
1.2.3 EIF4G INHIBITORS	13
1.3 CONCLUSION	14
1.4 REFERENCES.....	15
CHAPTER 2 DESIGN AND DEVELOPMENT OF PPI CAT-ELCCA	26
2.1 EFFORTS TO DEVELOP PEPPi CAT-ELCCA.....	29
2.1.1 RESEARCH DESIGN	29
2.1.2 PROTEIN LABELING.....	31

2.1.3	PEPPI CAT–ELCCA CLICK CHEMISTRY	32
2.1.3	PEPPI CAT–ELCCA ASSAY DEVELOPMENT	34
2.1.4	PEPPI CAT–ELCCA CONCLUSION	35
2.2	PPI CAT-ELCCA.....	36
2.3	RESULTS AND DISCUSSION	37
2.3.1	PROTEIN LABELING.....	37
2.3.2	PROOF OF CONCEPT: CUAAC PPI CAT–ELCCA	37
2.3.3	PROOF OF CONCEPT: IEDDA PPI CAT–ELCCA.....	39
2.3.4	EIF4E IMMOBILIZATION STABILITY	40
2.3.5	PPI CAT–ELCCA AND ELISA COMPARISON	41
2.3.6	IEDDA PPI CAT–ELCCA VALIDATIONS	43
2.4	CONCLUSION	45
2.5	EXPERIMENTAL	45
2.5.1	GENERAL INFORMATION	45
2.5.2	SYNTHETIC METHODS	48
2.5.3	PROTEIN EXPRESSION AND PURIFICATION.....	51
2.5.4	BIOCONJUGATION METHODS	53
2.5.5	PPI CAT–ELCCA PROTOCOL (384–WELL FORMAT).....	55
2.5.6	PEPPI CAT–ELCCA PROTOCOL.....	56
2.6	REFERENCES.....	58
CHAPTER 3 HIGH-THROUGHPUT SCREENING CAMPAIGN TARGETING THE CAP-		
DEPENDENT TRANSLATION INITIATION		
3.1	4EGI-1 DISCOVERY & VALIDATION	61
3.2	4E1RCAT DISCOVERY AND VALIDATION	64
3.4	HTS PPI CAT–ELCCA	67
3.4.1	PPI CAT–ELCCA AND AGGREGATORS	67

3.4.2	HTS SCREENING.....	68
3.5	CONCLUSION	73
3.6	HTS PPI CAT–ELCCA PROTOCOL (384–WELL FORMAT).....	73
3.7	EXPERIMENTAL	76
3.8	REFERENCES	77
CHAPTER 4 DESIGN, DEVELOPMENT, AND CHARACTERIZATIONS OF 4E–BP1		
	MIMETIC STAPLED PEPTIDES	81
4.1	DRUG DISCOVERY: PEPTIDES TARGETING PROTEIN–PROTEIN INTERACTIONS.....	81
4.1.1	PEPTIDES	82
4.1.2	ALPHA HELIX STAPLED PEPTIDES	83
4.1.3	HYDROCARBON STAPLED PEPTIDES TARGETING EIF4E PROTEIN–PROTEIN INTERACTIONS	85
4.2	RESEARCH DESIGN	86
4.3	HCS STAPLED PEPTIDES	89
4.3.1	4E–BP1 LINEAR SEQUENCE OPTIMIZATIONS.....	89
4.3.2	RING CLOSING METATHESIS.....	91
4.3.3	MHCS PEPTIDES	94
4.3.4	HCS PEPTIDES.....	96
4.3.5	CELLULAR TREATMENTS	98
4.4	HYDROCARBON STAPLED PEPTIDES: REGIOISOMERS	101
4.4.1	MHCS CASE STUDY.....	101
4.4.3	SURFACE PLASMON RESONANCE AND CIRCULAR DICHROISM.....	109
4.5	CONCLUSION	110
4.6	EXPERIMENTAL	111
4.6.1	GENERAL MATERIALS AND METHODS	111

4.6.2	CELLULAR TREATMENTS	114
4.7	CHAPTER IV REFERENCES	115
	CHAPTER 5 FUTURE DIRECTIONS	123
	5.1 REFERENCES.....	127
	APPENDIX.....	129
	NMR SPECTRA	129
	BIOTIN-PEG ₇ -HT LIGAND	129
	MTET-PEG ₇ -HT LIGAND.....	130
	SPR SENSOGRAMS.....	132
	CIRCULAR DICHROISM SPECTRAS	135

LIST OF TABLES

Table 1. Chemical structures and the inhibitory activities of inhibitors targeting the eIF4G – eIF4E interaction.....	13
Table 2. Validated hits from the BIC library. The binding affinities were All experiments were conducted in duplicates (n=2).....	72
Table 3. Peptides selected for further biophysical characterizations. Protocols for SPR and CD are detailed in appendix. mHCS-5i and mHCS-5ii were re-synthesized for SPR and CD experiments and were assigned label by the order of elution by LC. All the experiments were conducted in triplicates (n=3) and shown as the mean \pm SD.....	109

LIST OF FIGURES

Figure 1. Cap-dependent Translation. CdT is regulated through the PI3K–Akt–mTOR pathway and is highly dependent on the interactions of eIF4E.....	2
Figure 2. Known small molecule inhibitors of PI3K–Akt–mTOR pathway	3
Figure 3. eIF4E – 4E-BM structure. A) Structure of eIF4G 4E-BM (blue) and 4E-BP1 4E-BM (red) bound to eIF4E (yellow). B) E132 and H37-P38-Leu39 of eIF4E make critical hydrogen bond contact with 4E-BMs	9
Figure 4. Inhibitors targeting the eIF4F complex	10
Figure 5. cat–ELCCA and ELISA. A) generic schematic of cat-ELCCA. B) comparison of ELISA and PPI cat-ELCCA.....	27
Figure 6. PepPI cat–ELCCA CuAAC schematic.....	30
Figure 7. The mechanism of Halotag Protein labeling. A) Amine–reactive crosslinker NHS ester forms amide with surfaced exposed lysines on the protein, B) chloro–alkane linkers covalently react with Asp106 in the Halotag active site	31
Figure 8. PepPI cat-ELCCA proof-of-concept. A) <i>in solution</i> CuAAC conditions to conjugate alkynyl 4E–BP1 peptide and azido Rhodamine, B) CuAAC ligand THPTA fails to elicit notable S/B ratio whereas TBTA shows S/B of 4.2. ++, alkynyl 4E–BP1 and biotin eIF4E, +- alkynyl 4E–BP1 only (n = 3, shown as the mean ± SD).....	33
Figure 9. PepPI cat-ELCCA development. A) BSA incubation in PepPI cat–ELCCA dramatically increases the S/B between a positive interaction (++) and competition (++)	

competition), B) Synthetic Block BufferTM reduces the nonspecific binding of HRP induced by CuAAC condition, C) the unlabeled HT 4E–BP1 eliminates PepPI cat–ELCCA signal (++ WT) whereas equivalent addition of BSA does not (++ BSA). All experiments were conducted in triplicates (n=3) and shown as the mean \pm SD 35

Figure 10. 4E–BP1, eIF4E and eIF4G Labeling. A) PPI cat–ELCCA protein labeling verification. B) verification of successful biotinylation 37

Figure 11. CuAAC PPI cat–ELCCA. A) CuAAC PPI cat–ELCCA schematics. B) Proof of concept for CuAAC PPI cat–ELCCA. Addition of the WT 4E–BP1 lowers luminescence by 25-fold C) The interaction is dose dependent, and addition of WT 4E–BP1 reduces the number of the *active complexes*. All experiments were conducted in triplicates (n=3) and shown as the mean \pm SD. 38

Figure 12 IEDDA PPI cat–ELCCA. A) PPI cat–ELCCA for eIF4E PPIs. mTet = methyltetrazine; TCO = trans–cyclooctene. For the eIF4E–4E–BP1 assay, eIF4E was immobilized and 4E–BP1 mTet labeled. For the eIF4E–eIF4G assay, eIF4G was immobilized and eIF4E mTet labeled. B) Proof–of–concept data. X refers to protein. C) $K_{d,app}$ measurement. All experiments were conducted in triplicates (n=3) and shown as the mean \pm SD. 40

Figure 13. eIF4E in PPI cat–ELCCA. The alternative immobilization strategy, in which 4E–BP1 was immobilized and mTET–eIF4E was incubated, drastically reduced the S/B ratio and the apparent affinity. All experiments were conducted in triplicates (n=3) and shown as the mean \pm SD. 41

Figure 14. Sensitivity comparison between PPI cat–ELCCA and ELISA. A) ELISA yielded K_d of 19 ± 1 nM , in comparison to that of PPI cat–ELCCA at 3.8 ± 0.7 . B) Linear calibration curve generated from each assay. LOD and LOQ were calculated (LOD = $3.3\sigma/m$; LOQ = $10\sigma/m$;

where σ and m is the standard deviation and the slope of the response in the linear range. For ELISA, LOD = 0.15 ng and LOQ = 0.47 ng. For PPI cat-ELCCA, LOD = 0.014 ng and LOQ = 0.043 ng. All experiments were conducted in triplicates (n=3) and shown as the mean \pm SD. ... 42

Figure 15. Characterization of PPI cat-ELCCA for chemical probe discovery. (A) Inhibition by 4E-BP1 proteins. (B), (C) Inhibition of eIF4E-eIF4G and eIF4E-4E-BP1, respectively, by 4EGI-1 and 4E1RCat. (D) Inhibition by 4E-BP1 peptide. All experiments were conducted in triplicates (n=3) and shown as the mean \pm SD. 43

Figure 16. 4EGI-1. A) 4EGI-1 structure, 2-aminothiazole is highlighted in red; B) schematic of the HTS FP assay used by Moerke et al. and peptide probe sequence 61

Figure 17. 4E1RCat. A) 4E1RCat structure, promiscuous scaffold highlighted in red; B) schematic of the HTS TR-FRET assay used by Cencic et al1, and the eIF4G1 region used in the screen 65

Figure 18. Effect of aggregators on PPI cat-ELCCA. Aggregator characterization of PPI cat-ELCCA. A) Established aggregators, B) Effect of aggregators, C,D) Dose-dependence of Congo Red in the presence and absence of 0.01% Tween-20, respectively. All experiments were conducted in triplicates (n=3) and shown as the mean \pm SD. 68

Figure 19. PPI cat-ELCCA HTS Characterization. A) PPI cat-ELCCA exhibits Z' factor greater than 0.65, B) preliminary screening with fragment library compounds 69

Figure 20. The primary screening of the NPE library. $Z' = 0.62$. HTS statistics of the NPE library using PPI cat-ELCCA, representative CRCs of validated hits normalized to the assay controls. The CRC data was collected in duplicates (n=2). 70

Figure 21. The primary screening of the BIC library. $Z' = 0.7$. HTS statistics of the NPE library, and the representative CRCs of validated hits normalized to the assay controls. The CRCs were collected in duplicates ($n=2$) and shown as the mean \pm SD. 72

Figure 22. Common α -stabilizing strategies. 83

Figure 23. Stapled peptides targeting eIF4E interactions. A) FP design¹. FP probe sequence contained mutations that improved eIF4E binding affinity². B) K_d as reported through SPR and FP, and helicity as reported through CD..... 85

Figure 24. Overlay and amino acid sequences of the eIF4G mimetic sequence (blue, PDB: 5T46) and of the 4E-BP1 mimetic sequence (red, 4UED) bound to eIF4E (gray). Key side-chain residues of the canonical binding motif are displayed..... 87

Figure 25. Virtual sequential alanine mutagenesis on 4E-BP1. The docking poses of each 4E-BP1 mutant peptide with eIF4E were analyzed against that of the native 4E-BP1 with eIF4E using Glide, with (Minimized) and without (Rigid) energy minimization prior to Glide scoring. A higher Glide Score indicates an unfavorable mutation, and therefore, a greater contribution to the ligand binding affinity..... 88

Figure 26. Hydrocarbon stapled peptides. **mHCS** and **HCS** peptides are synthesized with monosubstituted pentenylglycine and disubstituted pentenylalanine, respectively..... 89

Figure 27. Linear sequence characterization. 4E-BP1 peptide mimetic sequence optimizations and inhibitory potencies. PPI cat-ELCCA dose response curves corresponding of linear peptides **4E-BP1** (black), **1** (red), **4** (blue), and **5** (green). All experiments were conducted in triplicates ($n=3$) and shown as the mean \pm SD. 90

Figure 28. Ring closing metathesis. A) Grubbs Generation I and II catalysts for RCMs. B) RCM mechanism categorized into 3 steps: Catalyst loading, Reaction, and Catalyst Regeneration. The

ligand *ortho*- to the ruthenium complex are tricyclohexylphosphine and N-heterocyclic carbenes for generation I and II, respectively. 92

Figure 29. mHCS-4E-BP1. A) mHCS peptides of 4E-BP1, 1 – 3, and 5 and their *in vitro* inhibitory potency. mHCS-1 was not assayed due to the lack of purity. **mHCS 4E-BP1** (black), **mHCS-2** (red), **mHCS-3** (blue), and **mHCS-5** (green). B) analytical HPLC spectra of stock **mHCS 4E-BP1** purity confirmed by LC-MS. The dose-responsive curves were conducted in triplicates (n=3) and shown as the mean \pm SD. 94

Figure 30. HCS peptides. A) HCS peptides of 4E-BP1, and sTIP-04 and the *in vitro* inhibitory potency. **HCS 4E-BP1** (black), **sTIP-04** (red). B) analytical HPLC spectra of stock **HCS 4E-BP1** purity confirmed by LC-MS. The dose-responsive curves were conducted in triplicates (n=3) and shown as the mean \pm SD. 96

Figure 31. Cellular assays for mHCS and HCS peptides. A) Cellular permeability of FITC-labeled HCS-4E-BP1 as determined via flow cytometry (n = 3) in MDA-MB-231 cells. Cells were treated at 1 μ M for 6 h. Ctrl: 1:2 DMF:H₂O v/v, Fl: dichlorofluoresceine. B) Cellular inhibitory activities of the linear 4E-BP1 and **HCS-4E-BP1** peptides as determined via m⁷GDP cap affinity chromatography. Inhibition of the eIF4E-4E-BP1 and eIF4E-eIF4G PPIs in C) MDA-MB-231 cells, and (C) HCT116 cells (2.5 μ M), and H1299 cells (2.5 μ M). In all cases, cells were treated for 6 h and eIF4E was used as a normalization control. 99

Figure 32. mHCS-4E-BP1 diastereomers. A) the semi-prep HPLC purification (left) and the analytical spectra (right) of **mHCS-i** (blue) and **mHCS-ii** (red) B) *in vitro* characterizations of **mHCS-i** and **mHCS-ii** by PPI cat-ELCCA (n=3) C) Cellular inhibitory activities of the **4E-BP1** peptide, **mHCS-i**, **mHCS-ii**, and **HCS 4E-BP1** as determined via m⁷GDP cap affinity

chromatography in MDA-MB-231 cells. In all cases, cells were treated for 6 h and eIF4E was used as a normalization control..... 101

Figure 33. Peptide diastereomer NMR. A) Overlaid 1D NMR spectra of **mHCS-i** (black) and **mHCS-ii** (red). B) 1D NMR spectra of **HCS 4E-BP1** (blue). Significant water contamination and the poor solubility yielded in unresolved low signal olefinic peaks in all cases..... 102

Figure 34. **mHCS-5i** and **mHCS-5ii** NMR. A) the analytical spectra of **mHCS-5i** (blue) and **mHCS-5ii** (red) B) in vitro characterizations of **mHCS-5i** and **mHCS-5ii** by PPI cat-ELCCA, and SPR (n=3). 1D NMR spectra and analysis of **mHCS-5i** (C) and **mHCS-5ii** (D) with alkene $^3J_{HH}$ values of 20 Hz and 8 Hz, respectively. 103

Figure 35. **sTIP-04** NMR. A) dqfCOSY 2D NMR of **sTIP-04**. The cross-peaks representative of the olefinic protons ($\delta 5.4 - 5.2$) and of the coupling methylene protons ($\delta 1.95 - 1.8$) were identified. B) Stacked **sTIP-04** 1D NMR (red) and homo-decoupling of the protons at a chemical shift of 2.0 – 1.8 ppm (blue) during the acquisition. The resulting coupling constant of 11 Hz suggest that **sTIP-04** is a Z- isomer..... 105

Figure 36. **mHCS-ii** NMR. A) TOCSY 2D NMR of **mHCS-ii**. The cross-peaks representative of the vinyl proton ($\delta 5.4 - \delta 5.2$) coupling methylene protons H_a ($\delta 2.1 - \delta 1.6$) and H_b ($\delta 1.4 - \delta 1.1$) were identified. B) Stacked **mHCS-ii** 1D NMR (red) and homo-decoupling of the protons at a chemical shift of 2.1– 1.6 ppm (blue) during the acquisition 107

Figure 37. Investigation of Grubbs' catalysts. A) the analytical spectra of **mHCS-G1** (red) and **mHCS-G2** (blue), B) in vitro characterizations of **mHCS-G1** and **mHCS-G2** by PPI cat-ELCCA, SPR, and CD (n=3), C) Cellular inhibitory activities of **mHCS-G1** and **mHCS-G2** as determined via m^7GDP cap affinity chromatography. Inhibition of the eIF4E-4E-BP1 and

eIF4E–eIF4G PPIs in MDA–MB–231 cells. In all cases, cells were treated for 6 h and eIF4E was used as a normalization control..... 108

ABSTRACT

Cap-dependent protein translation (CdT) is dysregulated in many types of cancer and leads to overexpression of oncogenes promoting angiogenesis, evasion of apoptosis, and cell proliferation. The protein-protein interactions (PPIs) involving eIF4E, 4E-BP1, and eIF4G1 dynamically regulate the initiation of the CdT and are therapeutic targets of interest in treatment of breast, pancreatic, ovarian, and prostate cancers; successful inhibition of the CdT could also provide selectivity towards targeting the protein translation addicted cancers over the healthy cells. In order to discover potent inhibitors of the CdT initiation, full-length eIF4E protein interactions were targeted using a two-pronged approach: small molecule discovered via high-throughput screening and rationally designed hydrocarbon stapled peptides.

To conduct a high-throughput screening campaign, the assay platform **catalytic enzyme-linked click chemistry assay (cat-ELCCA)** was expanded to screen against full-length PPIs to create PPI cat-ELCCA and implemented for the eIF4E–4E-BP1 interaction. PPI cat-ELCCA exhibited over 10-fold improvement in limits of detection and quantification over ELISA and was successfully miniaturized using automated liquid handlers with exceptional assay parameters ($Z' > 0.6$, signal-to-background > 30). Using PPI cat-ELCCA, over 50,000 natural product extracts (NPE) and custom compounds were screened, of which 18 NPE fractions and 9 compounds exhibited dose-dependent inhibition with hill slope ranging between -0.7 to -2.0. All the custom compounds were identified with micromolar inhibitory potency and 6 of the 9 compounds had demonstrated direct binding interaction to target protein eIF4E. Further re-

isolation and iterative screening are pending for the active NPE fractions, and compound structure disclosures of hit molecules are awaiting approval.

As an alternative drug discovery approach, the α -helical structure adopted by the 4E-BPs upon binding to eIF4E was exploited to design 4E-BP1 mimetic hydrocarbon stapled peptides (HCS). The lead HCS peptide **HCS 4E-BP1** exhibited 5-fold greater inhibitory potency and eIF4E direct binding affinity (4 nM and 4 nM, respectively) than the **linear 4E-BP1**, accompanied by a 250% increase in peptide helicity. **HCS 4E-BP1** successfully inhibited eIF4E PPIs with both 4E-BP1 and eIF4G1 in a dose-dependent manner *in cellulo* in presence of serum. Overall, the results from this two-pronged eIF4E inhibitor discovery campaign have pushed forward the current limits of targeting the CdT initiation and produced promising leads for further probe and drug development.

CHAPTER 1 CAP-DEPENDENT PROTEIN TRANSLATION BIOLOGY AND INHIBITORS

The cap-dependent protein translation (CdT) is upregulated by a variety of extracellular factors, such as mitogens, growth factors, insulin, amino acids, and overall nutrition levels provided to the cell³⁻⁵. CdT has garnered much investigation due to its dysregulation through the PI3K-AKT-mTORC1 pathway in tumor biology leading to aberrant regulation of the cell cycle, metabolism, genomic instability, and survival (**Figure 1**). Activated PI3K phosphorylates lipid phosphatidylinositol (3,4,5)-bisphosphate (PIP2) to phosphatidylinositol (3,4,5)-trisphosphate (PIP3), and PIP3 serves as the second messenger molecule that binds and recruits pleckstrin homology (PH) domain containing proteins such as phosphoinositide-dependent kinase-1 (PDK1) and protein kinase B (AKT) to the plasma membrane. This co-localization leads to PDK1 and mTOR complex 2 (mTORC2)-dependent phosphorylation and the activation of AKT⁸⁻¹⁰. The activation of AKT promotes cell cycle, cell survival, and more importantly for CdT, cell growth through phosphorylation and deactivation of GTPase-activating protein tuberous sclerosis complex 2 (TSC2). This likely inhibits the intrinsic GTPase activity of Ras homolog enriched in brain (RHEB) to maintain its GTP-bound state. Activated mTORC1 hyper-phosphorylates the gate-keeper of CdT, 4E binding protein 1 (4E-BP1), bound to eukaryotic initiation factor 4E (eIF4E) which promotes the initiation of CdT¹²⁻¹⁴.

1.1 PI3K–AKT–MTOR PATHWAY AND INHIBITORS

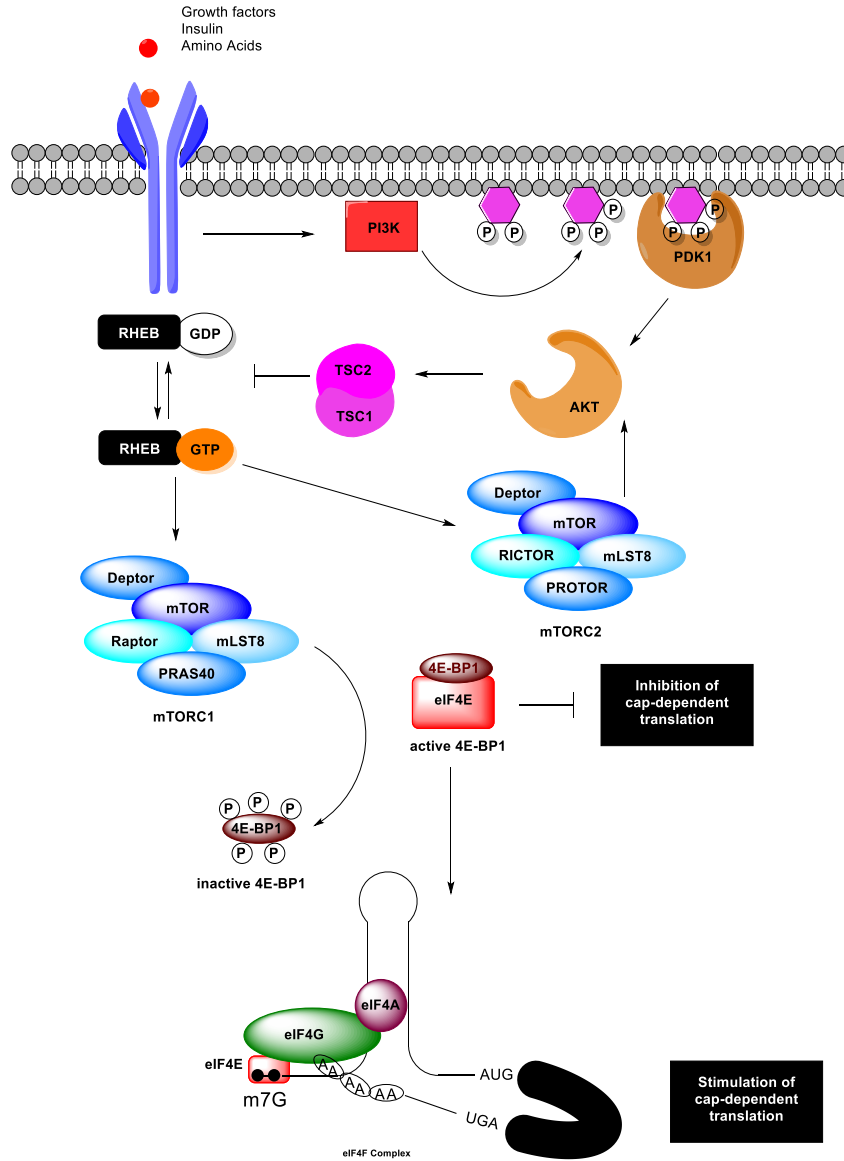


Figure 1. Cap-dependent Translation. CdT is regulated through the PI3K–Akt–mTOR pathway and is highly dependent on the interactions of eIF4E

The prevalence and the critical nature of the kinases involved in the PI3K–Akt–mTORC1 pathway has promoted extensive investigation into the discovery of kinase inhibitors against these enzymes. However, while kinases are excellent “druggable” targets due to the well–defined substrate and target binding pockets, the cells face rapid resistance to overcome the

inhibition of these critical signaling enzymes through various mechanisms. Despite this hurdle, researchers have discovered and classified five general types of kinase inhibitors targeting the PI3K–AKT–mTOR signaling cascade, and to an extent, the CdT initiation pathway: pan–class I PI3K inhibitors, isoform–selective PI3K inhibitors, pan–PI3K–mTOR kinase inhibitors, AKT inhibitors, mTORC1 inhibitors, and active site mTOR kinase inhibitors (**Figure 2**).

Pan–class I PI3K inhibitors (GDC–0941 (Genentech), NVP–BKM120 (Novartis)) target the various isoforms of PI3K and their redundant functions in oncogenic signaling¹⁷ (**Figure 2**). However, this multi–targeted approach often leads to over– or under–dosing depending on the

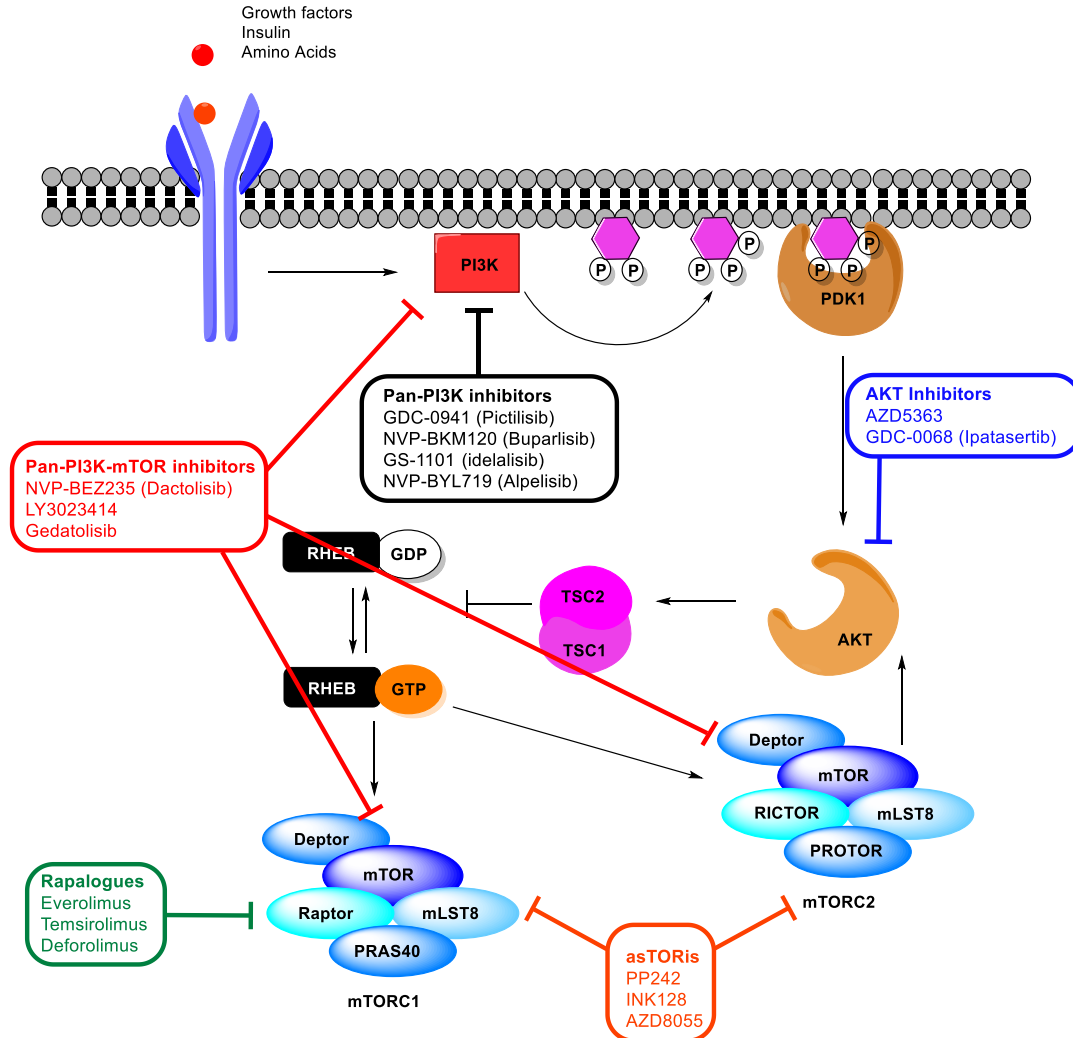


Figure 2. Known small molecule inhibitors of PI3K–Akt–mTOR pathway

disease biology and context. Furthermore, the lack of isoform selectivity generally expands outside of PI3K isoforms and into other PI3K-related kinase family such as mTOR¹⁸. For instance, GDC-0941 was reported as a potent kinase inhibitor of p110 α , β , and δ isoforms with low nanomolar and low micromolar IC₅₀ values *in vitro* and in human glioblastoma and ovarian cancer cell lines, respectively¹⁹. After its success through phase I clinical trial, growing concerns over the inherent resistance mechanisms of targeting PI3K²⁰ led to combination therapy with cisplatin to treat triple-negative breast cancer. Unfortunately, the study met an early termination²¹, but GDC-0941 appears promising in a combination therapy with paclitaxel to treat metastatic breast cancer (NCT01740336).

In contrast to pan-class I PI3K inhibitors, isoform-selective PI3K inhibitors target the disease prevalent isoform of PI3K, minimalizing the overall over- and under- dosing, and consequently, the toxicities associated with off-target inhibition (**Figure 2**). Successful development of p110 β isoform inhibitors remain elusive due to its redundant functionalities with the p110 α isoform, and the prevalence of solid tumors expressing malignant p110 α and p110 β had placed p110 δ and p110 γ inhibitor development in pre-clinical stages. p110 δ inhibitor GS-1101 is an exception, and has been approved for combination therapy with rituximab to treat chronic lymphocytic leukemia²². An exhaustive medicinal chemistry campaign by Novartis led to a p110 α specific inhibitor NVP-BYL719 that exhibited greater than 50-fold selectivity over the p110 β and p110 δ isoforms *in vitro*, and inhibited growth of p110 α -driven tumors in xenograft mouse models²³. NVP-BYL719 is currently being investigated for its efficacy in neck/head tumors (NCT02145312) and advanced breast cancers (NCT02506556). The particular importance of p110 β in certain prostate and breast cancer²⁴ cells lacking in PTEN may drive future research in identifying p110 β inhibitors as well.

Investigators have also tried to capitalize on the broad inhibition profile of pan-PI3K inhibitors that target the structurally-related mTOR kinase by developing pan-PI3K-mTOR kinase inhibitors (**Figure 2**). Despite the increased potential for higher toxicity, the rationale behind this class of inhibitors lies in shutting down the crosstalk and the feedback at mTORC2 (**Figure 1**). NVP-BEZ235 showed antiproliferative results early on in glioblastoma and prostate cancer xenograft models,²⁵ but failed to translate as a single agent to human pathology due to high toxicity²⁶. A synergized combination therapy to inhibit mTOR and p110 α is being pursued to treat advanced nonhematologic malignancies (NCT01899053) and appears promising. LY3023414 (Lilly) is another hopeful molecule that caused G1 cell-cycle arrests in broad panel of cancer cells and in xenograft models of glioblastoma, bladder, colon, breast, ovarian and renal cancer²⁷. Gedatolisib (Phase I) also showed promising results treating advanced colorectal cancers and ovarian cancers in combinatorial therapies²⁸, and is currently in Phase II clinical trials.

Like the other kinases in this signaling cascade, AKT also promotes growth factor-mediated cell survival, cell proliferation and inhibits apoptosis²⁹, and is frequently dysregulated in many types of cancers. Despite the critical nature of AKT, therapeutic inhibitors remain elusive (**Figure 2**). The function, tissue distribution, and ligand affinities of the three different AKT isoforms significantly complicates ATP-competitive inhibitor design³⁰. However, certain AKT inhibitors in combination therapy with other agents appear promising and in-route to various stages of clinical trials. For instance, AZD5363 and Ipatasertib (GDC-0068) inhibit all AKT isoforms with low nanomolar potency, reduce tumor growth in certain breast cancer xenograft mice models³¹⁻³² and prostate cancer cells, and are currently in separate Phase II trials in combination with paclitaxel for the treatment of triple-negative metastatic breast cancer

(NCT02423603, NCT02301988). AZD5363 is also being investigated in additional Phase II trials for treating advanced gastric cancers (NCT02451956) and prostate cancers (NCT02121639); similarly, Ipatasertib is involved in a Phase II trial for treating prostate cancers (NCT01485861).

Further downstream in the cascade, specific allosteric mTOR inhibitors rapamycin and rapalogues such as everolimus, temsirolimus and deforolimus, showed tolerated safety profiles³³ but limited therapeutic efficacy (**Figure 2**). Rapamycin and rapalogues bind to the intracellular receptor FKBP12 and the FRB domain of mTOR, thereby reducing substrate accessibility to the mTOR catalytic site³⁵. These compounds selectively inhibit mTORC1 rather than the mTORC2³⁶⁻³⁷. Rapalogues such as everolimus and temsirolimus were FDA approved to treat neuroendocrine tumors and advanced renal cell carcinoma³⁸; however, others have caused cytostatic effects (reduction in protein translation, increased autophagy) in cells rather than cytotoxicity⁴⁰, most likely due to the incomplete inhibition of mTORC1 and mTORC2, and the mTORC1–S6K1–dependent negative feedback loop. Unchecked mTORC2 results in increased phosphorylation of AKT at S473⁴¹, resulting in hyperactivation of AKT⁴² and its regulated downstream effectors such as FOXO proteins, cyclin D1, MDM2, caspase–9, and BAD to drive tumorigenesis⁴³⁻⁴⁵. In addition, inhibition of mTOR substrate S6K1 eliminates the negative feedback loop to IRS–1 upstream to PI3K activation, and limits the rapalogue efficacy. More importantly, rapalogues only partially inhibit mTORC1; while S6K phosphorylation is effectively inhibited, 4E-BP1, the master regulator of CdT, is re-phosphorylated and unresponsive to long-term rapalogue treatment under similar conditions. Dowling et al⁴⁷⁻⁴⁸ showed that mTORC1–mediated inhibition of 4E–BPs led to significant reduction in cell proliferation, whereas inhibition of S6Ks drove reduction in cell size. This suggested that the

regulation of cell size and proliferation may be uncoupled in mammalian cells, and a complete inhibition of 4E-BP1 may be necessary to elicit cell death. Rapalogues' incomplete inhibition of mTOR activity fails to kill malignant cells and have found alternative utilities as combination agent targeting breast cancers⁴⁹⁻⁵⁰.

Despite the similarities between the PI3K and mTOR kinase domains and the overlapping inhibition profiles between the two, extensive medicinal chemistry efforts have led to kinase inhibitors with greater selectivity for mTOR. These active site mTOR inhibitors, or asTORis, bind and block the ATP-binding cleft of mTOR kinase, effectively shutting down both mTORC1 and mTORC2 (**Figure 2**). PP242 and INK128 are potent asTORis that suppress both mTORC1-dependent 4E-BP1 phosphorylation as well as tumor growth in AKT-driven rapalogue resistant mice models⁵¹. INK128 is currently in numerous clinical trials targeting renal cell carcinoma (NCT02724020), breast cancer (NCT02719691), and liver cancer (NCT02575339). AZD8055 potently inhibits mTOR kinases with excellent selectivity profile and induces autophagy and cell death in cancer cells⁵³⁻⁵⁴, but its therapeutic efficacy remains unclear. Overall, asTORi exhibit a greater cytostatic effect than the rapalogues in certain cancer cell lines. However, most advanced tumors tend to have high eIF4E to 4E-BP ratios in response to prolonged mTOR inhibition⁵⁵⁻⁵⁹ and may limit asTORi efficacy as a single agent.

1.2 EIF4F BIOLOGY AND INHIBITORS

The limited success of kinase inhibitors in treating PI3K-AKT-mTOR-driven cancers led to studies further downstream of mTOR, to the effectors that directly regulate the protein translation. In theory, successful inhibition downstream of these effectors should exert far less selective pressure to the cells than inhibiting the signaling kinases, and in turn, hamper the development of rapid resistance to the therapy. In particular, the effectors driving CdT initiation

are of therapeutic interest because it is the rate limiting step in protein translation and is highly regulated through a critical signaling hub known as 4E-binding proteins (4E-BPs) and eIF4F.

4E-BPs are intrinsically disordered proteins (IDPs) and have little secondary structure while free in solution. They are critical in dynamically regulating eIF4E and the CdT in different tissues, but of the family (4E-BP1, 2, and 3), 4E-BP1 alterations are the most commonly reported in a wide range of cancers and have been extensively reviewed^{49, 61}. Briefly, loss of 4E-BP1 results in accelerated tumorigenesis, and non-phosphorylatable mutant actively binds and suppresses eIF4F complex formation, suppressing cellular proliferation and neoplastic growth⁶². Active 4E-BP1 serve as a metabolic brake and exerts significant control over fat metabolism, and may find utility in diabetes/obesity treatments¹¹. Furthermore, a *Drosophila* model suggests that overexpression of Thor, a 4E-BP homolog, is able to suppress the pathologic phenotypes of parkinsonism, making 4E-BP mimetics as an attractive therapeutic approach to neurodegenerative diseases⁵⁷⁻⁵⁸.

eIF4F is a heterotrimeric protein complex composed of the 7-methylguanosine (m7G) cap binding protein eIF4E, the large scaffolding protein eIF4G⁶⁴, and the DNA helicase protein eIF4A⁶⁴⁻⁶⁵. Artificial eIF4G1 overexpression has distinct transforming activity in mouse embryonic fibroblasts, and in xenograft nude mice⁶⁶. In inflammatory breast cancer⁶⁷⁻⁶⁹ and in squamous lung carcinoma, eIF4G was found to be overexpressed in the absence of corresponding increase in eIF4E and 4E-BP1. It is likely that eIF4G overexpression switches certain mRNAs from CdT to IRES-dependent translation to trigger pro-angiogenic and pro-survival signaling cascades.

Under starvation and nutrient deficiency, 4E-BPs bind and suppress eIF4E through a small canonical eIF4E binding motif (4E-BM, shared by eIF4G) – YX₄LΦ where Y,X,L, and Φ

denote Tyr, any amino acid, Leu, and hydrophobic residue, respectively (**Figure 3A**), and a lateral binding non-canonical binding motif (4E–NBM). 4E–BMs bind on the dorsal region of eIF4E, the opposite side to the cap-binding site; studies have noted that binding to 4E–BP1 suppresses the ability of eIF4E to bind effectively to m7G cap⁷¹ and provides increased limitations on initiating the CdT. The conserved Tyr forms a hydrogen bond to the backbone of the His–Pro–Leu motif of eIF4E, and R614 (eIF4G)^{11, 72} and R56 (4E–BP1) makes salt bridge with E132 on eIF4E to stabilize the interaction, as well as to partially cover the hydrophobic W73 (**Figure 3B**).

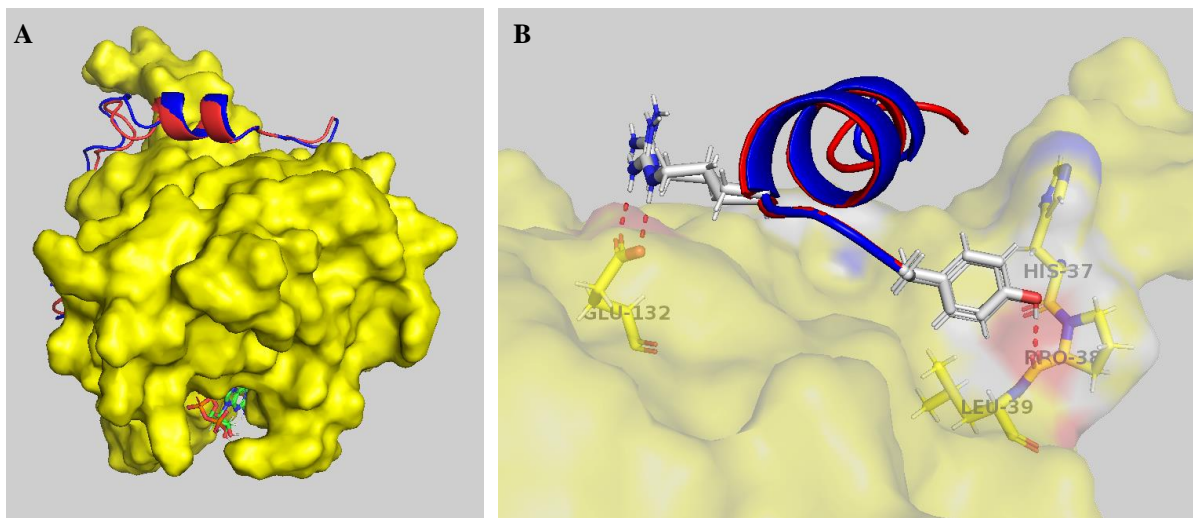


Figure 3. eIF4E – 4E-BM structure. A) Structure of eIF4G 4E-BM (blue) and 4E-BP1 4E-BM (red) bound to eIF4E (yellow). B) E132 and H37-P38-Leu39 of eIF4E make critical hydrogen bond contact with 4E-BMs

Under nutrient-rich conditions, activated PI3K–AKT–mTOR leads to mTOR–dependent hyper-phosphorylation of 4E–BP1 and result in significant reduction in its binding affinity to eIF4E. eIF4G exploits this weakened interaction and competitively binds (4E–BMs of eIF4G also bind to the dorsal, hydrophobic surface of eIF4E⁷³⁻⁷⁴) to eIF4E to initiate the formation of the eIF4F complex, and recruits eIF4A, and eIF3 to the 40S PIC. Successful eIF4E–eIF4G

binding interaction increases the binding affinity to m⁷G cap, possibly through decreasing the entropy to the 4E-BP/eIF4G binding region⁷⁵, and stabilizes the RNA-eIF4E complex. The contrasting binding affinities of 4E-BPs and eIF4G stem from the different binding affinity contributions that their respective C-terminal 4E-NBM make upon binding to the lateral surface of eIF4E. Gruner et al⁷² and Peter et al⁸⁰ solved the structures of 4E-BMs and 4E-NBMs of eIF4G and 4E-BPs and concluded that the greater flexibility of the eIF4G linker connecting the 4E-BMs to the 4E-NBMs allows for higher chances for 4E-BPs to compete with eIF4G. NMR spectroscopy titration experiments⁸¹⁻⁸² and small angle X-ray scattering experiments suggests that 4E-BP1 has a greater binding interface than eIF4G, offering additional evidence that 4E-BP1 sequesters eIF4G effectively. And while the majority of the stimulants (growth factors, amino acids) modestly increase global protein translation, subsets of mRNAs containing relatively long, highly structured 5' UTR that depend on eIF4F have increased translation rates. These subset of mRNAs are typically involved in oncogenesis such as cell proliferation (c-myc, CDK2, cyclin D1), evasion of apoptosis (MCL-1, BCL-2, survivin), angiogenesis (VEGF, FGF2), and metastasis (MMP9, heparanase)⁸³⁻⁸⁵. The eIF4F complex is an attractive alternative

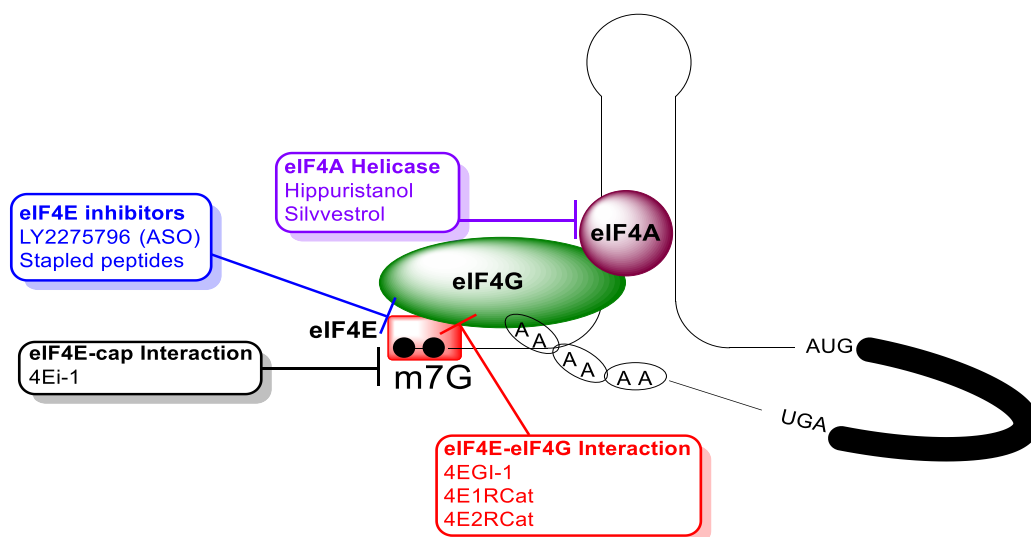


Figure 4. Inhibitors targeting the eIF4F complex

to shutting down and killing PI3K–AKT–mTOR driven cancers, and its inhibitors can be broadly categorized by targets: eIF4E, eIF4A, and eIF4G (**Figure 4**).

1.2.1 EIF4E INHIBITORS

In-depth studies have identified eIF4E as a highly dysregulated agent in oncology. Elevated total eIF4E in combination with 4E–BP1 hyper–phosphorylation has been observed in numerous types of breast and prostate cancer, and correlates strongly with a decrease in disease progression and overall survival. Healthy cells are reported to contain just enough free eIF4E to maintain basal levels of translation⁸⁹⁻⁹⁰, and increased eIF4E significantly upregulates the translation the mRNA sequences with excessive secondary structure in their 5' UTR⁹¹. The eIF4E gene is also amplified in human breast and head and neck cancers in comparison to the healthy cells⁹². Due to its important nature, eIF4E overexpression and amplification has been postulated as a useful biomarker to predict therapeutic efficacy, disease progression, survival and relapse^{69, 93}.

eIF4E binds to the 5' terminal cap structure m⁷GpppN (denoted m⁷G), where N is the first transcribed nucleotide held through a 5' to 5' triphosphate linkage⁹⁴. This site, more commonly referred to as the cap–binding site, is an attractive target for small molecule inhibition due to its defined molecular architecture. Cap analogues remain valuable tools for the eIF4E studies⁹⁶, but the required phosphodiester moiety in the molecules results in poor permeability and stability *in vivo*⁹⁷. On-going investigations are attempting to address these issues with pro–nucleotide drugs containing phosphoramidates that are rapidly converted to the corresponding 5'-monophosphate nucleotides in cell (4Ei–1)⁹⁸⁻⁹⁹ and with the use of virus–like particles (**Figure 4**).

eIF4E was targeted using antisense oligonucleotides (ASOs) with promising anti-tumorigenic results¹⁰⁰ (**Figure 4**). Further optimizations to the ASOs led to reduction in breast and prostate cancer xenograft mice models with minimal toxicity¹⁰², and accompanying greater reduction in pro-survival and pro-growth protein levels compared to the global protein level. ASO LY2275796 targeting the eIF4E mRNA completed its phase I trial in combination with irinotecan against solid tumors and irinotecan-resistant colorectal cancers¹⁰³, and showed minimal toxicity.

Alternatively, researchers exploited the fact that 4E-BMs adopt the α -helix secondary structure upon binding to eIF4E and designed α -helix mimetic stapled peptides to inhibit eIF4E PPIs¹⁰⁴. The stapled eIF4G peptides yielded enhanced binding affinity and helicity compared to the linear peptides, but unfortunately indicated poor cell permeability¹⁰⁵. Further medicinal chemistry campaign on these peptides could likely increase the cell permeability¹⁰⁶ and demonstrated that eIF4F complex can be targeted through stapled peptides.

1.2.2 EIF4A INHIBITORS

eIF4A is an ATP-dependent RNA-stimulated DEAD-box helicase that unwinds RNA duplexes¹⁰⁷ and is the reported target for Hippuristanol and Silvestrol (**Figure 4**). Hippuristanol is a steroid that prevents eIF4A from interacting with RNA¹⁰⁸, and has shown efficacy in T-cell leukemia mouse models¹⁰⁸. Silvestrol shuts down eIF4A by possibly inducing protein dimerization and enhancing its binding activity to RNA, effectively removing the free eIF4A from binding to the eIF4F complex¹⁰⁹. Silvestrol has modest efficacies in breast cancer and prostate cancer xenograft mouse models¹⁰⁸. eIF4A inhibitors have not yet progressed to the clinical trials due to their rapid clearance¹¹⁰⁻¹¹². However, eIF4A inhibitors (as single agents)

remain well-tolerated and may help restore chemosensitivity to selected types of cancers and synergize with other chemotherapeutic agents.

1.2.3 EIF4G INHIBITORS

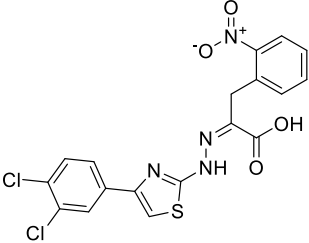
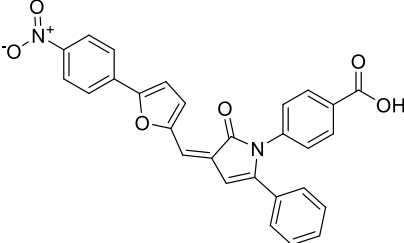
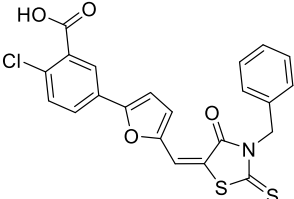
Inhibitor	Structure	IC ₅₀ (μM)	K _d (μM)
4EGI-1		125 (<i>in vitro</i>) 6 - 60 (<i>in cellulo</i>)	25 ± 11
4E1RCat		3.2 (<i>in vitro</i>)	N/A
4E2RCat		13.5 (<i>in vitro</i>)	N/A

Table 1. Chemical structures and the inhibitory activities of inhibitors targeting the eIF4G – eIF4E interaction

The growing evidence of the eIF4E nexus in cancer, metabolic, and neurodegenerative pathology led to a few high-throughput screening (HTS) campaigns to identify novel small molecule inhibitors of eIF4E – eIF4G PPIs. 4EGI-1, 4E1RCat, and 4E2RCat are documented inhibitors of this PPI (**Table 1**), discovered through HTS targeting the PPI between the 4E-BMs of eIF4G/4E-BP1 and eIF4E. 4EGI-1 effectively inhibited CdT, proved to be active in numerous cancer cell lines, and reduced tumor growth in xenograft breast cancer and melanoma

mice models¹¹⁵. 4E1RCat and 4E2RCat target the 4E-BMs and inhibit both 4E-BP1 and eIF4G from binding to eIF4E¹¹⁶. The initial studies indicated that 4E1RCat restores the chemosensitivity in *myc*-driven lymphoma model, and could find utility in treating coronavirus infection as well¹¹⁷. Despite the *in vitro* evidence of 4EGI-1 and 4E1RCat potency, there are no on-going clinical trials utilizing these small molecules yet, likely due to the possible target promiscuities and their structural similarities to PAIN compounds.

More recently, Feng et al discovered another eIF4F disrupting molecule, SBI-756¹¹⁸. Although SBI-756 was an analog derived from the AKT kinase inhibitor BI-69A11¹, the investigators identified eIF4G1 as a binding protein and that in combination with BRAF inhibitors, SBI-756 had reduced the formations of BRAF inhibitor resistant tumors. The investigators are currently working on the next generation of this molecule for clinical trials.

1.3 CONCLUSION

The current literature on hyperactivated PI3K-AKT-mTOR pathology and medicine makes two things very clear, i) that targeting The CdT in pathological cells through kinase inhibitors up-stream to the effectors is imperfect, and ii) prior drug discovery efforts to target the downstream eIF4F complex have yet to reveal compounds amenable for drug development. The Garner group has been working on the latter issue with a simple thought in mind: imperfect tools lead to imperfect products. These imperfect compounds are the natural products of imperfect tools, or more specifically, the HTS assays used to identify the hit compounds during the discovery stage. For instance, although fast and inexpensive, the fluorescence-based HTS methods such as fluorescence polarization suffer from well-documented poor sensitivity, high false positive and negative hits of aggregators and fluorescence quenchers. A more robust, sensitive, and applicable HTS methods would greatly improve the chances of identifying a

scaffold capable of inhibiting strong PPIs for further medicinal chemistry while minimizing the time and resources.

1.4 REFERENCES

1. Svitkin, Y. V.; Herdy, B.; Costa-Mattioli, M.; Gingras, A.-C.; Raught, B.; Sonenberg, N., Eukaryotic Translation Initiation Factor 4E Availability Controls the Switch between Cap-Dependent and Internal Ribosomal Entry Site-Mediated Translation. *Molecular and Cellular Biology* **2005**, *25* (23), 10556-10565.
2. Fruman, D. A.; Rommel, C., PI3K and cancer: lessons, challenges and opportunities. **2014**, *13*, 140.
3. Beagle, B.; Fruman, David A., A Lipid Kinase Cousin Cooperates to Promote Cancer. *Cancer Cell* **2011**, *19* (6), 693-695.
4. Soler, A.; Serra, H.; Pearce, W.; Angulo, A.; Guillermet-Guibert, J.; Friedman, L. S.; Viñals, F.; Gerhardt, H.; Casanovas, O.; Graupera, M.; Vanhaesebroeck, B., Inhibition of the p110 α isoform of PI 3-kinase stimulates nonfunctional tumor angiogenesis. *The Journal of Experimental Medicine* **2013**, *210* (10), 1937-1945.
5. Hirsch, E.; Ciraolo, E.; Franco, I.; Ghigo, A.; Martini, M., PI3K in cancer-stroma interactions: bad in seed and ugly in soil. *Oncogene* **2014**, *33* (24), 3083-3090.
6. Bozulis, L.; Hemmings, B. A., PIKKing on PKB: regulation of PKB activity by phosphorylation. *Current Opinion in Cell Biology* **2009**, *21* (2), 256-261.
7. DiNitto, J. P.; Lambright, D. G., Membrane and juxtamembrane targeting by PH and PTB domains. *Biochimica et Biophysica Acta (BBA) - Molecular and Cell Biology of Lipids* **2006**, *1761* (8), 850-867.
8. Sun, Y.; Fang, Y.; Yoon, M.-S.; Zhang, C.; Rocco, M.; Zwartkruis, F. J.; Armstrong, M.; Brown, H. A.; Chen, J., Phospholipase D1 is an effector of Rheb in the mTOR pathway. *Proceedings of the National Academy of Sciences* **2008**, *105* (24), 8286-8291.
9. Bai, X.; Ma, D.; Liu, A.; Shen, X.; Wang, Q. J.; Liu, Y.; Jiang, Y., Rheb Activates mTOR by Antagonizing Its Endogenous Inhibitor, FKBP38. *Science* **2007**, *318* (5852), 977-980.
10. Sengupta, S.; Peterson, T. R.; Sabatini, D. M., Regulation of the mTOR Complex 1 Pathway by Nutrients, Growth Factors, and Stress. *Molecular Cell* **2010**, *40* (2), 310-322.
11. Haghighat, A.; Mader, S.; Pause, A.; Sonenberg, N., Repression of cap-dependent translation by 4E-binding protein 1: competition with p220 for binding to eukaryotic initiation factor-4E. *EMBO J.* **1995**, *14*, 5701-5709.

12. Holohan, C.; Van Schaeybroeck, S.; Longley, D. B.; Johnston, P. G., Cancer drug resistance: an evolving paradigm. *Nat Rev Cancer* **2013**, *13* (10), 714-726.
13. Barouch-Bentov, R.; Sauer, K., Mechanisms of Drug-Resistance in Kinases. *Expert opinion on investigational drugs* **2011**, *20* (2), 153-208.
14. Janne, P. A.; Gray, N.; Settleman, J., Factors underlying sensitivity of cancers to small-molecule kinase inhibitors. *Nat Rev Drug Discov* **2009**, *8* (9), 709-723.
15. Foukas, L. C.; Berenjano, I. M.; Gray, A.; Khwaja, A.; Vanhaesebroeck, B., Activity of any class IA PI3K isoform can sustain cell proliferation and survival. *Proceedings of the National Academy of Sciences* **2010**, *107* (25), 11381-11386.
16. Brachmann, S. M.; Kleylein-Sohn, J.; Gaulis, S.; Kauffmann, A.; Blommers, M. J. J.; Kazic-Legueux, M.; Laborde, L.; Hattenberger, M.; Stauffer, F.; Vaxelaire, J.; Romanet, V.; Henry, C.; Murakami, M.; Guthy, D. A.; Sterker, D.; Bergling, S.; Wilson, C.; Brümmendorf, T.; Fritsch, C.; Garcia-Echeverria, C.; Sellers, W. R.; Hofmann, F.; Maira, S.-M., Characterization of the Mechanism of Action of the Pan Class I PI3K Inhibitor NVP-BKM120 across a Broad Range of Concentrations. *Molecular Cancer Therapeutics* **2012**, *11* (8), 1747-1757.
17. Folkes, A. J.; Ahmadi, K.; Alderton, W. K.; Alix, S.; Baker, S. J.; Box, G.; Chuckowree, I. S.; Clarke, P. A.; Depledge, P.; Eccles, S. A.; Friedman, L. S.; Hayes, A.; Hancox, T. C.; Kugendradas, A.; Lensun, L.; Moore, P.; Olivero, A. G.; Pang, J.; Patel, S.; Pergl-Wilson, G. H.; Raynaud, F. I.; Robson, A.; Saghir, N.; Salphati, L.; Sohal, S.; Ultsch, M. H.; Valenti, M.; Wallweber, H. J. A.; Wan, N. C.; Wiesmann, C.; Workman, P.; Zhyvoloup, A.; Zvelebil, M. J.; Shuttleworth, S. J., The Identification of 2-(1H-Indazol-4-yl)-6-(4-methanesulfonyl-piperazin-1-ylmethyl)-4-morpholin-4-yl-thieno[3,2-d]pyrimidine (GDC-0941) as a Potent, Selective, Orally Bioavailable Inhibitor of Class I PI3 Kinase for the Treatment of Cancer. *Journal of Medicinal Chemistry* **2008**, *51* (18), 5522-5532.
18. Workman, P.; Clarke, P. A.; Raynaud, F. I.; van Montfort, R. L. M., Drugging the PI3 Kinome: From Chemical Tools to Drugs in the Clinic. *Cancer Research* **2010**, *70* (6), 2146-2157.
19. Abramson, V. G.; Lehmann, B.; Mayer, I. A.; Arteaga, C. L.; Pietenpol, J. A.; Consortium, I. o. t. T. B. C. R., TBCRC028: A phase Ib/II trial of GDC-0941 (a PI3K inhibitor) in combination with cisplatin in metastatic androgen receptor-negative triple-negative breast cancer (TNBC). *Journal of Clinical Oncology* **2014**, *32* (15_suppl), TPS1148-TPS1148.
20. Furman, R. R.; Sharman, J. P.; Coutre, S. E.; Cheson, B. D.; Pagel, J. M.; Hillmen, P.; Barrientos, J. C.; Zelenetz, A. D.; Kipps, T. J.; Flinn, I.; Ghia, P.; Eradat, H.; Ervin, T.; Lamanna, N.; Coiffier, B.; Pettitt, A. R.; Ma, S.; Stilgenbauer, S.; Cramer, P.; Aiello, M.; Johnson, D. M.; Miller, L. L.; Li, D.; Jahn, T. M.; Dansey, R. D.; Hallek, M.; O'Brien, S. M., Idelalisib and Rituximab in Relapsed Chronic Lymphocytic Leukemia. *New England Journal of Medicine* **2014**, *370* (11), 997-1007.
21. Fritsch, C.; Huang, A.; Chatenay-Rivauday, C.; Schnell, C.; Reddy, A.; Liu, M.; Kauffmann, A.; Guthy, D.; Erdmann, D.; De Pover, A.; Furet, P.; Gao, H.; Ferretti, S.; Wang, Y.;

- Trappe, J.; Brachmann, S. M.; Maira, S.-M.; Wilson, C.; Boehm, M.; Garcia-Echeverria, C.; Chene, P.; Wiesmann, M.; Cozens, R.; Lehar, J.; Schlegel, R.; Caravatti, G.; Hofmann, F.; Sellers, W. R., Characterization of the Novel and Specific PI3K α Inhibitor NVP-BYL719 and Development of the Patient Stratification Strategy for Clinical Trials. *Molecular Cancer Therapeutics* **2014**, *13* (5), 1117-1129.
22. Jia, S.; Liu, Z.; Zhang, S.; Liu, P.; Zhang, L.; Lee, S. H.; Zhang, J.; Signoretti, S.; Loda, M.; Roberts, T. M.; Zhao, J. J., Essential roles of PI(3)K–p110 β in cell growth, metabolism and tumorigenesis. *Nature* **2008**, *454*, 776.
23. Maira, S.-M.; Stauffer, F.; Brueggen, J.; Furet, P.; Schnell, C.; Fritsch, C.; Brachmann, S.; Chène, P.; De Pover, A.; Schoemaker, K.; Fabbro, D.; Gabriel, D.; Simonen, M.; Murphy, L.; Finan, P.; Sellers, W.; García-Echeverría, C., Identification and characterization of NVP-BEZ235, a new orally available dual phosphatidylinositol 3-kinase/mammalian target of rapamycin inhibitor with potent *in vivo* antitumor activity. *Molecular Cancer Therapeutics* **2008**, *7* (7), 1851-1863.
24. Fazio, N.; Buzzoni, R.; Baudin, E.; Antonuzzo, L.; Hubner, R. A.; Lahner, H.; De Herder, W. W.; Raderer, M.; Teulé, A.; Capdevila, J.; Libutti, S. K.; Kulke, M. H.; Shah, M.; Dey, D.; Turri, S.; Aimone, P.; Massacesi, C.; Verslype, C., A Phase II Study of BEZ235 in Patients with Everolimus-resistant, Advanced Pancreatic Neuroendocrine Tumours. *Anticancer Research* **2016**, *36* (2), 713-719.
25. Smith, M. C.; Mader, M. M.; Cook, J. A.; Iversen, P.; Ajamie, R.; Perkins, E.; Bloem, L.; Yip, Y. Y.; Barda, D. A.; Waid, P. P.; Zeckner, D. J.; Young, D. A.; Sanchez-Felix, M.; Donoho, G. P.; Wacheck, V., Characterization of LY3023414, a Novel PI3K/mTOR Dual Inhibitor Eliciting Transient Target Modulation to Impede Tumor Growth. *Molecular Cancer Therapeutics* **2016**, *15* (10), 2344-2356.
26. Wainberg, Z. A.; Alsina, M.; Soares, H. P.; Braña, I.; Britten, C. D.; Del Conte, G.; Ezeh, P.; Houk, B.; Kern, K. A.; Leong, S.; Pathan, N.; Pierce, K. J.; Siu, L. L.; Vermette, J.; Tabernero, J., A Multi-Arm Phase I Study of the PI3K/mTOR Inhibitors PF-04691502 and Gedatolisib (PF-05212384) plus Irinotecan or the MEK Inhibitor PD-0325901 in Advanced Cancer. *Targeted Oncology* **2017**, *12* (6), 775-785.
27. Arcaro, A.; Guerreiro, A. S., The Phosphoinositide 3-Kinase Pathway in Human Cancer: Genetic Alterations and Therapeutic Implications. *Current Genomics* **2007**, *8* (5), 271-306.
28. Mattmann, M. E.; Stoops, S. L.; Lindsley, C. W., Inhibition of Akt with small molecules and biologics: historical perspective and current status of the patent landscape. *Expert opinion on therapeutic patents* **2011**, *21* (9), 1309-1338.
29. Davies, B. R.; Greenwood, H.; Dudley, P.; Crafter, C.; Yu, D.-H.; Zhang, J.; Li, J.; Gao, B.; Ji, Q.; Maynard, J.; Ricketts, S.-A.; Cross, D.; Cosulich, S.; Chresta, C. C.; Page, K.; Yates, J.; Lane, C.; Watson, R.; Luke, R.; Ogilvie, D.; Pass, M., Preclinical Pharmacology of AZD5363, an Inhibitor of AKT: Pharmacodynamics, Antitumor Activity, and Correlation of Monotherapy Activity with Genetic Background. *Molecular Cancer Therapeutics* **2012**, *11* (4), 873-887.

30. Lin, J.; Sampath, D.; Nannini, M. A.; Lee, B. B.; Degtyarev, M.; Oeh, J.; Savage, H.; Guan, Z.; Hong, R.; Kassees, R.; Lee, L. B.; Risom, T.; Gross, S.; Liederer, B. M.; Koeppen, H.; Skelton, N. J.; Wallin, J. J.; Belvin, M.; Punnoose, E.; Friedman, L. S.; Lin, K., Targeting Activated Akt with GDC-0068, a Novel Selective Akt Inhibitor That Is Efficacious in Multiple Tumor Models. *Clinical Cancer Research* **2013**, *19* (7), 1760-1772.
31. Yuan, R.; Kay, A.; Berg, W. J.; Lebowitz, D., Targeting tumorigenesis: development and use of mTOR inhibitors in cancer therapy. *Journal of Hematology & Oncology* **2009**, *2* (1), 45.
32. Sankhala, K.; Mita, A.; Kelly, K.; Mahalingam, D.; Giles, F.; Mita, M., The emerging safety profile of mTOR inhibitors, a novel class of anticancer agents. *Targeted Oncology* **2009**, *4* (2), 135-142.
33. Yang, H.; Rudge, D. G.; Koos, J. D.; Vaidialingam, B.; Yang, H. J.; Pavletich, N. P., mTOR kinase structure, mechanism and regulation. *Nature* **2013**, *497*, 217.
34. Loewith, R.; Jacinto, E.; Wullschleger, S.; Lorberg, A.; Crespo, J. L.; Bonenfant, D.; Oppliger, W.; Jenoe, P.; Hall, M. N., Two TOR Complexes, Only One of which Is Rapamycin Sensitive, Have Distinct Roles in Cell Growth Control. *Molecular Cell* **2002**, *10* (3), 457-468.
35. Pusceddu, S.; Verzoni, E.; Prinzi, N.; Mennitto, A.; Femia, D.; Grassi, P.; Concas, L.; Vernieri, C.; Lo Russo, G.; Procopio, G., Everolimus treatment for neuroendocrine tumors: latest results and clinical potential. *Therapeutic Advances in Medical Oncology* **2017**, *9* (3), 183-188.
36. Kwitkowski, V. E.; Prowell, T. M.; Ibrahim, A.; Farrell, A. T.; Justice, R.; Mitchell, S. S.; Sridhara, R.; Pazdur, R., FDA Approval Summary: Temsirolimus as Treatment for Advanced Renal Cell Carcinoma. *The Oncologist* **2010**, *15* (4), 428-435.
37. Buti, S.; Leonetti, A.; Dallatomasina, A.; Bersanelli, M., Everolimus in the management of metastatic renal cell carcinoma: an evidence-based review of its place in therapy. *Core Evidence* **2016**, *11*, 23-36.
38. Hung, C.-M.; Garcia-Haro, L.; Sparks, C. A.; Guertin, D. A., mTOR-Dependent Cell Survival Mechanisms. *Cold Spring Harbor Perspectives in Biology* **2012**, *4* (12), a008771.
39. Sarbassov, D. D.; Guertin, D. A.; Ali, S. M.; Sabatini, D. M., Phosphorylation and Regulation of Akt/PKB by the Rictor-mTOR Complex. *Science* **2005**, *307* (5712), 1098-1101.
40. Altomare, D. A.; Testa, J. R., Perturbations of the AKT signaling pathway in human cancer. *Oncogene* **2005**, *24*, 7455.
41. Manning, B. D.; Cantley, L. C., AKT/PKB Signaling: Navigating Downstream. *Cell* **2007**, *129* (7), 1261-1274.
42. Zhang, J.; Gao, Z.; Yin, J.; Quon, M. J.; Ye, J., S6K Directly Phosphorylates IRS-1 on Ser-270 to Promote Insulin Resistance in Response to TNF- α Signaling through IKK2. *Journal of Biological Chemistry* **2008**, *283* (51), 35375-35382.

43. Choo, A. Y.; Yoon, S.-O.; Kim, S. G.; Roux, P. P.; Blenis, J., Rapamycin differentially inhibits S6Ks and 4E-BP1 to mediate cell-type-specific repression of mRNA translation. *Proceedings of the National Academy of Sciences* **2008**, *105* (45), 17414-17419.
44. Thoreen, C. C.; Kang, S. A.; Chang, J. W.; Liu, Q.; Zhang, J.; Gao, Y.; Reichling, L. J.; Sim, T.; Sabatini, D. M.; Gray, N. S., An ATP-competitive mammalian target of rapamycin inhibitor reveals rapamycin-resistant functions of mTORC1. *Journal of Biological Chemistry* **2009**, *284* (12), 8023-8032.
45. Feldman, M. E.; Apsel, B.; Uotila, A.; Loewith, R.; Knight, Z. A.; Ruggero, D.; Shokat, K. M., Active-site inhibitors of mTOR target rapamycin-resistant outputs of mTORC1 and mTORC2. *PLoS biology* **2009**, *7* (2), e1000038.
46. Dowling, R. J. O.; Topisirovic, I.; Alain, T.; Bidinosti, M.; Fonseca, B. D.; Petroulakis, E.; Wang, X.; Larsson, O.; Selvaraj, A.; Liu, Y.; Kozma, S. C.; Thomas, G.; Sonenberg, N., mTORC1-Mediated Cell Proliferation, But Not Cell Growth, Controlled by the 4E-BPs. *Science* **2010**, *328* (5982), 1172-1176.
47. Singh, J. C.; Novik, Y.; Stein, S.; Volm, M.; Meyers, M.; Smith, J.; Omene, C.; Speyer, J.; Schneider, R.; Jhaveri, K.; Formenti, S.; Kyriakou, V.; Joseph, B.; Goldberg, J. D.; Li, X.; Adams, S.; Tiersten, A., Phase 2 trial of everolimus and carboplatin combination in patients with triple negative metastatic breast cancer. *Breast Cancer Research* **2014**, *16* (2), R32.
48. Meng, L.-h.; Zheng, X. F. S., Toward rapamycin analog (rapalog)-based precision cancer therapy. *Acta Pharmacologica Sinica* **2015**, *36* (10), 1163-1169.
49. Hsieh, A. C.; Costa, M.; Zollo, O.; Davis, C.; Feldman, M. E.; Testa, J. R.; Meyuhas, O.; Shokat, K. M.; Ruggero, D., Genetic dissection of the oncogenic mTOR pathway reveals druggable addiction to translational control via 4EBP-eIF4E. *Cancer cell* **2010**, *17* (3), 249-261.
50. Apsel, B.; Blair, J. A.; Gonzalez, B.; Nazif, T. M.; Feldman, M. E.; Aizenstein, B.; Hoffman, R.; Williams, R. L.; Shokat, K. M.; Knight, Z. A., Targeted polypharmacology: discovery of dual inhibitors of tyrosine and phosphoinositide kinases. *Nature Chemical Biology* **2008**, *4*, 691.
51. Marshall, G.; Howard, Z.; Dry, J.; Fenton, S.; Heathcote, D.; Gray, N.; Keen, H.; Logie, A.; Holt, S.; Smith, P.; Guichard, Sylvie M., Benefits of mTOR kinase targeting in oncology: pre-clinical evidence with AZD8055. *Biochemical Society Transactions* **2011**, *39* (2), 456-459.
52. Benjamin, D.; Colombi, M.; Moroni, C.; Hall, M. N., Rapamycin passes the torch: a new generation of mTOR inhibitors. *Nature Reviews Drug Discovery* **2011**, *10*, 868.
53. Alain, T.; Sonenberg, N.; Topisirovic, I., mTOR inhibitor efficacy is determined by the eIF4E/4E-BP ratio. *Oncotarget* **2012**, *3* (12), 1491-1492.
54. Martineau, Y.; Azar, R.; Müller, D.; Lasfargues, C.; El Khawand, S.; Anesia, R.; Pelletier, J.; Bousquet, C.; Pyronnet, S., Pancreatic tumours escape from translational control through 4E-BP1 loss. *Oncogene* **2013**, *33*, 1367.

55. Hershey, J. W. B.; Sonenberg, N.; Mathews, M. B., Principles of Translational Control: An Overview. *Cold Spring Harbor Perspectives in Biology* **2012**, *4* (12), a011528.
56. Mamane, Y.; Petroulakis, E.; Rong, L.; Yoshida, K.; Ler, L. W.; Sonenberg, N., eIF4E--from translation to transformation. *Oncogene* **2004**, *23* (18), 3172-9.
57. Mark, L.; Evrim, A.; Amit, M.; Nahum, S., Mechanisms governing the control of mRNA translation. *Physical Biology* **2010**, *7* (2), 021001.
58. Richter, J. D.; Sonenberg, N., Regulation of cap-dependent translation by eIF4E inhibitory proteins. *Nature* **2005**, *433* (7025), 477-480.
59. Sonenberg, N., eIF4E, the mRNA cap-binding protein: from basic discovery to translational research. *Biochem Cell Biol* **2008**, *86* (2), 178-83.
60. Musa, J.; Orth, M. F.; Dallmayer, M.; Baldauf, M.; Pardo, C.; Rotblat, B.; Kirchner, T.; Leprieux, G.; Grünwald, T. G. P., Eukaryotic initiation factor 4E-binding protein 1 (4E-BP1): a master regulator of mRNA translation involved in tumorigenesis. *Oncogene* **2016**, *35*, 4675.
61. Avdulov, S., Activation of translation complex eIF4F is essential for the genesis and maintenance of the malignant phenotype in human mammary epithelial cells. *Cancer Cell* **2004**, *5*, 553-563.
62. Teleman, A. A.; Chen, Y.-W.; Cohen, S. M., 4E-BP functions as a metabolic brake used under stress conditions but not during normal growth. *Genes & Development* **2005**, *19* (16), 1844-1848.
63. Tain, L. S.; Mortiboys, H.; Tao, R. N.; Ziviani, E.; Bandmann, O.; Whitworth, A. J., Rapamycin activation of 4E-BP prevents parkinsonian dopaminergic neuron loss. *Nature Neuroscience* **2009**, *12*, 1129.
64. Fukuchi-Shimogori, T.; Ishii, I.; Kashiwagi, K.; Mashiba, H.; Ekimoto, H.; Igarashi, K., Malignant Transformation by Overproduction of Translation Initiation Factor eIF4G. *Cancer Research* **1997**, *57* (22), 5041-5044.
65. Silvera, D.; Arju, R.; Darvishian, F.; Levine, P. H.; Zolfaghari, L.; Goldberg, J.; Hochman, T.; Formenti, S. C.; Schneider, R. J., Essential role for eIF4GI overexpression in the pathogenesis of inflammatory breast cancer. *Nature Cell Biology* **2009**, *11*, 903.
66. Bauer, C.; Diesinger, I.; Brass, N.; Steinhart, H.; Iro, H.; Meese, E. U., Translation initiation factor eIF-4G is immunogenic, overexpressed, and amplified in patients with squamous cell lung carcinoma. *Cancer* **2001**, *92* (4), 822-829.
67. Grüner, S.; Peter, D.; Weber, R.; Wohlbold, L.; Chung, M.-Y.; Weichenrieder, O.; Valkov, E.; Igreja, C.; Izaurralde, E., The Structures of eIF4E-eIF4G Complexes Reveal an Extended Interface to Regulate Translation Initiation. *Molecular Cell* **64** (3), 467-479.

68. Mader, S.; Lee, H.; Pause, A.; Sonenberg, N., The translation initiation factor eIF-4E binds to a common motif shared by the translation factor eIF-4[gamma] and the translational repressors 4E-binding proteins. *Mol. Cell. Biol.* **1995**, *15*, 4990-4997.
69. Marcotrigiano, J.; Gingras, A.-C.; Sonenberg, N.; Burley, S. K., Cocystal Structure of the Messenger RNA 5' Cap-Binding Protein (eIF4E) Bound to 7-methyl-GDP. *Cell* **1997**, *89* (6), 951-961.
70. Haghghat, A.; Sonenberg, N., eIF4G Dramatically Enhances the Binding of eIF4E to the mRNA 5'-Cap Structure. *Journal of Biological Chemistry* **1997**, *272* (35), 21677-21680.
71. Peter, D.; Igreja, C.; Weber, R.; Wohlbold, L.; Weiler, C.; Ebertsch, L.; Weichenrieder, O.; Izaurralde, E., Molecular Architecture of 4E-BP Translational Inhibitors Bound to eIF4E. *Molecular Cell* **2015**, *57* (6), 1074-1087.
72. Matsuo, H.; Li, H.; McGuire, A. M.; Fletcher, C. M.; Gingras, A.-C.; Sonenberg, N.; Wagner, G., Structure of translation factor eIF4E bound to m7GDP and interaction with 4E-binding protein. *Nature Structural Biology* **1997**, *4*, 717.
73. Volpon, L.; Osborne, M. J.; Topisirovic, I.; Siddiqui, N.; Borden, K. L., Cap-free structure of eIF4E suggests a basis for conformational regulation by its ligands. *The EMBO Journal* **2006**, *25* (21), 5138-5149.
74. von der Haar, T.; Ball, P. D.; McCarthy, J. E. G., Stabilization of Eukaryotic Initiation Factor 4E Binding to the mRNA 5'-Cap by Domains of eIF4G. *Journal of Biological Chemistry* **2000**, *275* (39), 30551-30555.
75. Niedzwiecka, A.; Marcotrigiano, J.; Stepinski, J.; Jankowska-Anyszka, M.; Wyslouch-Cieszynska, A.; Dadlez, M.; Gingras, A.-C.; Mak, P.; Darzynkiewicz, E.; Sonenberg, N.; Burley, S. K.; Stolarski, R., Biophysical Studies of eIF4E Cap-binding Protein: Recognition of mRNA 5' Cap Structure and Synthetic Fragments of eIF4G and 4E-BP1 Proteins. *Journal of Molecular Biology* **2002**, *319* (3), 615-635.
76. Igreja, C.; Peter, D.; Weiler, C.; Izaurralde, E., 4E-BPs require non-canonical 4E-binding motifs and a lateral surface of eIF4E to repress translation. *Nature Communications* **2014**, *5*, 4790.
77. Kinkelin, K.; Veith, K.; Grünwald, M.; Bono, F., Crystal structure of a minimal eIF4E–Cap complex reveals a general mechanism of eIF4E regulation in translational repression. *RNA* **2012**, *18* (9), 1624-1634.
78. Paku, Keum S.; Umenaga, Y.; Usui, T.; Fukuyo, A.; Mizuno, A.; In, Y.; Ishida, T.; Tomoo, K., A conserved motif within the flexible C-terminus of the translational regulator 4E-BP is required for tight binding to the mRNA cap-binding protein eIF4E. *Biochemical Journal* **2012**, *441* (1), 237-245.

79. Lukhele, S.; Bah, A.; Lin, H.; Sonenberg, N.; Forman-Kay, Julie D., Interaction of the Eukaryotic Initiation Factor 4E with 4E-BP2 at a Dynamic Bipartite Interface. *Structure* **2013**, *21* (12), 2186-2196.
80. Gosselin, P.; Oulhen, N.; Jam, M.; Ronzca, J.; Cormier, P.; Czjzek, M.; Cosson, B., The translational repressor 4E-BP called to order by eIF4E: new structural insights by SAXS. *Nucleic Acids Research* **2011**, *39* (8), 3496-3503.
81. Konicek, B. W.; Dumstorf, C. A.; Graff, J. R., Targeting the eIF4F translation initiation complex for cancer therapy. *Cell Cycle* **2008**, *7* (16), 2466-2471.
82. Silvera, D.; Formenti, S. C.; Schneider, R. J., Translational control in cancer. *Nature reviews. Cancer* **2010**, *10* (4), 254.
83. Coleman, L.; Peter, M.; Teall, T.; Brannan, R.; Hanby, A.; Honarpisheh, H.; Shaaban, A.; Smith, L.; Speirs, V.; Verghese, E., Combined analysis of eIF4E and 4E-binding protein expression predicts breast cancer survival and estimates eIF4E activity. *British journal of cancer* **2009**, *100* (9), 1393.
84. Flowers, A.; Chu, Q. D.; Panu, L.; Meschonat, C.; Caldito, G.; Lowery-Nordberg, M.; Li, B. D., Eukaryotic initiation factor 4E overexpression in triple-negative breast cancer predicts a worse outcome. *Surgery* **2009**, *146* (2), 220-226.
85. Rojo, F.; Najera, L.; Lirola, J.; Jiménez, J.; Guzmán, M.; Sabadell, M. D.; Baselga, J.; y Cajal, S. R., 4E-binding protein 1, a cell signaling hallmark in breast cancer that correlates with pathologic grade and prognosis. *Clinical Cancer Research* **2007**, *13* (1), 81-89.
86. Graff, J. R.; Konicek, B. W.; Lynch, R. L.; Dumstorf, C. A.; Dowless, M. S.; McNulty, A. M.; Parsons, S. H.; Brail, L. H.; Colligan, B. M.; Koop, J. W., eIF4E activation is commonly elevated in advanced human prostate cancers and significantly related to reduced patient survival. *Cancer research* **2009**, *69* (9), 3866-3873.
87. Duncan, R.; Milburn, S. C.; Hershey, J. W., Regulated phosphorylation and low abundance of HeLa cell initiation factor eIF-4F suggest a role in translational control. Heat shock effects on eIF-4F. *J. Biol. Chem.* **1987**, *262*, 380-383.
88. Rau, M.; Ohlmann, T.; Morley, S. J.; Pain, V. M., A reevaluation of the cap-binding protein, eIF4E, as a rate-limiting factor for initiation of translation in reticulocyte lysate. *J. Biol. Chem.* **1996**, *271*, 8983-8990.
89. Gingras, A. C.; Raught, B.; Sonenberg, N., eIF4 initiation factors: effectors of mRNA recruitment to ribosomes and regulators of translation. *Annu. Rev. Biochem.* **1999**, *68*, 913-963.
90. Graff, J. R.; Zimmer, S. G., Translational control and metastatic progression: enhanced activity of the mRNA cap-binding protein eIF-4E selectively enhances translation of metastasis-related mRNAs. *Clin. Exp. Metastasis* **2003**, *20*, 265-273.

91. Sorrells, D. L.; Ghali, G. E.; Meschonat, C.; DeFatta, R. J.; Black, D.; Liu, L.; Benedetti, A. D.; Nathan, C. A. O.; Li, B. D., Competitive PCR to detect eIF4E gene amplification in head and neck cancer. *Head & neck* **1999**, *21* (1), 60-65.
92. Shatkin, A. J., Capping of eucaryotic mRNAs. *Cell* **1976**, *9* (4, Part 2), 645-653.
93. von der Haar, T.; Gross, J. D.; Wagner, G.; McCarthy, J. E., The mRNA cap-binding protein eIF4E in post-transcriptional gene expression. *Nature Struct. Mol. Biol.* **2004**, *11*, 503-511.
94. Chen, X.; Kopecky, D. J.; Mihalic, J.; Jeffries, S.; Min, X.; Heath, J.; Deignan, J.; Lai, S.; Fu, Z.; Guimaraes, C.; Shen, S.; Li, S.; Johnstone, S.; Thibault, S.; Xu, H.; Cardozo, M.; Shen, W.; Walker, N.; Kayser, F.; Wang, Z., Structure-Guided Design, Synthesis, and Evaluation of Guanine-Derived Inhibitors of the eIF4E mRNA–Cap Interaction. *Journal of Medicinal Chemistry* **2012**, *55* (8), 3837-3851.
95. Wagner, C. R.; Iyer, V. V.; McIntee, E. J., Pronucleotides: Toward the in vivo delivery of antiviral and anticancer nucleotides. *Medicinal Research Reviews* **2000**, *20* (6), 417-451.
96. Ghosh, B.; Benyumov, A. O.; Ghosh, P.; Jia, Y.; Avdulov, S.; Dahlberg, P. S.; Peterson, M.; Smith, K.; Polunovsky, V. A.; Bitterman, P. B.; Wagner, C. R., Nontoxic Chemical Interdiction of the Epithelial-to-Mesenchymal Transition by Targeting Cap-Dependent Translation. *ACS Chemical Biology* **2009**, *4* (5), 367-377.
97. Zochowska, M.; Piguet, A.-C.; Jemielity, J.; Kowalska, J.; Szolajska, E.; Dufour, J.-F.; Chroboczek, J., Virus-like particle-mediated intracellular delivery of mRNA cap analog with in vivo activity against hepatocellular carcinoma. *Nanomedicine: Nanotechnology, Biology and Medicine* **2015**, *11* (1), 67-76.
98. De Benedetti, A.; Joshi-Barve, S.; Rinker-Schaeffer, C.; Rhoads, R. E., Expression of antisense RNA against initiation factor eIF-4E mRNA in HeLa cells results in lengthened cell division times, diminished translation rates, and reduced levels of both eIF-4E and the p220 component of eIF-4F. *Molecular and Cellular Biology* **1991**, *11* (11), 5435-5445.
99. Rinker-Schaeffer, C. W.; Graff, J. R.; De Benedetti, A.; Zimmer, S. G.; Rhoads, R. E., Decreasing the level of translation initiation factor 4E with antisense rna causes reversal of ras-mediated transformation and tumorigenesis of cloned rat embryo fibroblasts. *International Journal of Cancer* **1993**, *55* (5), 841-847.
100. Graff, J. R.; Konicek, B. W.; Vincent, T. M.; Lynch, R. L.; Monteith, D.; Weir, S. N.; Schwier, P.; Capen, A.; Goode, R. L.; Dowless, M. S.; Chen, Y.; Zhang, H.; Sissons, S.; Cox, K.; McNulty, A. M.; Parsons, S. H.; Wang, T.; Sams, L.; Geeganage, S.; Douglass, L. E.; Neubauer, B. L.; Dean, N. M.; Blanchard, K.; Shou, J.; Stancato, L. F.; Carter, J. H.; Marcusson, E. G., Therapeutic suppression of translation initiation factor eIF4E expression reduces tumor growth without toxicity. *The Journal of Clinical Investigation* **2007**, *117* (9), 2638-2648.
101. Duffy, A. G.; Makarova-Rusher, O. V.; Ulahannan, S. V.; Rahma, O. E.; Fioravanti, S.; Walker, M.; Abdullah, S.; Raffeld, M.; Anderson, V.; Abi-Jaoudeh, N.; Levy, E.; Wood, B. J.;

- Lee, S.; Tomita, Y.; Trepel, J. B.; Steinberg, S. M.; Revenko, A. S.; MacLeod, A. R.; Peer, C. J.; Figg, W. D.; Greten, T. F., Modulation of tumor eIF4E by antisense inhibition: A phase I/II translational clinical trial of ISIS 183750—an antisense oligonucleotide against eIF4E—in combination with irinotecan in solid tumors and irinotecan-refractory colorectal cancer. *International Journal of Cancer* **2016**, *139* (7), 1648-1657.
102. Lama, D.; Quah, S. T.; Verma, C. S.; Lakshminarayanan, R.; Beuerman, R. W.; Lane, D. P.; Brown, C. J., Rational Optimization of Conformational Effects Induced By Hydrocarbon Staples in Peptides and their Binding Interfaces. **2013**, *3*, 3451.
103. BROWN, C. J.-C., Singapore 2, 13863, SG), LANE, David Philip (#20-10 Connexis, Singapore 2, 13863, SG), QUAH, Soo Tng (#20-10 Connexis, Singapore 2, 13863, SG), LAMA, Dilraj (#20-10 Connexis, Singapore 2, 13863, SG), VERMA, Chandra Shekhar (#20-10 Connexis, Singapore 2, 13863, SG) STAPLING eIF4E INTERACTING PEPTIDES. 2014.
104. Bird, G. H.; Mazzola, E.; Opoku-Nsiah, K.; Lammert, M. A.; Godes, M.; Neuberger, D. S.; Walensky, L. D., Biophysical determinants for cellular uptake of hydrocarbon-stapled peptide helices. *Nature Chemical Biology* **2016**, *12*, 845.
105. Rogers, G. W.; Richter, N. J.; Merrick, W. C., Biochemical and Kinetic Characterization of the RNA Helicase Activity of Eukaryotic Initiation Factor 4A. *Journal of Biological Chemistry* **1999**, *274* (18), 12236-12244.
106. Bordeleau, M.-E.; Mori, A.; Oberer, M.; Lindqvist, L.; Chard, L. S.; Higa, T.; Belsham, G. J.; Wagner, G.; Tanaka, J.; Pelletier, J., Functional characterization of IRESes by an inhibitor of the RNA helicase eIF4A. *Nature Chemical Biology* **2006**, *2*, 213.
107. Tsumuraya, T.; Ishikawa, C.; Machijima, Y.; Nakachi, S.; Senba, M.; Tanaka, J.; Mori, N., Effects of hippuristanol, an inhibitor of eIF4A, on adult T-cell leukemia. *Biochemical Pharmacology* **2011**, *81* (6), 713-722.
108. Cencic, R.; Carrier, M.; Galicia-Vázquez, G.; Bordeleau, M.-E.; Sukarieh, R.; Bourdeau, A.; Brem, B.; Teodoro, J. G.; Greger, H.; Tremblay, M. L.; Porco, J. A.; Pelletier, J., Antitumor Activity and Mechanism of Action of the Cyclopenta[b]benzofuran, Silvestrol. *PLoS ONE* **2009**, *4* (4), e5223.
109. Gupta, S. V.; Sass, E. J.; Davis, M. E.; Edwards, R. B.; Lozanski, G.; Heerema, N. A.; Lehman, A.; Zhang, X.; Jarjoura, D.; Byrd, J. C.; Pan, L.; Chan, K. K.; Kinghorn, A. D.; Phelps, M. A.; Grever, M. R.; Lucas, D. M., Resistance to the Translation Initiation Inhibitor Silvestrol is Mediated by ABCB1/P-Glycoprotein Overexpression in Acute Lymphoblastic Leukemia Cells. *The AAPS Journal* **2011**, *13* (3), 357.
110. Moerke, N. J.; Aktas, H.; Chen, H.; Cantel, S.; Reibarkh, M. Y.; Fahmy, A.; Gross, J. D.; Degtarev, A.; Yuan, J.; Chorev, M., Small-molecule inhibition of the interaction between the translation initiation factors eIF4E and eIF4G. *Cell* **2007**, *128* (2), 257-267.

111. Yi, T.; Kabha, E.; Papadopoulos, E.; Wagner, G., 4EGI-1 targets breast cancer stem cells by selective inhibition of translation that persists in CSC maintenance, proliferation and metastasis. *Oncotarget* **2014**, *5* (15), 6028-6037.
112. De, A.; Jacobson, B. A.; Peterson, M. S.; Jay-Dixon, J.; Kratzke, M. G.; Sadiq, A. A.; Patel, M. R.; Kratzke, R. A., 4EGI-1 represses cap-dependent translation and regulates genome-wide translation in malignant pleural mesothelioma. *Investigational New Drugs* **2017**.
113. Chen, L.; Aktas, B. H.; Wang, Y.; He, X.; Sahoo, R.; Zhang, N.; Denoyelle, S.; Kabha, E.; Yang, H.; Freedman, R. Y.; Supko, J. G.; Chorev, M.; Wagner, G.; Halperin, J. A., Tumor suppression by small molecule inhibitors of translation initiation. *Oncotarget* **2012**, *3* (8), 869-881.
114. Cencic, R.; Hall, D. R.; Robert, F.; Du, Y.; Min, J.; Li, L.; Qui, M.; Lewis, I.; Kurtkaya, S.; Dingleline, R.; Fu, H.; Kozakov, D.; Vajda, S.; Pelletier, J., Reversing chemoresistance by small molecule inhibition of the translation initiation complex eIF4F. *Proceedings of the National Academy of Sciences of the United States of America* **2011**, *108* (3), 1046-1051.
115. Cencic, R.; Desforages, M.; Hall, D. R.; Kozakov, D.; Du, Y.; Min, J.; Dingleline, R.; Fu, H.; Vajda, S.; Talbot, P. J.; Pelletier, J., Blocking eIF4E-eIF4G Interaction as a Strategy To Impair Coronavirus Replication. *Journal of Virology* **2011**, *85* (13), 6381-6389.
116. Feng, Y.; Pinkerton, A. B.; Hulea, L.; Zhang, T.; Davies, M. A.; Grotegut, S.; Cheli, Y.; Yin, H.; Lau, E.; Kim, H.; De, S. K.; Barile, E.; Pellecchia, M.; Bosenberg, M.; Li, J.-L.; James, B.; Hassig, C. A.; Brown, K. M.; Topisirovic, I.; Ronai, Z. e. A., SBI-0640756 Attenuates the Growth of Clinically Unresponsive Melanomas by Disrupting the eIF4F Translation Initiation Complex. *Cancer Research* **2015**, *75* (24), 5211-5218.
117. Gaitonde, S.; De Surya, K.; Tcherpakov, M.; Dewing, A.; Yuan, H.; Riel-Mehan, M.; Krajewski, S.; Robertson, G.; Pellecchia, M.; Ronai, Z. e., BI-69A11-mediated inhibition of AKT leads to effective regression of xenograft melanoma. *Pigment Cell & Melanoma Research* **2009**, *22* (2), 187-195.
118. Feng, Y.; Pinkerton, A. B.; Hulea, L.; Zhang, T.; Davies, M. A.; Grotegut, S.; Cheli, Y.; Yin, H.; Lau, E.; Kim, H.; De, S. K.; Barile, E.; Pellecchia, M.; Bosenberg, M.; Li, J.-L.; James, B.; Hassig, C. A.; Brown, K. M.; Topisirovic, I.; Ronai, Z. e. A., SBI-0640756 Attenuates the Growth of Clinically Unresponsive Melanomas by Disrupting the eIF4F Translation Initiation Complex. *Cancer Research* **2015**, *75* (24), 5211-5218.

CHAPTER 2 DESIGN AND DEVELOPMENT OF PPI CAT-ELCCA¹

In the present toolbox of high-throughput screening (HTS) assays for PPIs, a missing piece is the ability to screen against *full-length* protein systems in a non-cellular format. The most commonly used biochemical assays for PPIs are fluorescence polarization (FP), fluorescence resonance energy transfer (FRET), and time-resolved FRET (TR-FRET)¹. Although easy to implement due to their homogeneous conditions, these assays are mostly limited to the analysis of motif-domain or domain-domain interactions due to size and labeling requirements¹⁻². Thus, by using these methods, probe discovery efforts are focused solely on hot spot interactions, while eliminating the possibility of targeting potentially more druggable allosteric binding sites. Moreover, these approaches require structural knowledge about the PPI in order to design appropriate peptide substrates (e.g. FP) or for proximity-matched labeling (e.g. FRET), which also may be difficult, particularly for large or disordered proteins, as the cases of 4EGI-1 and 4E1RCat HTS campaigns have shown. Other disadvantages of these approaches include single-turnover readout, which limits the sensitivity of the measurement and compound interference by assay-specific interferents (e.g. fluorescent molecules or fluorescence quenchers) yielding many false positive and negative hits. In order to efficiently assay and discover chemical modulators of *full-length* PPIs, which are more biologically relevant, ELISA and SPR are better suited despite their disadvantages with respect to lower screening throughput. Specifically, the Garner group has been interested in developing novel assays that retain the

¹ This work was published in ACS Combinatorial Science in 2017 under the title “High-Throughput Chemical Probing of Full-Length Protein-Protein Interactions”. Co-authors include: Menon, Arya (eIF4G1 protein preparation); Mitchell, Dylan (eIF4G1 plasmid preparation); Johnson, Oleta (eIF4E protein preparation)

advantages of ELISA and minimize its disadvantages while expanding its applications. Garner et al. invented a new platform assay technology termed catalytic enzyme-linked click chemistry assay, or cat-ELCCA, as a robust method to monitor the fatty acid acyltransferase activity of Ghrelin O-Acyltransferase^{1, 3-4}. Later on, cat-ELCCA was re-conceptualized to target DICER-driven maturation of pre-miRNAs and eIF4E PPIs (**Figure 5A**). The latter assay platform was termed PPI cat-ELCCA⁶⁻⁷.

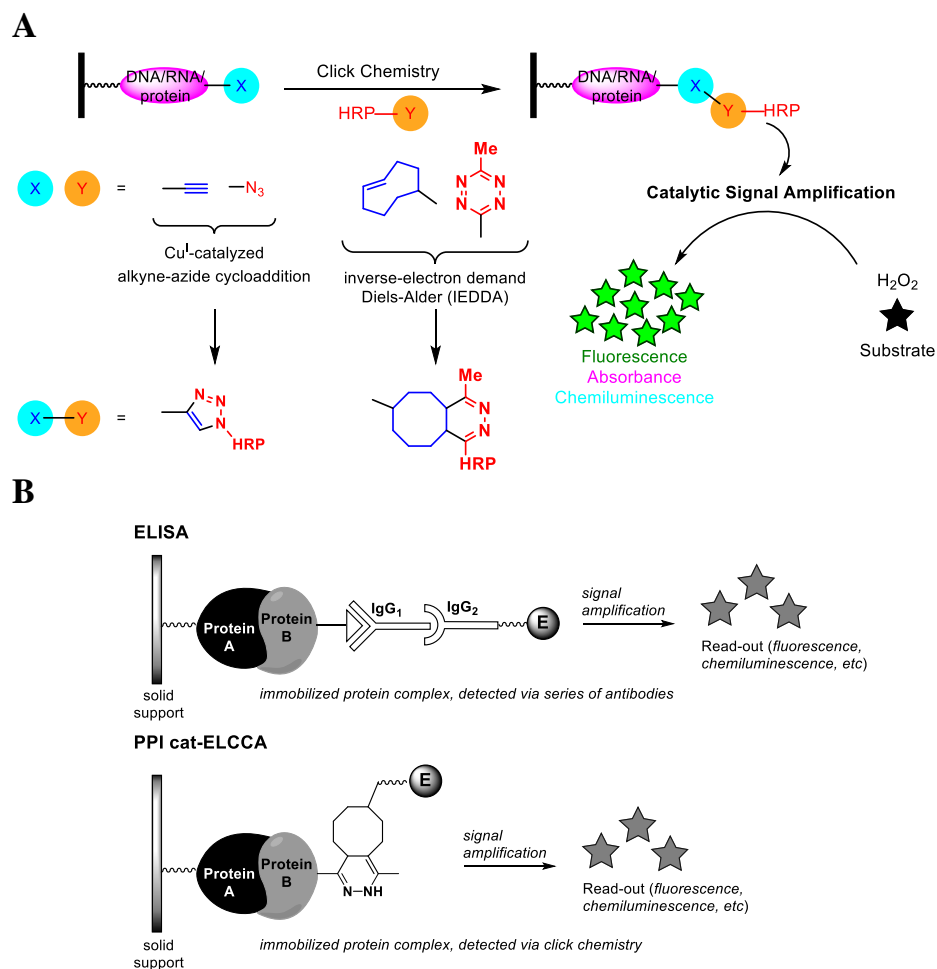


Figure 5. cat-ELCCA and ELISA. A) generic schematic of cat-ELCCA. B) comparison of ELISA and PPI cat-ELCCA

PPI cat-ELCCA derives its origin from ELISA (**Figure 5B**), and as such, share its core advantages (high sensitivity and low chemical interference) to its disadvantages (mid-throughput

and heterogeneous assay conditions). Briefly, one of the binding partners in the PPI is immobilized to the well surface through passive adsorption to the plastic (ELISA) or through tag–affinity driven interactions (PPI cat-ELCCA, biotin–streptavidin). Following the immobilization and the subsequent washing, the second binding partner is then added. In ELISA, after another brief wash, the binding event is then detected through the antibody specific to the second binding partner and quantified through an enzyme–conjugated secondary antibody. PPI cat-ELCCA eliminates the need for antibodies and relies on the click-chemistry reaction between the protein complex and chemically modified HRP for direct detection.

Although few in number, (9 primary screens as of January 2018) ELISA has been used for primary screening campaigns. In general, ELISA is suboptimal for the large primary screening due to its three greatest drawbacks: it is labor intensive, it has relatively low throughput in comparison to FP and TR–FRET and plagued by the inconsistencies and availabilities of antibodies. The washing steps must be automated and optimized through robotic handlers, and in most cases, the plates must be manually handled in between the washing steps. HTS campaign using ELISA could potentially be days or even weeks longer than a similar campaign using FP and TR–FRET. Furthermore, the lot–to–lot and even vial–to–vial variations in sensitivity and selectivity of commercially available antibodies plague researchers and contributes to the rising undependability of published studies.

Despite the glaring disadvantages of HTS ELISA, its strengths could enable screening of difficult PPI targets. ELISA utilizes readily available instrumentation and reagents in a typical laboratory, from generic fluorescence/absorbance/luminescence plate readers to primary and secondary antibodies of interest. Its enhanced sensitivity from enzyme–driven signal detection enables compound screening to be performed at low nanomolar concentrations, saving reagents,

and more importantly, dramatically increasing the chances of discovering even weak inhibitors to a particularly strong PPI. This advantage is critical in screening for inhibitors of eIF4E PPIs because of the reported high binding affinity of 4E–BP1 and eIF4G to eIF4E. Although labor intensive, the washing steps separate the screening step and the signal detection step, reducing the library chemical interference (fluorescence/luminescence quenchers, fluorophores, etc.) while greatly increasing the diversity of potential libraries. Furthermore, optimized protein immobilization (specifically enzymes) in biotechnology often leads to greater temperature, pH, and organic solvent stabilities¹⁻²; thus, protein engineering that accounts for proper active orientation, and distance from the immobilized surface could allow screening of the PPIs involving unstable protein(s). PPI cat-ELCCA had eliminated the washing and the incubation steps required for the secondary antibodies, which led to reduction in assay time and improvements in HTS statistics. And while the first generation of cat-ELCCAs utilized CuAAC^{3-4, 8} in the assay design, the second generation cat-ELCCAs use IEDDA which provided far superior reaction kinetics, greater throughput and HTS screening statistics, and required less labor. In design and practice, PPI cat-ELCCA is a faster and more sensitive alternative to ELISA for PPI drug discovery campaigns.

2.1 EFFORTS TO DEVELOP PepPI CAT-ELCCA

2.1.1 RESEARCH DESIGN

Prior to the invention of PPI cat-ELCCA, the Garner group sought to develop an alternative assay for the biological systems in which full-length proteins were unavailable and FP/TR-FRET HTS campaigns had been unsuccessful. To fill this unique target gap – especially in regard to the CdT initiation and the eIF4E interactions – the **Peptide-Protein Interaction cat-**

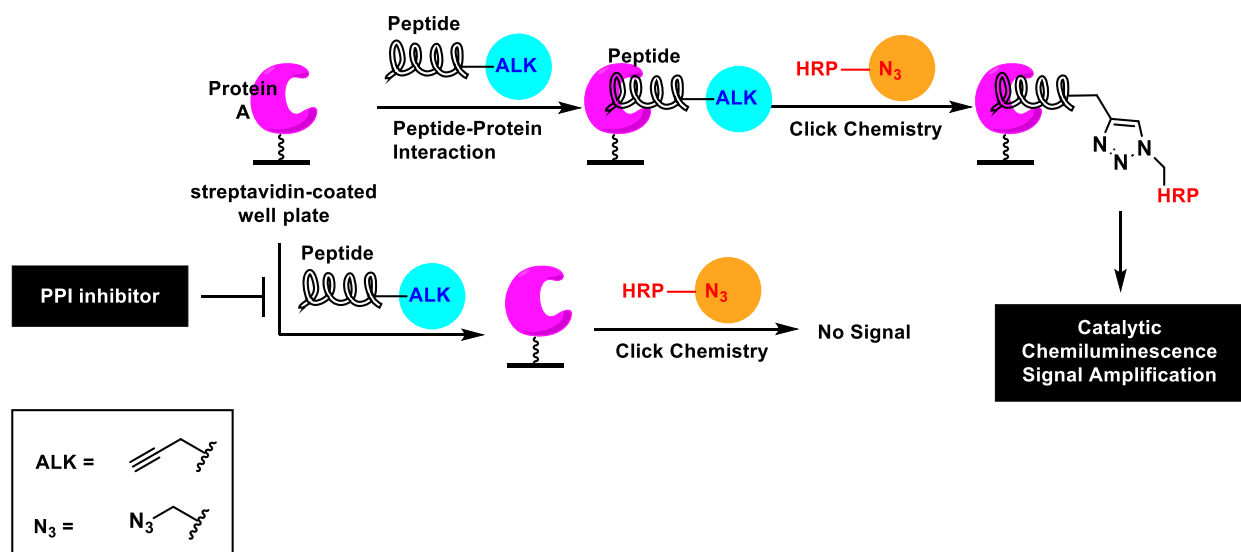


Figure 6. PepPI cat-ELCCA CuAAC schematic

ELCCA, or PepPI cat-ELCCA was developed (**Figure 6**). For all the proposed advantages of developing HTS campaign assays against full-length PPIs, sometimes the full interaction is impossible to recapitulate *in vitro*. For example, the full-length eIF4E-eIF4G1 interaction was unsuitable to be developed into a HTS campaign due to difficult preparation and procurement of eIF4G1 for the assays and its instability. A comprehensive study in 2003 revealed that only about 10% of full-length proteins from *Eukarya* can be expressed and purified in *E. coli* systems⁶⁻⁷, and that the probability of success decreases significantly for proteins with molecular weights greater than 60 kDa. Unsurprisingly, the shorter and simpler domains could be expressed as a recombinant protein or synthesized as peptides, and are less prone to poor translation, misfolding, and aggregation than the full-length protein. Thus, for many targets of interest, peptide-protein interactions and FP/TR-FRET assays may be one of the few options for conducting HTS campaigns.

In PepPI cat-ELCCA, the biotinylated protein is immobilized in the wells of a streptavidin-coated microtiter plate. Following the protein immobilization, a click chemistry-armed peptide-binding partner is added to form the peptide-protein interaction. In this assay

platform, the direct binding affinities of the chemically modified peptide probes could be measured without the need for immuno-affinity tags, antibodies, and SPR instrumentation. It would also benefit from the increased protein complex stability (temperature, pH, organic solvent, and etc.) from protein immobilization¹¹ and exhibit reduced screening chemical interference while maintaining the high sensitivity and the robustness of ELISA.

2.1.2 PROTEIN LABELING

cat-ELCCAs utilizes chemically labeled proteins: one with a biotin moiety for immobilization to the streptavidin-functionalized plate, and another with a click chemistry

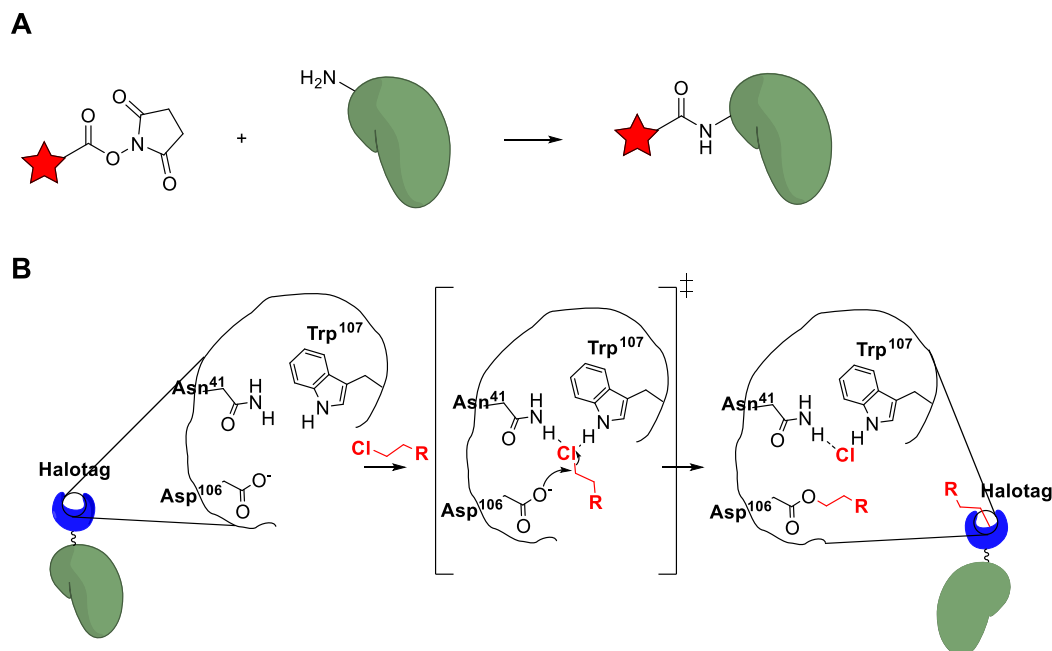


Figure 7. The mechanism of Halotag Protein labeling. A) Amine-reactive crosslinker NHS ester forms amide with surfaced exposed lysines on the protein, B) chloro-alkane linkers covalently react with Asp106 in the Halotag active site

handle (alkyne, azide, TCO, or mTET) for a bioconjugation to the HRP. A common strategy to label proteins is by using amine reactive crosslinkers such as N-hydroxysuccinimide (NHS) esters to target the surface-exposed lysines (**Figure 7A**) on the proteins. However, this approach

can randomly functionalize the target protein with varying numbers of desired chemical groups and will result in heterogenous biophysical orientations during the immobilization and the interaction. As previously discussed, the protein immobilization step could potentially be advantageous with the right protein engineering to increase protein stability and activity; thus, the bioconjugation method should yield one functional group per protein, and on the identical residue(s). Both PepPI and PPI cat-ELCCAs were designed using HaloTag-fusion™ proteins (HT). HT is a 34 kDa enzymatic tag that covalently reacts to a chloroalkane ligand, displacing the electrophilic chlorine in a S_N2 reaction (**Figure 7B**). HT fusion protein limits labeling to just one chemical group per protein on HT Asp106, and provide a homogenous labeling.

2.1.3 PEPI CAT-ELCCA CLICK CHEMISTRY

Alkynyl 4E-BP1 peptide was prepared through solid phase peptide chemistry and verified by reacting with azido-functionalized rhodamine; azido-HRP was labeled with a diazotransfer reagent¹ and verified similarly with alkynyl-functionalized rhodamine. The reactions were tested using both THPTA (Tris(3-hydroxypropyltriazolylmethyl)amine) and TBTA (Tris[(1-benzyl-1H-1,2,3-triazol-4-yl)methyl]amine) as the CuAAC ligand (**Figure 8A**). However, while both post-translational modification cat-ELCCA³⁻⁴ and pre-microRNA maturation cat-ELCCA had worked effectively using the ligand THPTA, PepPI cat-ELCCA failed under the identical conditions and only yielded notable signal-to-background (S/B) using TBTA (**Figure 8B**). The lack of translation between the reactivities of immobilized and in-solution substrates highlights the difficulties of bioconjugation and the necessary assay developments for each biological systems and substrates.

Unfortunately, the IEDDA reaction utilized by the second-generation cat-ELCCAs^{1, 3} was not amenable to PepPI cat-ELCCA and the assay could not capitalize on its superior

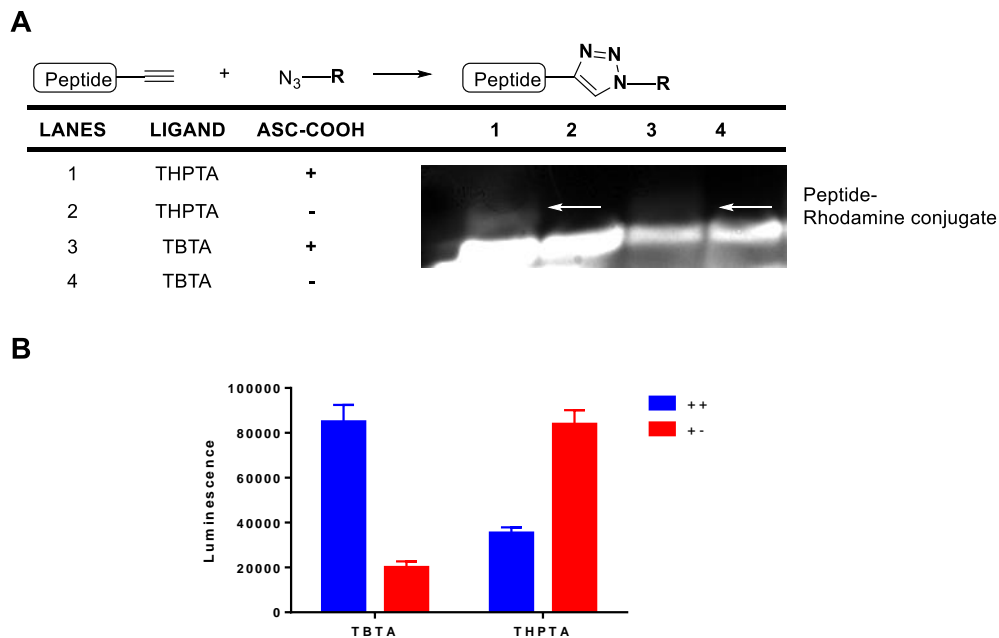
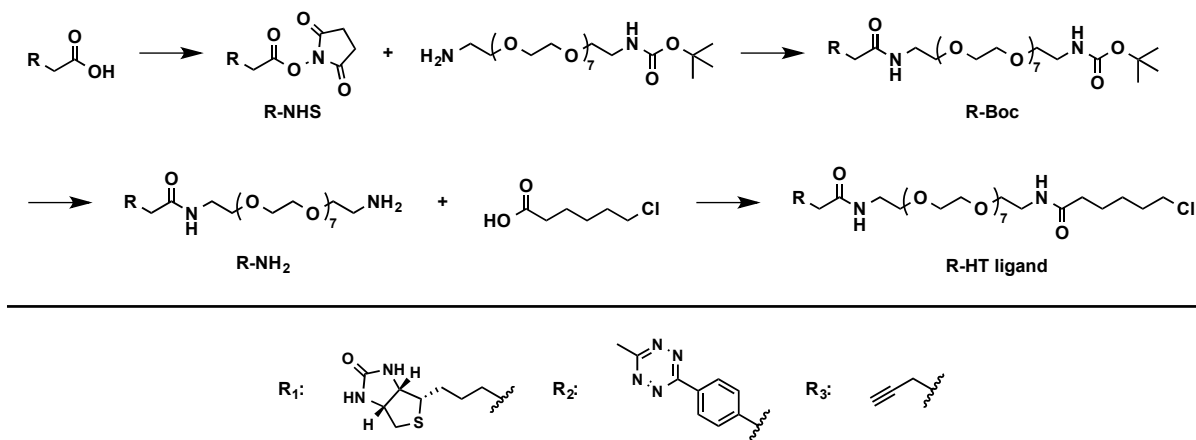


Figure 8. PepPI cat-ELCCA proof-of-concept. A) *in solution* CuAAC conditions to conjugate alkyne 4E-BP1 peptide and azido Rhodamine, B) CuAAC ligand THPTA fails to elicit notable S/B ratio whereas TBTA shows S/B of 4.2. ++, alkyne 4E-BP1 and biotin eIF4E, +- alkyne 4E-BP1 only (n = 3, shown as the mean \pm SD)

reaction kinetics. Despite the noted stability of methyl-tetrazine (mTET) to trifluoroacetic acid (TFA) as shown by the synthesis of mTET HaloTag probe (**Scheme 1**), global TFA deprotection of the mTET functionalized 4E-BP1 peptide had failed to materialize the desired product. Although the mTET moiety had previously been successfully incorporated into either of the termini and into the mid-peptide sequence¹⁵, these peptides all consisted of amino acids without any side-chain protecting groups (V, F, A, and G). Since the global TFA deprotection of 4E-BP1 peptide releases highly reactive protecting groups, the added scavengers may be insufficient to prevent the side reactions with mTET moiety. The incorporation of the *trans*-cyclooctene (TCO) moiety into the 4E-BP1 peptide was not attempted due to its documented isomerization under global deprotection conditions¹⁶.



Scheme 1. Synthetic schemes of Biotin- (R_1), mTet- (R_2), and alkynyl- (R_3) Halotag ligands.

2.1.3 PEPPi CAT-ELCCA ASSAY DEVELOPMENT

Supplementing the assay and the wash buffers with BSA significantly improved the S/B between the positive interaction (++) and the competition (++ competition) from 1.4 to 10.1 (**Figure 9A**). BSA is a common blocking reagent utilized in ELISAs, western blotting, FP, and other laboratory techniques. In PepPI cat-ELCCA, BSA likely prevented nonspecific adherence of the 4E-BP1 peptides (both alkynyl and native) and azido-HRP to the well surfaces. In fact, the high signal observed in absence of both BSA and alkynyl 4E-BP1 peptide indicated that the CuAAC condition alone was sufficient to cause nonspecific adherence of azido-HRP, which could be prevented by using a commercial blocking reagent (**Figure 9B**). Alkynyl 4E-BP1-eIF4E interaction failed to reach saturation signal above 5 μ M despite the reported binding affinity of 15 nM to 85 nM by SPR¹⁶ (++, **Figure 9C**), which indicated possible peptide aggregation at the high concentrations. However, the assay did demonstrate a complete inhibition of alkynyl 4E-BP1 peptide-eIF4E interaction-dependent signal in the presence of the unlabeled 4E-BP1 protein, and only a slight loss in presence of BSA (**Figure 9C**); confirming that the observed signal in the PepPI cat-ELCCA was indeed 4E-BP1-eIF4E interaction specific.

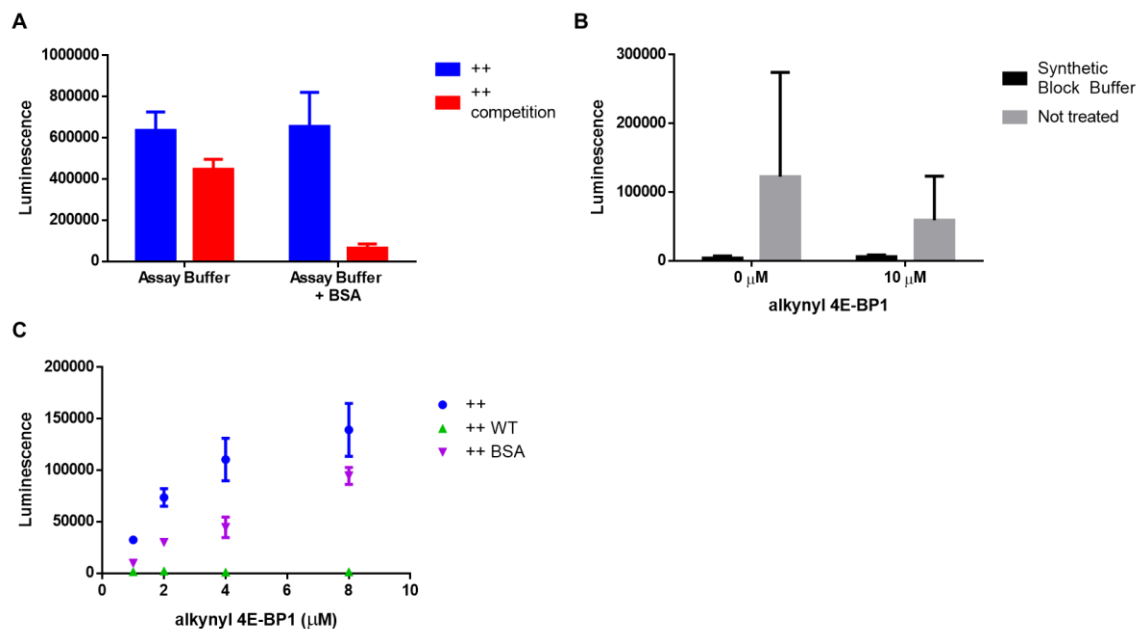


Figure 9. PepPI cat-ELCCA development. A) BSA incubation in PepPI cat-ELCCA dramatically increases the S/B between a positive interaction (++) and competition (++ competition), B) Synthetic Block BufferTM reduces the nonspecific binding of HRP induced by CuAAC condition, C) the unlabeled HT 4E-BP1 eliminates PepPI cat-ELCCA signal (++ WT) whereas equivalent addition of BSA does not (++ BSA). All experiments were conducted in triplicates (n=3) and shown as the mean \pm SD

2.1.4 PEPI CAT-ELCCA CONCLUSION

Although PepPI cat-ELCCA was confirmed to be 4E-BP1-eIF4E interaction dependent, and the nonspecific signals arising from CuAAC conditions had been resolved, the extensive assay optimizations to arrive to a modest S/B with data fluctuations made it undesirable for HTS screening. Successful transition of PepPI cat-ELCCA to IEDDA chemistry may have improved its screening statistics; however, with the successful development of PPI cat-ELCCA, PepPI cat-ELCCA had lost much of its relevance for the HTS purposes. The suspected peptide aggregation was later confirmed through PPI cat-ELCCA (**Figure 16D**) but was never resolved despite the extensive peptide sequence optimizations, buffer salts and ionic strength variations, and additions of reducing and/or chaotropic reagents. In summary, PepPI cat-ELCCA demonstrated

the difficulties of designing peptide-protein interaction-based assays. Their limited solubilities and susceptibilities to the aggregation requires careful peptide sequence design, and a difficult compromise between optimizing for the desired binding affinity and for the necessary reagent/assay conditions of the HTS campaign. Although the development of HTS capable PepPI cat-ELCCA proved unsuccessful, it laid the foundation for the design and the establishment of a more biologically relevant, full-length protein interaction targeting PPI cat-ELCCA.

2.2 PPI CAT-ELCCA

As previously noted, PPI cat-ELCCA shares much of its foundation with ELISA and PepPI cat-ELCCA. Similar to PepPI cat-ELCCA, a biotinylated protein is first immobilized in the wells of a streptavidin-coated microtiter plate. However, in place of adding in a click chemistry-armed *peptide*-binding partner, the wells are incubated with a click chemistry-armed *protein*-binding partner to form the PPI. Detection occurs through a click reaction with a labeled horseradish peroxidase (HRP), followed by addition of a HRP substrate and chemiluminescence measurement. Importantly, this catalytic system retains the major advantages of ELISA and minimizes the disadvantages of ELISA by eliminating the requirement for antibodies, which results in two distinct benefits: 1) the facile implementation to PPI targets for which monoclonal antibodies may not already exist or are difficult to generate against, and 2) the removal of one washing step without sacrificing the sensitivity and the low compound interference. As a proof-of-concept, PPI cat-ELCCA was developed for two interactions that play a crucial role in the initiation of the CdT, between that of eIF4E–4E-BP1 and of eIF4E–eIF4G.

2.3 RESULTS AND DISCUSSION

2.3.1 PROTEIN LABELING

Alkyne-, mTet-, and biotin-functionalized chloroalkane HT probes were synthesized (**Scheme 1**) and purified. Azide–NHS esters and TCO–NHS esters were used to label HRP; the biophysical orientations and the varying number of labeling (3–4 surface-exposed lysines that were labeled) on HRP were of minimal concern, as the reactive functional groups were already restricted by the active protein complexes. The successful labeling and activity of the chemical groups were verified (**Figure 10A**) and the biotin labeling was verified through streptavidin–HRP blot (**Figure 10B**).

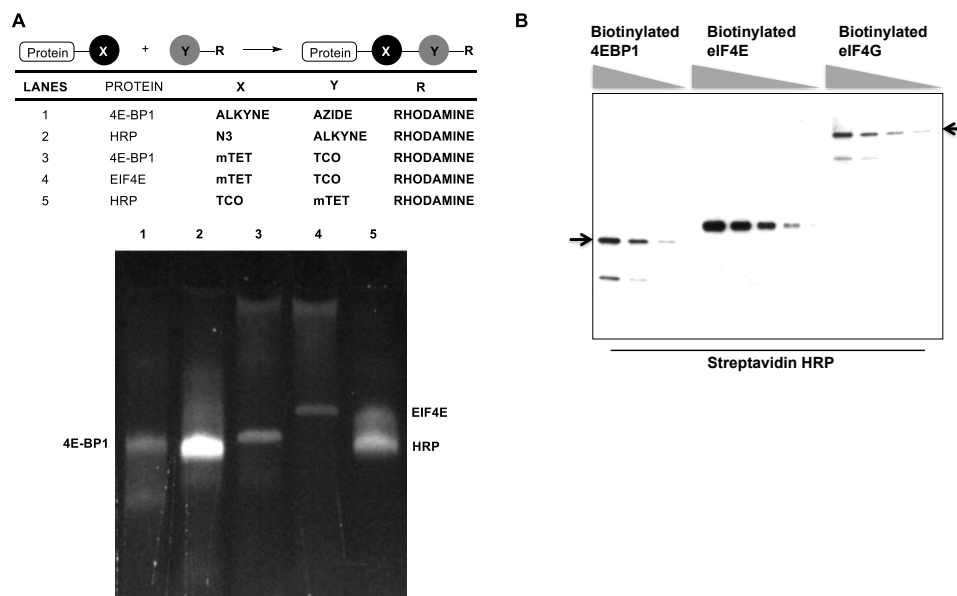


Figure 10. 4E-BP1, eIF4E and eIF4G Labeling. A) PPI cat–ELCCA protein labeling verification. B) verification of successful biotinylation

2.3.2 PROOF OF CONCEPT: CUAAC PPI CAT–ELCCA

PPI cat–ELCCA was first established with eIF4E–4E–BP1 as a model interaction and using CuAAC as the click chemistry reaction (**Figure 11A**). Biotinylated eIF4E was first

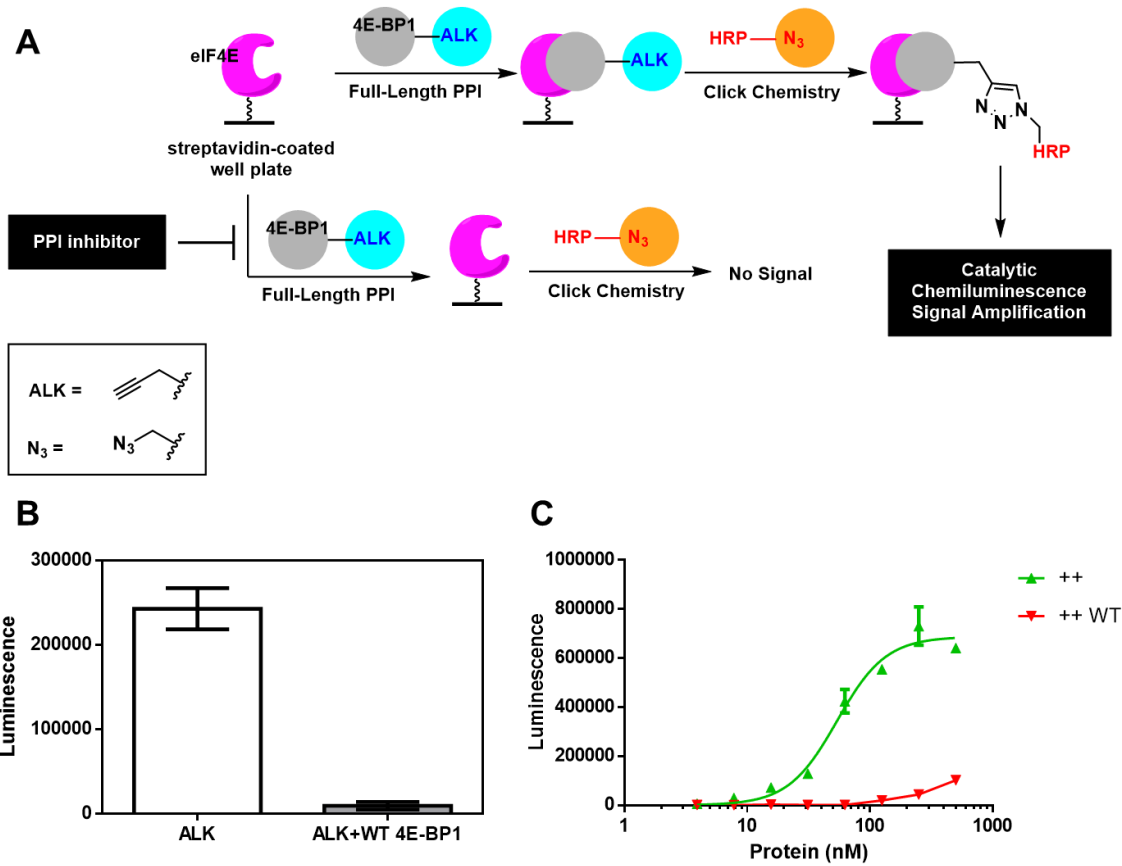


Figure 11. CuAAC PPI cat-ELCCA. A) CuAAC PPI cat-ELCCA schematics. B) Proof of concept for CuAAC PPI cat-ELCCA. Addition of the WT 4E-BP1 lowers luminescence by 25-fold C) The interaction is dose dependent, and addition of WT 4E-BP1 reduces the number of the *active complexes*. All experiments were conducted in triplicates (n=3) and shown as the mean \pm SD.

immobilized in the wells of a 384-well streptavidin plate and incubated with alkyne-4E-BP1. Following a click reaction with azido-HRP, the wells were treated with SuperSignal West Pico and chemiluminescence signal was measured. In this proof-of-concept, alkyne-4E-BP1 showed high luminescence and the addition of unlabeled WT HaloTag-4E-BP1 (WT 4E-BP1) reduced the signal to the base level (**Figure 11B**). The interaction was also found to be dose-dependent, yielding apparent K_d values of 54 ± 5 nM for 4E-BP1-eIF4E interaction (++, **Figure 11C**), which were comparable to the hot spots that drive the interaction. Furthermore, the addition of WT 4E-BP1 reduced the luminescence signal, indicating that the observed interaction was specific to that between eIF4E-4E-BP1.

2.3.3 PROOF OF CONCEPT: IEDDA PPI CAT-ELCCA

Although CuAAC yielded acceptable results, the reaction conditions were labor intensive. Thus, PPI cat-ELCCA was re-modeled to the second-generation approach utilizing inverse-electron demand Diels-Alder (IEDDA) chemistry (**Figure 12A**), in which the HRP and 4E-BP1 were labeled with TCO and mTET, respectively. Previously, the Garner group had demonstrated that due to its kinetic superiority, replacing the first-generation CuAAC click chemistry detection step¹⁶ with IEDDA yielded improved sensitivity and reproducibility, enabling automated HTS. Similar to CuAAC PPI cat-ELCCA, biotinylated eIF4E or eIF4G was first immobilized in the wells of a 384-well streptavidin plate and incubated with mTet-4E-BP1 or -eIF4E, respectively. Of note, for the eIF4E-eIF4G PPI, eIF4G was immobilized due to its large size (220 kDa) and crude preparation from overexpressing HEK293T cells (**Figure 12B**), as eIF4G cannot be purified to homogeneity. Following the click reaction with HRP-TCO, the wells were treated with SuperSignal West Pico and chemiluminescence signal was measured. The preliminary experiments using IEDDA were successful and >500-fold chemiluminescence signal increases were observed for both PPIs, whereas controls without either protein yielded no signal as expected (**Figure 12B**). Importantly, this is the first time that the full-length eIF4G protein has been used in a biochemical assay of eIF4E binding, as the previous reports have focused solely on eIF4G peptide or protein fragments due to its size, instability, and limitations of the assay formats used (FP and TR-FRET).. The interactions were also found to be dose-dependent, yielding apparent K_d values of 3.8 ± 0.7 and 8.3 ± 0.5 nM for 4E-BP1 and eIF4G binding, respectively (**Figure 12C**). These values are in line with previous biophysical affinity measurements of 4E-BP1 protein and eIF4G fragments for eIF4E since the full-length PPIs should yield greater affinity to eIF4E. Thus, IEDDA PPI cat-ELCCA had significantly

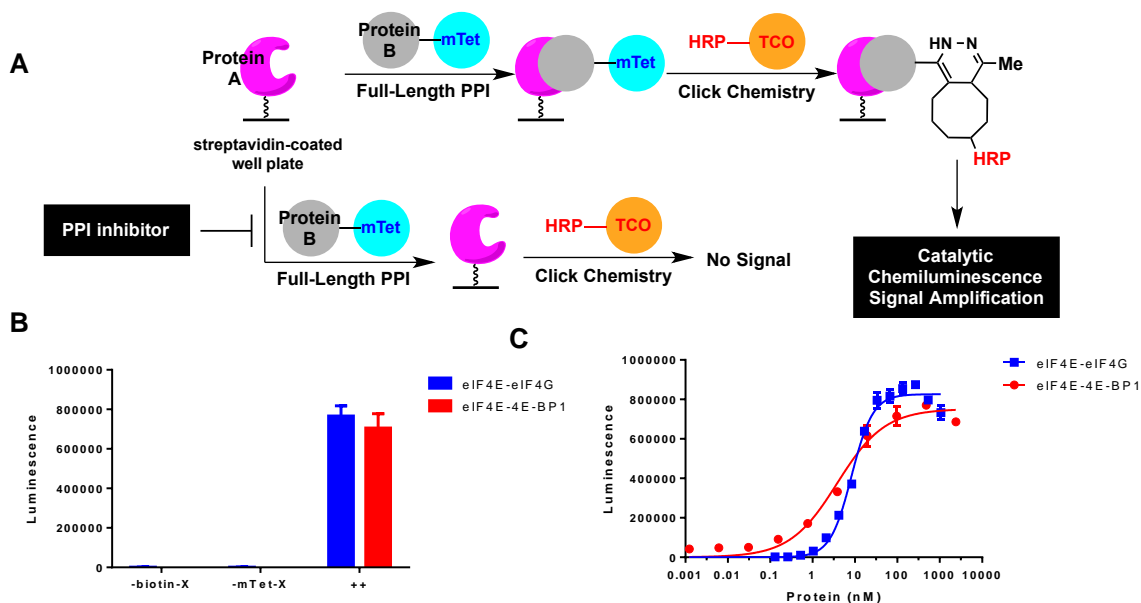


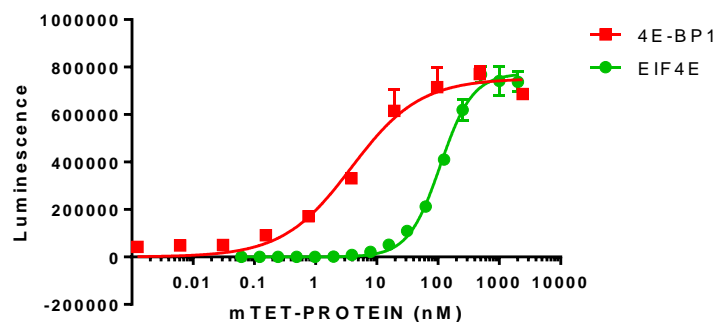
Figure 12 IEDDA PPI cat-ELCCA. A) PPI cat-ELCCA for eIF4E PPIs. mTet = methyltetrazine; TCO = trans-cyclooctene. For the eIF4E-4E-BP1 assay, eIF4E was immobilized and 4E-BP1 mTet labeled. For the eIF4E-eIF4G assay, eIF4G was immobilized and eIF4E mTet labeled. B) Proof-of-concept data. X refers to protein. C) $K_{d,app}$ measurement. All experiments were conducted in triplicates ($n=3$) and shown as the mean \pm SD.

improved the overall sensitivity of the assay and revealed the extent to which CuAAC PPI cat-ELCCA had understated the interaction affinity. As previously mentioned, the screening conditions must account for the native binding affinity of the interaction and ensure that assay is performed ideally under the saturating conditions to improve the chances of getting hits in HTS campaigns. Fortunately, IEDDA PPI cat-ELCCA has the sensitivity to allow screening to be done at mere single digit nanomolar concentrations of the protein complex.

2.3.4 EIF4E IMMOBILIZATION STABILITY

Of note, a complete loss of signal (eIF4E-eIF4G) or drastic increase in the apparent K_d (eIF4E-4E-BP1) was observed when eIF4E was exposed to a freeze/thaw cycle for long-term storage (**Figure 13**). Interestingly, this phenomenon was observed only when eIF4E was free in solution as the mTet-labeled substrate. Because the eIF4E instability is well-documented in the

literature, the immobilization likely enhances its stability during the assay. A similar result



S/B				
HT PROBE	PROTEIN	NEW	STORED	Kd (nM)
mTET	eIF4E	292	26	109 ± 5
biotin	4E-BP1			
mTET	4E-BP1	245	308	3.8 ± 0.7
biotin	eIF4E			

Figure 13. eIF4E in PPI cat-ELCCA. The alternative immobilization strategy, in which 4E-BP1 was immobilized and mTET-eIF4E was incubated, drastically reduced the S/B ratio and the apparent affinity. All experiments were conducted in triplicates (n=3) and shown as the mean ± SD.

was observed with eIF4G, and the assay using mTet-eIF4G in solution failed. As previously noted, increased protein stability through immobilization is not a novel phenomenon; thus, despite the associated washing steps, immobilization-based assay platforms like ELISA, SPR, and now PPI cat-ELCCA may enable a more comprehensive analysis of the full-length proteins that exhibit stability issues.

2.3.5 PPI CAT-ELCCA AND ELISA COMPARISON

To provide a direct comparison of PPI cat-ELCCA to ELISA, binding affinities of the eIF4E-4E-BP1 PPI was measured through ELISA, which yielded a K_d of 19 ± 1 nM (**Figure 14A**). Next, limit of detection (LOD) and limit of quantitation (LOQ) parameters were determined for both assays. PPI cat-ELCCA exhibited a superior limit of detection (0.014 ng for PPI cat-ELCCA and 0.15 ng for ELISA) and a limit of quantitation (0.43 and 0.047 ng,

respectively) than ELISA by approximately 10-fold. The LOD and LOQ differences reasonably explains the observed

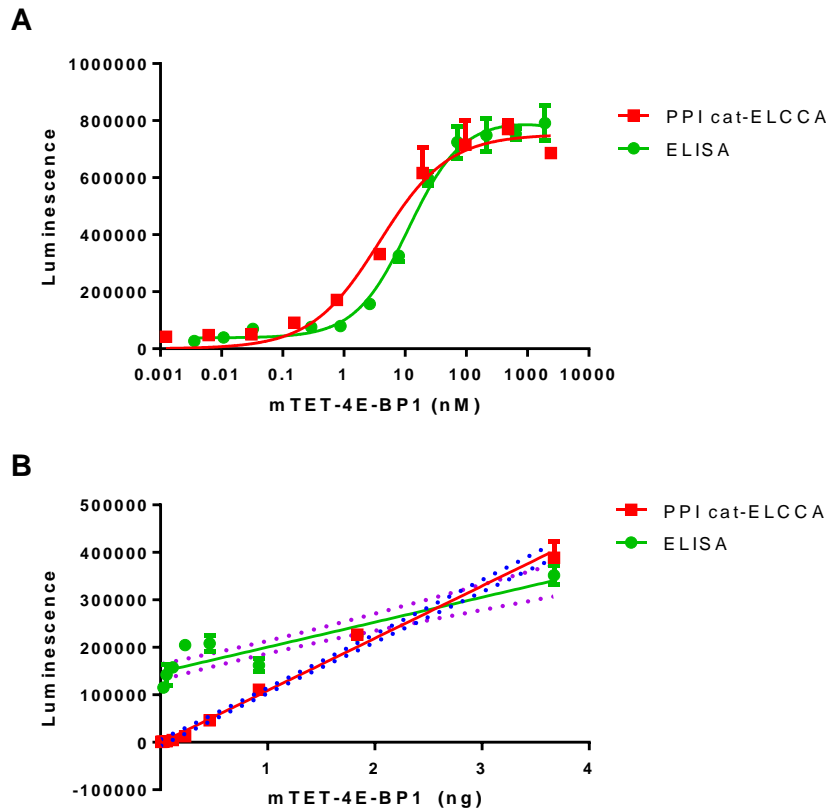


Figure 14. Sensitivity comparison between PPI cat-ELCCA and ELISA. A) ELISA yielded K_d of 19 ± 1 nM, in comparison to that of PPI cat-ELCCA at 3.8 ± 0.7 . B) Linear calibration curve generated from each assay. LOD and LOQ were calculated ($LOD = 3.3\sigma/m$; $LOQ = 10\sigma/m$; where σ and m is the standard deviation and the slope of the response in the linear range. For ELISA, $LOD = 0.15$ ng and $LOQ = 0.47$ ng. For PPI cat-ELCCA, $LOD = 0.014$ ng and $LOQ = 0.043$ ng. All experiments were conducted in triplicates ($n=3$) and shown as the mean \pm SD.

differences in the measured binding affinities, and offers a concrete evidence that PPI cat-ELCCA has greater sensitivity than ELISA. In addition, PPI cat-ELCCA was faster by 2 h due to the elimination of additional incubation step with the enzyme-linked secondary antibody and the related washing steps. A similar ELISA for the eIF4E-eIF4G PPI could not be performed, due to the necessity of using crude eIF4G protein, which was contaminated with endogenous

eIF4E and would yield false results as the primary antibody would detect both endogenous and exogenous eIF4E.

2.3.6 IEDDA PPI CAT-ELCCA VALIDATIONS

Because the goal was to use PPI cat-ELCCA to discover inhibitory chemical probes, the competitive effect of 4E-BP1 proteins and of the previously reported small molecule modulators of the eIF4E-eIF4G PPI were assayed²⁴. WT 4E-BP1 protein was able to readily compete with mTET-4E-BP1 (**Figure 15A**, IC₅₀ value of 11.0 ± 0.1 nM); whereas, null-binding 4E-BP1 mutants exhibited reduced inhibition of the PPI-dependent signal (IC₅₀ values

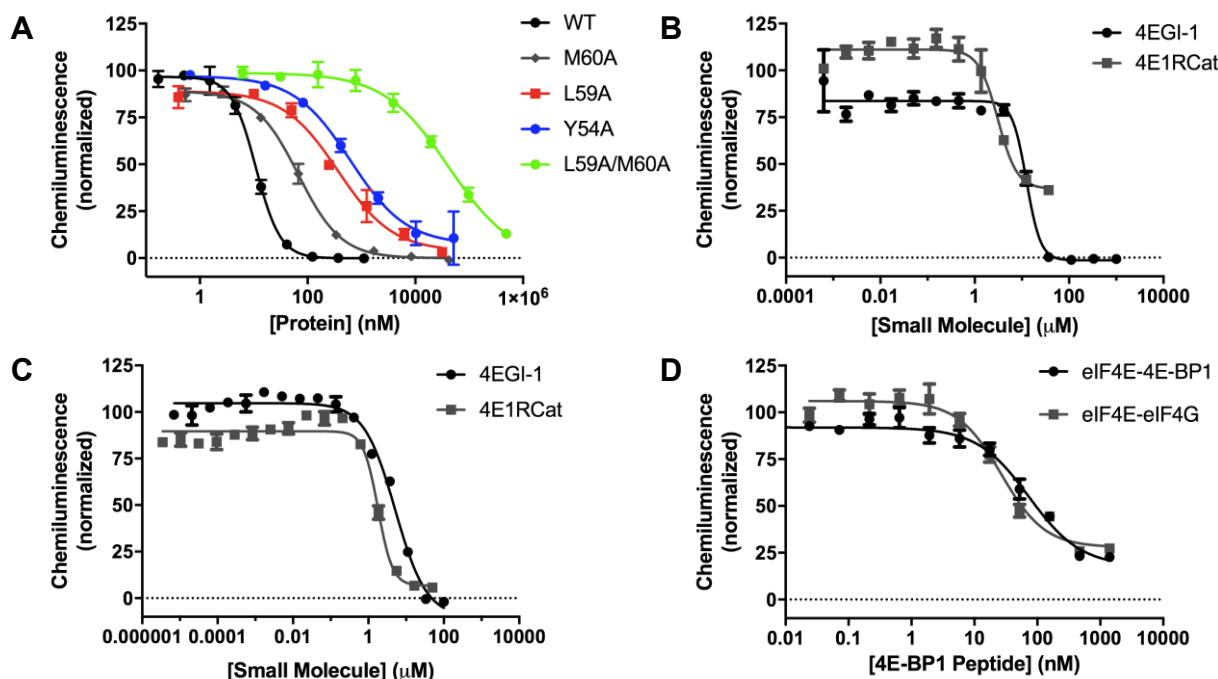


Figure 15. Characterization of PPI cat-ELCCA for chemical probe discovery. (A) Inhibition by 4E-BP1 proteins. (B), (C) Inhibition of eIF4E-eIF4G and eIF4E-4E-BP1, respectively, by 4EGI-1 and 4E1RCat. (D) Inhibition by 4E-BP1 peptide. All experiments were conducted in triplicates (n=3) and shown as the mean ± SD.

of 67, 370, 618 and 41,000 nM for M60A, L59A, Y54A, and L59A/M60A mutants, respectively). For the small molecules, **4EGI-1** and **4E1RCat**, apparent IC₅₀ values of 12 ± 1

and $3.1 \pm 0.4 \mu\text{M}$ for eIF4E–eIF4G and 5.1 ± 0.1 and $1.8 \pm 0.6 \mu\text{M}$ for eIF4E–4E–BP1 were measured, respectively (**Figures 15B, 15C**). Importantly, this is the first study demonstrating that these molecules can directly disrupt eIF4E–4E–BP1 binding.²⁴ For **4EGI–1**, this is in contrast to its initial report, which indicated that it stabilized 4E–BP1 binding to eIF4E in cells. However, this is likely due to its complex cellular activity, and inhibition of 4E–BP1 binding by this molecule has never been analyzed in a biochemical or biophysical assay. **4EGI–1** was recently found to bind allosterically to eIF4E at its lateral surface, which is distinct from that of eIF4G and 4E–BP1, which competitively bind at the dorsal surface. Since both eIF4G²⁴ and 4E–BP1 contain second, yet weaker, binding sites at this lateral surface of eIF4E, it is not surprising that **4EGI–1** would disrupt the binding of both. It is important to note, however, that both **4EGI–1** and **4E1RCat** exhibit potentially non-specific inhibitory mechanisms for the PPIs, as indicated by their steep Hill slopes (< -2). On the other hand, a 4E–BP1 peptide (Gly49–Asn64) exhibited specific inhibition of both PPIs with apparent IC_{50} values of $27 \pm 4 \text{ nM}$ and $74 \pm 5 \text{ nM}$ for the eIF4E–eIF4G and eIF4E–4E–BP1 PPIs, respectively (**Figure 15D**), and Hill slopes of -1 . At the higher dosage of linear 4E–BP1 peptides, a steep increase in the luminescence was observed (10 – 100-fold greater intensity than the negative controls) which was likely contributed by the linear 4E–BP1 peptides' poor solubility, a high tendency to precipitate from solution (from minor, erratic perturbations like sudden change in temperature, pH, solvent composition, and mixing), and aggregation. Subsequent testing of known aggregators in PPI cat–ELCCA exhibited similar trends, and suggested the problem was in peptide aggregations.

2.4 CONCLUSION

PPI cat-ELCCA is a new assay technology that readily facilitates the analysis of the full-length PPIs. Despite its similarity to ELISA, it boasts about 10-fold greater LOD and LOQ due to the elimination of the primary and the secondary antibodies, and the respective washing steps. PPI cat-ELCCA was readily adapted to two PPIs of interest, eIF4E-4E-BP1 and eIF4E-eIF4G1; as PPIs are of great interest in both basic science and drug discovery, this assay system will provide a key methodology in advancing various PPI-targeted investigations and chemical probe discovery. The robustness and notable resistance to assay interfering chemicals make PPI cat-ELCCA an ideal assay system to screen complex, yet chemically diverse libraries such as the natural product extract (NPE) library. Furthermore, the high sensitivity of the assay allows HTS screening to be completed at protein complex concentration as low as 4 nM, increasing the likelihood of finding a disruptor of this high affinity interaction and reducing the chances of protein aggregation and precipitation. In summary, PPI cat-ELCCA is highly robust and sensitive, and readily accommodates potentially unstable proteins and complexes for HTS campaigns.

2.5 EXPERIMENTAL

2.5.1 GENERAL INFORMATION

2.5.1.1 GENERAL CHEMISTRY METHODS

Reactions were carried out under a nitrogen atmosphere with dry, freshly distilled solvents under anhydrous conditions, unless otherwise noted. Reaction were monitored by thin-layer chromatography (TLC) carried out on 0.25-mm SiliCycle silica gel plates (60F-254) using UV-light (254 nm) or ninhydrin staining.

RP-HPLC was performed using binary gradients of solvents A and B, where A is 0.1% HCO₂H in water and B is 0.1% HCO₂H in acetonitrile (analytical RP-HPLC) or 0.1% HCO₂H in methanol (preparative RP-HPLC). Analytical RP-HPLC was performed using an Agilent 1260 Infinity HPLC equipped with a ZORBAX Eclipse SB-C18 column (4.6 × 150 mm; 5 μm) at a flow rate of 1 mL/min, with detection at 214 and 254 nm. Preparative RP-HPLC was performed using an Agilent 1260 Infinity HPLC equipped with a PrepHT SB-C18 column (21.2 × 150 mm; 5 μm) at a flow rate of 18mL/min, with detection at 214 and 254 nm. In all cases, fractions were analyzed off-line using an Agilent Q-TOF HPLC-MS.

NMR spectra were recorded on Varian 500MHz instrument. The following abbreviations are used to indicate the multiplicities: s, singlet; d, doublet; t, triplet; q, quartet; m, multiplet; br, broad.

Fmoc-protected amino acids and Rink amide MBHA resin were purchased from P3 Biosystems and used as received. TCO-PEG4-NHS was purchased from Click Chemistry Tools and used as received.

2.5.1.2 GENERAL ASSAY AND BIOLOGY METHODS

Chemiluminescence data was collected on a BioTek Cytation3. Gels were imaged on a ProteinSimple Fluorchem M Gel Imager. BL21DE3 *E. coli* were used for protein expression. HEK293T cells were cultured in DMEM (Corning) supplemented with 2 mM L-glutamine, 1% Penicillin/streptomycin (Gibco) and 10% FBS (Atlanta Biologicals). Cells were incubated at 37 °C in a humidified atmosphere containing 5% CO₂. Horseradish peroxidase (HRP), streptavidin-coated 384-well plates (white, high binding capacity; cat #15505), and SuperSignal West Pico Chemiluminescent substrate kit were purchased from Pierce. eIF4GI-HaloTag® human ORF in

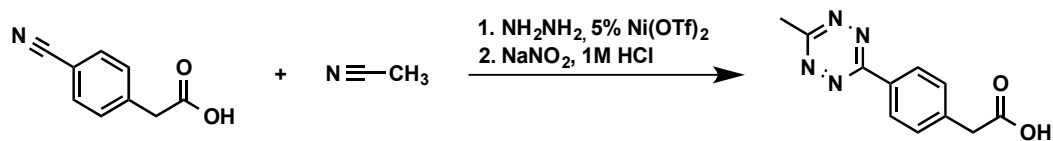
pFN21A was purchased from Promega. eIF4EBP1–HaloTag® human ORF in pFN21A was purchased from Promega. pFN29K His6HaloTag® T7 Flexi® vector and the Flexi® System cloning kit were purchased from Promega. pHA–eIF4E (Plasmid #17343) was purchased from Addgene. All data was analyzed using GraphPad Prism version 6.0c for Mac OS X (GraphPad Software, www.graphpad.com).

2.5.1.3 GENERAL PEPTIDE SYNTHESIS

4E–BP1 peptide (Gly49–Asn64) was synthesized on a 0.2–mmol scale in a 20–mL fritted syringe using MBHA Rink amide resin (0.4 mmol/g resin, average). In brief, the resin was initially washed with DMF (3 × 10 mL) and CH₂Cl₂ (3 × 10 mL) and allowed to swell for 30 min at 25 °C in 1:1 DMF/CH₂Cl₂. Fmoc groups were removed following addition of a 20% piperidine/DMF solution (10 mL) and gentle agitation for 20 min at 25°C. After each Fmoc deprotection and amino acid couplings, the resin was thoroughly washed with NMP (3 × 10 mL), CH₂Cl₂ (3 × 10 mL), and DMF (3 × 10 mL). Amino acid couplings were performed by addition of amino acid (0.8 mmol) pre–activated with HBTU (0.72 mmol), *N,N*–diisopropylethylamine (1.28 mmol) in NMP (4 mL), and agitation for 2 h at 25 °C. Upon completion of the sequence, the *N*–terminus was acetylated, and the peptide was cleaved from the resin using TFA/thioanisole/triisopropylsilane/water (90:0.4:0.4:0.2) for 5 h at 25 °C. The resulting solution was added to glacial ether (~200 mL) for peptide precipitation. The precipitates were then centrifuged, dissolved in ACN–water mixture, and purified via RP–HPLC. Fractions containing the desired peptide were confirmed via Q–TOF HPLC–MS, lyophilized, acetic acid exchanged, lyophilized again, and then dissolved in 33% DMF/H₂O. Peptide stock concentrations were quantified via amino acid analysis.

2.5.2 SYNTHETIC METHODS

Synthesis of 2-(4-(6-methyl-1,2,4,5-tetrazin-3-yl)phenyl)acetic acid



The synthesis was adapted from that reported¹⁻². In a 5-mL pressure-resistant vial, 2-(4-cyanophenyl)acetic acid (80.6 mg, 0.5 mmol) was dissolved in acetonitrile (260 μL , 5 mmol). Fresh $\text{Ni}(\text{OTf})_2$ (90.9 mg, 0.5 mmol) and anhydrous hydrazine (800 μL , 25 mmol) were subsequently added. The vial was then flushed with nitrogen and sealed, and the reaction was heated to 60 $^\circ\text{C}$. After 24 h, the reaction was cooled to 25 $^\circ\text{C}$ and transferred to a 1-L beaker. In a separate beaker, NaNO_2 (690 mg, 10 mmol) was dissolved in H_2O (10 mL). The resulting NaNO_2 solution was then slowly added to reaction, followed by slow addition of 1M HCl , during which the solution turned bright red/pink in color and gas evolved from reaction. Addition of 1M HCl was continued until the gas stopped evolving from the solution and the pH remained at 3. (**Caution!** This step generates a large amount of toxic nitrogen oxide gas and should be performed in a well-ventilated fume hood.) The reaction mixture was extracted with CH_2Cl_2 , washed brine, and dried with Na_2SO_4 . The solvent was removed *in vacuo*, and the resulting residue was purified by chromatography (10% $\text{MeOH}/\text{CH}_2\text{Cl}_2$) on silica gel to afford **1** in 48% yield. ^1H NMR (500 MHz, CDCl_3 , 293K): δ 8.51 (d, $J = 8.0$ Hz, 2H), 7.47 (d, $J = 8.0$ Hz, 2H), 3.73 (s, 2H), 3.05 (s, 3H).

Synthesis of R-NHS. To a 10-mL round-bottom flask was added, **R₁₋₃-carboxylic acid** (0.15 mmols), *N,N'*-disuccinimidyl carbonate (0.16 mmols), *N,N*-diisopropylethylamine (0.3 mmols), and CH₂Cl₂ (5 mL). The resulting mixture was then stirred for 4 h at 25 °C. The reaction was quenched with water, and organic layer was washed with brine and dried with Na₂SO₄. The solvent was removed *in vacuo*, and the resulting **R₁₋₃-NHS** was used without further purification.

Synthesis of R-Boc. To a 10-mL round-bottom flask was added, **R₁₋₃-NHS** (0.11 mmols), *N,N*-diisopropylethylamine (0.43 mmols), *O*-(2-Aminoethyl)-*O'*-[2-(Boc-amino)ethyl]hexaethylene glycol (0.11 mmols) and CH₂Cl₂ (4 mL). The resulting mixture was then stirred overnight at 25 °C. The solvent was removed *in vacuo*, and the resulting residue was dissolved in DMSO and water and purified via RP-HPLC. **R₁-Boc**: HRMS (ESI+) calcd for 694.3823, found 595.2 [M+H-Boc]. **R₂-Boc**: HRMS (ESI+) calcd for 680.3745, found 681.3819 [M+H]. **R₃-Boc**: HRMS (ESI+) calcd for 548.3309, found 449.1 [M+H-Boc].

Synthesis of R-NH₂. To a 10-mL round-bottom flask was added, **R₁₋₃-Boc** (0.05mmols) and TFA (10 mL). The resulting mixture was stirred for 2 h at at 25 °C. TFA was then removed *in vacuo* overnight . The resulting **R₁₋₂-NH₂** was used without further purification.

Synthesis of R-HT. To a scintillation vial was added, **R₁₋₃-NH₂** (0.05 mmols), 6-chlorohexanoic acid (0.2 mmols), EDC (0.2 mmols), *N,N*-diisopropylethylamine (0.4 mmols), and CH₂Cl₂ (5 mL). The solvent was removed *in vacuo*, and the resulting residue was dissolved in DMSO and water and purified via RP-HPLC.

Biotin-PEG₇-HT ligand. HRMS (ESI+) calcd for 726.3640, found 727.3721 [M+H]. ¹H NMR (400 MHz, DMSO-*d*₆, 293K): δ 4.30 (dd, *J* = 7.7, 5.0 Hz, 1H), 4.16 – 4.07 (m, 1H), 3.61 (t, *J* = 6.6 Hz, 2H), 3.50 (s, 25H), 3.38 (t, *J* = 5.9 Hz, 4H), 3.18 (q, *J* = 5.8 Hz, 4H), 3.09 (dt, *J* = 10.3, 5.5 Hz, 1H), 2.81 (dd, *J* = 12.4, 5.1 Hz, 1H), 2.57 (d, *J* = 12.8 Hz, 1H), 2.06 (td, *J* = 7.3, 2.1 Hz, 4H), 1.76 – 1.18 (m, 12H).

***mTet*-PEG₇-HT ligand.** HRMS (ESI+) calcd for 712.3563, found 713.3648 [M+H]. ¹H NMR (500 MHz, DMSO-*d*₆, 293K): δ 8.39 (d, *J* = 8.2 Hz, 2H), 8.24 (t, *J* = 5.7 Hz, 1H), 7.83 (t, *J* = 5.7 Hz, 1H), 7.54 (d, *J* = 8.2 Hz, 2H), 3.61 (t, *J* = 6.4 Hz, 2H), 3.57 (s, 1H), 3.53 – 3.47 (m, 24H), 3.43 (t, *J* = 5.7 Hz, 2H), 3.38 (t, *J* = 5.9 Hz, 3H), 3.24 (q, *J* = 5.7 Hz, 2H), 3.18 (q, *J* = 5.9 Hz, 2H), 2.99 (s, 3H), 2.06 (t, *J* = 7.3 Hz, 2H), 1.69 (h, *J* = 6.6 Hz, 3H), 1.49 (p, *J* = 7.7 Hz, 3H), 1.41 – 1.29 (m, 3H).

Alkyne-PEG₇-HT ligand. HRMS (ESI+) calcd for 580.3127, found 581.3277 [M+H]. ¹H NMR (500 MHz, DMSO-*d*₆, 293K): δ 2.40 – 2.34 (m, 24H), 2.30 (t, *J* = 6.4 Hz, 2H), 2.28 (dd, *J* = 5.5, 2.8 Hz, 4H), 2.10 (q, *J* = 5.6 Hz, 4H), 1.20 (ddd, *J* = 9.1, 5.5, 2.3 Hz, 2H), 1.14 (dd, *J* = 7.8, 5.6 Hz, 2H), 1.02 (t, *J* = 2.6 Hz, 1H), 0.96 (t, *J* = 7.4 Hz, 2H), 0.52 (p, *J* = 6.8 Hz, 2H), 0.38 (p, *J* = 7.5 Hz, 2H), 0.21 (p, *J* = 7.6, 7.0 Hz, 2H).

Native 4E-BP1 – CH₃CO-GTRIIYDRKFLMECRN-NH₂

HRMS (ESI+) calcd for 2055.0506, found 2056.0606 [M+H].

Alkynyl 4E-BP1 – >RIIYDRKFLMECRN-NH₂, & = 5-pentynoic acid

HRMS (ESI+) calcd for 2080.10, found 2081.11 [M+H]

2.5.3 PROTEIN EXPRESSION AND PURIFICATION

HaloTag-eIF4E. Human eIF4E cDNA was cloned from pHA-eIF4E with engineered Sgf1 and PmeI restriction enzyme sites. The resulting product was ligated into a pFN29K vector via built-in Sgf1 and PmeI restriction sites. Overnight culture of *E. coli* carrying pFN29K eIF4E was diluted (1:400) into LB media, and incubated at 37 °C until an OD₆₀₀ of 0.6 was achieved. The resulting culture was induced with 0.5 mM IPTG overnight at 20 °C. Cells were pelleted, re-suspended in lysis buffer (50 mM phosphate buffer, 100 mM NaCl, 0.5 mM PMSF, 0.5 mM EDTA, 5 mM DTT, 5 mM β-mercaptoethanol, 0.5% Tween-20), and lysed via ultrasonication. The resulting lysate was centrifuged at 25,000 RPM for 1 h at 4 °C. The supernatant was collected, incubated with m⁷GDP agarose resin and gently agitated on a rocker at 4 °C for 1 h. The resin was washed twice with wash buffer (50 mM phosphate buffer, 100 mM NaCl, 5 mM DTT), and eluted with 10 mM m⁷G in wash buffer. The protein was dialyzed overnight in wash buffer containing 2 mM DTT, concentrated in a 50-mL conical concentrator, and quantified via the Bradford assay.

HaloTag-4E-BP1. eIF4EBP1-HaloTag® human ORF in pFN21A was transferred into the pFN29K His6HaloTag® T7 Flexi® vector using the Flexi® System. Overnight culture of *E. coli* carrying pFN29K 4E-BP1 was diluted (1:400) into LB media, and incubated at 37 °C until an OD₆₀₀ of 0.6 was achieved, and induced with 0.5 mM IPTG for 3 h. Cells were pelleted, re-

suspended in lysis buffer (50 mM phosphate buffer, 100 mM NaCl, 0.5 mM PMSF, 5 mM DTT, 1% Triton-100), and lysed via ultrasonication. The resulting lysate was centrifuged at 25,000 RPM for 1 h at 4 °C. The supernatant was collected and incubated with Ni-NTA resin for 30 min @ 4°C. The resin was then washed with wash buffer (50 mM phosphate buffer, 100 mM NaCl, 2 mM DTT), and eluted with increasing concentrations of imidazole (10–500mM). The protein was dialyzed overnight at 4°C in wash buffer and further purified by FPLC on a S200 column. Protein quantification was determined via the Bradford Assay.

HaloTag-eIF4G. eIF4GI-HaloTag® human ORF in pFN21A was purchased from Promega. eIF4GI isoform 1 cDNA was purchased from Promega. A C-terminal 5×His tag was subsequently added by ligating annealed oligos encoding for the 5×His tag into the PmeI restriction site. HEK293T cells at 60% confluence in a 15-cm plate were transfected with 15 ug of purified DNA using linear PEI 25,000MW (Polysciences, Inc.); media was changed 18 h after transfection. 24 h later, media was aspirated, cells were washed once with 25 mL ice-cold 1X PBS, and then harvested by scraping into 3 mL of 1X TBS pH 7.5 containing 7 µg/mL pepstatin, 5 µg/mL leupeptin, and 10 µg/mL aprotinin. Cells were lysed by passing through a sterile, 28.5-gauge syringe (5×) on ice, and lysates were cleared by centrifugation at 18,000×g for 10 min at 4 °C. Cleared lysates were incubated end-over-end with pre-washed Ni-NTA resin for 2 h at 4 °C, then washed 3× with lysis buffer for 30 min each. ‘Semi-purified’ His-HaloTag-eIF4G was eluted with 500 mM imidazole in 1X TBS pH 7.5, before dialyzing overnight at 4 °C. Protein quantification was determined via the Bradford Assay.

Mutagenesis. The following oligonucleotides were used to create point mutations in the HaloTag-4E-BP1 coding sequence using site-directed mutagenesis. cDNA sequences were confirmed by Sanger sequencing.

Y54A, Forward: 5'-GGGAGGTACCAGGATCATCGCTGACCGGAAATTCCTG-3';

Reverse: 5'-CAGGAATTTCCGGTCAGCGATGATCCTGGTACCTCCC-3'

L59A, Forward: 5'-CTATGACCGGAAATTCGCGATGGAGTGTCGGAACTCAC-3';

Reverse: 5'-GTGAGTTCCGACACTCCATCGCGAATTTCCGGTCATAG-3'

M60A, Forward: 5'-CTATGACCGGAAATTCCTGGCGGAGTGTCGGAACTCAC-3';

Reverse: 5'-GTGAGTTCCGACACTCCGCCAGGAATTTCCGGTCATAG-3'

L59A/M60A, Forward: 5'-

CTATGACCGGAAATTCGCGGCGGAGTGTCGGAACTCAC-3'; Reverse: 5'-

GTGAGTTCCGACACTCCGCCGCGAATTTCCGGTCATAG-3'

2.5.4 BIOCONJUGATION METHODS

Biotinylation of eIF4E, eIF4G and 4E-BP1. HaloTag-eIF4E, -eIF4G, and -4E-BP1 were biotinylated by addition of **Biotin-PEG₇-HT ligand** (20 equiv) in reaction buffer (50 mM phosphate buffer, 100 mM NaCl, pH 7.4, 5 mM DTT, 10% glycerol) and incubation overnight at 4 °C. The resulting mixture was concentrated in wash buffer (50 mM phosphate buffer, 100 mM NaCl, 5 mM DTT), buffer exchanged with wash buffer (6 × 20 mL), and quantified via the Bradford assay. Successful biotinylation was confirmed via Western blot with streptavidin-HRP.

mTet and Alkyne Labeling of 4E-BP1. HaloTag-4E-BP1 was labeled by addition of **mTet-PEG₇-HT ligand** or **Alkyne-PEG₇-HT ligand** (20 equiv) in reaction buffer (50 mM phosphate

buffer, 100 mM NaCl, pH 7.4, 5 mM DTT, 10% glycerol) and incubation overnight at 4 °C. The resulting mixture was concentrated again in wash buffer (50 mM phosphate buffer, 100 mM NaCl, 2 mM DTT), buffer exchanged with wash buffer (6 × 20 mL), and quantified via the Bradford assay. Successful labeling was confirmed via click chemistry with a click handle–labeled rhodamine.

HRP–N₃. HRP–N₃ was prepared following an established procedure and stored at 4°C in phosphate buffer (50 mM, pH 7.4).⁴ Successful introduction of azide was confirmed via reaction with Rhod–alkyne

HRP–TCO.⁵ HRP (10 mg) was dissolved in phosphate buffer (50 mM, pH 7.4; 2 mL). TCO–PEG₄–NHS (20 equiv in DMSO) was subsequently added, and the reaction was gently agitated overnight at 4 °C. The resulting solution was concentrated and buffer exchanged with phosphate buffer. Successful HRP modification was confirmed via reaction with Rhod–mTet (**Figure S2**).

CuAAC condition. TBTA (0.1 μL of 50 mM stock in DMSO, 0.5 mM final), CuSO₄ (0.5 μL of 2 mM stock in H₂O, 0.1 mM final), and HRP–N₃ (0.1 μL of 50 μM stock in phosphate buffer (pH 7.4), 0.5 μM final) were diluted in phosphate buffer (pH 7.4) and agitated gently in a vial. Sodium ascorbate solution (0.5 μL of 100 mM stock in H₂O, 5.0 mM final) was freshly made prior to use and added to initiate the CuAAC reaction. The reaction mixture (10 μL) was then added to assay wells, covered with plate–sealing tape, and agitated at 25 °C for 2 h. For the validations of HRP–N₃, alkyneyl 4E–BP1 peptide, and ALK–4E–BP1, 1 μM of alkyneyl–rhodamine, azido–rhodamine, and azido–rhodamine, respectively, were incubated with the same

TBTA–CuAAC conditions. THPTA ligand driven CuAAC conditions were followed as documented¹.

2.5.5 PPI CAT–ELCCA PROTOCOL (384–WELL FORMAT)

Buffer A: 50 mM Phosphate Buffer (pH 7.4), 100 mM NaCl, 0.01% Tween–20, 2 mM DTT

Buffer B: 50 mM Phosphate Buffer (pH 7.4)

1. Immobilization of biotin–eIF4E (10 μ L of 50 nM in Buffer A)
 - a. POS Ctrl: add Buffer A (10 μ L)
 - b. NEG Ctrl: add biotin–eIF4E (10 μ L)
 - c. Cover the wells with plate–sealing tape
 - d. Overnight incubation (4 °C)
2. Remove well contents
3. Wash the wells with Buffer A (3 \times 50 μ L)
 - a. Incubate for 5 min between each wash
4. PPI incubation
 - a. Ctrls (POS & NEG): Add mTet 4E–BP1 (5 μ L of 8 nM in Buffer A), dilute to 10 μ L with Buffer A
 - b. Inhibitor incubations (Titrations)
 - i. Inhibitors diluted to varying concentrations in Buffer A
 - ii. Add inhibitor samples (5 μ L), and then add mTet–4E–BP1 (5 μ L of 8 nM in Buffer A)
 - c. Cover the wells with plate–sealing tape
 - d. Incubate at 4 °C for 60 min

5. Remove well contents
6. Wash the wells with Buffer A ($3 \times 50 \mu\text{L}$)
 - a. Incubate for 5 min between each wash
7. Click chemistry with TCO–HRP ($10 \mu\text{L}$ of $1 \mu\text{M}$ in Buffer A)
 - a. Cover the wells with plate–sealing tape
 - b. Incubate at $25 \text{ }^\circ\text{C}$ for 1 h
8. Wash the wells with Buffer A ($3 \times 50 \mu\text{L}$)
 - a. Incubate for 5 min between each wash
9. Wash the wells with Buffer B ($3 \times 50 \mu\text{L}$)
 - a. Incubate for 5 min between each wash
10. For chemiluminescence detection:
 - a. Add $30 \mu\text{L}$ SuperSignal West Pico Chemiluminescent Substrate (prepared following kit instructions)

2.5.6 PEPPI CAT–ELCCA PROTOCOL

Buffer A: 50 mM Phosphate Buffer (pH 7.4), 100 mM NaCl, 0.01% Tween–20, 2 mM DTT, 0.08mg/mL bovine serum albumin

Buffer B: 50 mM Phosphate Buffer (pH 7.4)

1. Immobilization of biotin–eIF4E ($10 \mu\text{L}$ of 50 nM in Buffer A)
 - a. POS Ctrl: add Buffer A ($10 \mu\text{L}$)
 - b. NEG Ctrl: add biotin–eIF4E ($10 \mu\text{L}$)
 - c. Cover the wells with plate–sealing tape

- d. Overnight incubation (4 °C)
2. Remove well contents
3. Wash the wells with Buffer A (3 × 50 µL)
 - a. Incubate for 5 min between each wash
4. Peptide–protein incubation
 - a. Ctrls (POS & NEG): Add alkynyl 4E–BP1 (10 µL of 250 nM in Buffer A)
 - b. Inhibitor incubations (Titrations)
 - i. Dilute the inhibitors to desired concentrations in Buffer A
 - ii. Add inhibitor samples (5 µL), and then add alkynyl 4E–BP1 (5 µL of 500 nM in Buffer A)
 - c. Cover the wells with plate–sealing tape
 - d. Incubate at 4 °C for 120 min
5. Remove well contents
6. Wash the wells with Buffer A (3 × 50 µL)
 - a. Incubate for 5 min between each wash
7. Click chemistry with N₃–HRP (10 µL of 0.5 µM in Buffer B, see **BIOCONJUGATION METHODS**)
 - a. Cover the wells with plate–sealing tape
 - b. Incubate at 25 °C for 2 h
8. Wash the wells with Buffer A (3 × 50 µL)
 - a. Incubate for 5 min between each wash
9. Wash the wells with Buffer B (3 × 50 µL)
 - a. Incubate for 5 min between each wash

10. For chemiluminescence detection:

- a. Add 30 μ L SuperSignal West Pico Chemiluminescent Substrate (prepared following kit instructions)

2.6 REFERENCES

1. Lorenz, D. A.; Song, J. M.; Garner, A. L., High-Throughput Platform Assay Technology for the Discovery of pre-microRNA-Selective Small Molecule Probes. *Bioconjugate Chemistry* **2015**, *26* (1), 19-23.
2. Garner, A. L.; Janda, K. D., cat - ELCCA: A Robust Method To Monitor the Fatty Acid Acyltransferase Activity of Ghrelin O - Acyltransferase (GOAT). *Angewandte Chemie International Edition* **2010**, *49* (50), 9630-9634.
3. Song, J. M.; Menon, A.; Mitchell, D. C.; Johnson, O. T.; Garner, A. L., High-Throughput Chemical Probing of Full-Length Protein–Protein Interactions. *ACS Combinatorial Science* **2017**, *19* (12), 763-769.
4. Lorenz, D. A.; Garner, A. L., A click chemistry-based microRNA maturation assay optimized for high-throughput screening. *Chemical Communications* **2016**, *52* (53), 8267-8270.
5. Johnson, M. P., H. , Antibody Quality *MATER METHODS* **2014**, *4* (572).
6. Mateo, C.; Palomo, J. M.; Fernandez-Lorente, G.; Guisan, J. M.; Fernandez-Lafuente, R., Improvement of enzyme activity, stability and selectivity via immobilization techniques. *Enzyme and Microbial Technology* **2007**, *40* (6), 1451-1463.
7. Singh, R.; Tiwari, M.; Singh, R.; Lee, J.-K., From Protein Engineering to Immobilization: Promising Strategies for the Upgrade of Industrial Enzymes. *International Journal of Molecular Sciences* **2013**, *14* (1), 1232.
8. Lorenz, D. A.; Kaur, T.; Kerk, S. A.; Gallagher, E. E.; Sandoval, J.; Garner, A. L., Expansion of cat-ELCCA for the Discovery of Small Molecule Inhibitors of the Pre-let-7–Lin28 RNA–Protein Interaction. *ACS Medicinal Chemistry Letters* **2018**.
9. Braun, P.; LaBaer, J., High throughput protein production for functional proteomics. *Trends in Biotechnology* *21* (9), 383-388.
10. Structural Genomics, C.; Architecture et Fonction des Macromolécules, B.; Berkeley Structural Genomics, C.; China Structural Genomics, C.; Integrated Center for, S.; Function, I.; Israel Structural Proteomics, C.; Joint Center for Structural, G.; Midwest Center for Structural, G.; New York Structural Genomi, X. R. C. f. S. G.; Northeast Structural Genomics, C.; Oxford

Protein Production, F.; Protein Sample Production Facility, M. D. C. f. M. M.; Initiative, R. S. G. P.; Complexes, S., Protein production and purification. *Nature Methods* **2008**, *5*, 135.

11. Goddard-Borger, E. D.; Stick, R. V., An Efficient, Inexpensive, and Shelf-Stable Diazotransfer Reagent: Imidazole-1-sulfonyl Azide Hydrochloride. *Organic Letters* **2007**, *9* (19), 3797-3800.
12. Ni, Z.; Zhou, L.; Li, X.; Zhang, J.; Dong, S., Tetrazine-Containing Amino Acid for Peptide Modification and Live Cell Labeling. *PLOS ONE* **2015**, *10* (11), e0141918.
13. Zeglis Brian, M.; Emmetiere, F.; Pillarsetty, N.; Weissleder, R.; Lewis Jason, S.; Reiner, T., Building Blocks for the Construction of Bioorthogonally Reactive Peptides via Solid - Phase Peptide Synthesis. *ChemistryOpen* **2014**, *3* (2), 48-53.
14. Selvaraj, R.; Fox, J. M., trans-Cyclooctene — a stable, voracious dienophile for bioorthogonal labeling. *Current opinion in chemical biology* **2013**, *17* (5), 753-760.
15. Abiko, F.; Tomoo, K.; Mizuno, A.; Morino, S.; Imataka, H.; Ishida, T., Binding preference of eIF4E for 4E-binding protein isoform and function of eIF4E N-terminal flexible region for interaction, studied by SPR analysis. *Biochemical and Biophysical Research Communications* **2007**, *355* (3), 667-672.
16. Lama, D.; Quah, S. T.; Verma, C. S.; Lakshminarayanan, R.; Beuerman, R. W.; Lane, D. P.; Brown, C. J., Rational optimization of conformational effects induced by hydrocarbon staples in peptides and their binding interfaces. *Sci. Rep.* **2013**, *3*, 3451.
17. Lama, D.; Quah, S. T.; Verma, C. S.; Lakshminarayanan, R.; Beuerman, R. W.; Lane, D. P.; Brown, C. J., Rational Optimization of Conformational Effects Induced By Hydrocarbon Staples in Peptides and their Binding Interfaces. **2013**, *3*, 3451.
18. Marcotrigiano, J.; Gingras, A.-C.; Sonenberg, N.; Burley, S. K., Cap-dependent translation initiation in eukaryotes is regulated by a molecular mimic of eIF4G. *Molecular cell* **1999**, *3* (6), 707-716.
19. Gross, J. D., Ribosome loading onto the mRNA cap is driven by conformational coupling between eIF4G and eIF4E. *Cell* **2003**, *115*, 739-750.
20. Lukhele, S.; Bah, A.; Lin, H.; Sonenberg, N.; Forman-Kay, Julie D., Interaction of the Eukaryotic Initiation Factor 4E with 4E-BP2 at a Dynamic Bipartite Interface. *Structure* **2013**, *21* (12), 2186-2196.
21. Volpon, L.; Osborne, M. J.; Topisirovic, I.; Siddiqui, N.; Borden, K. L., Cap - free structure of eIF4E suggests a basis for conformational regulation by its ligands. *The EMBO Journal* **2006**, *25* (21), 5138-5149.
22. Moerke, N. J.; Aktas, H.; Chen, H.; Cantel, S.; Reibarkh, M. Y.; Fahmy, A.; Gross, J. D.; Degtarev, A.; Yuan, J.; Chorev, M., Small-molecule inhibition of the interaction between the translation initiation factors eIF4E and eIF4G. *Cell* **2007**, *128* (2), 257-267.

23. Cencic, R.; Hall, D. R.; Robert, F.; Du, Y.; Min, J.; Li, L.; Qui, M.; Lewis, I.; Kurtkaya, S.; Dingle, R.; Fu, H.; Kozakov, D.; Vajda, S.; Pelletier, J., Reversing chemoresistance by small molecule inhibition of the translation initiation complex eIF4F. *Proceedings of the National Academy of Sciences of the United States of America* **2011**, *108* (3), 1046-1051.
24. Yang, J.; Karver, M. R.; Li, W.; Sahu, S.; Devaraj, N. K., Metal - Catalyzed One - Pot Synthesis of Tetrazines Directly from Aliphatic Nitriles and Hydrazine. *Angewandte Chemie International Edition* **2012**, *51* (21), 5222-5225.
25. Ederly, I.; Altmann, M.; Sonenberg, N., High-level synthesis in Escherichia coli of functional cap-binding eukaryotic initiation factor eIF-4E and affinity purification using a simplified cap-analog resin. *Gene* **1988**, *74* (2), 517-525.

CHAPTER 3 HIGH-THROUGHPUT SCREENING CAMPAIGN TARGETING THE CAP-DEPENDENT TRANSLATION INITIATION

3.1 4EGI-1 DISCOVERY & VALIDATION

4EGI-1 (**Figure 16A**) was the product of a HTS campaign by Moerke et al³ using a fluorescence polarization or anisotropy (FP) assay. FP is a very common mix-and-read HTS

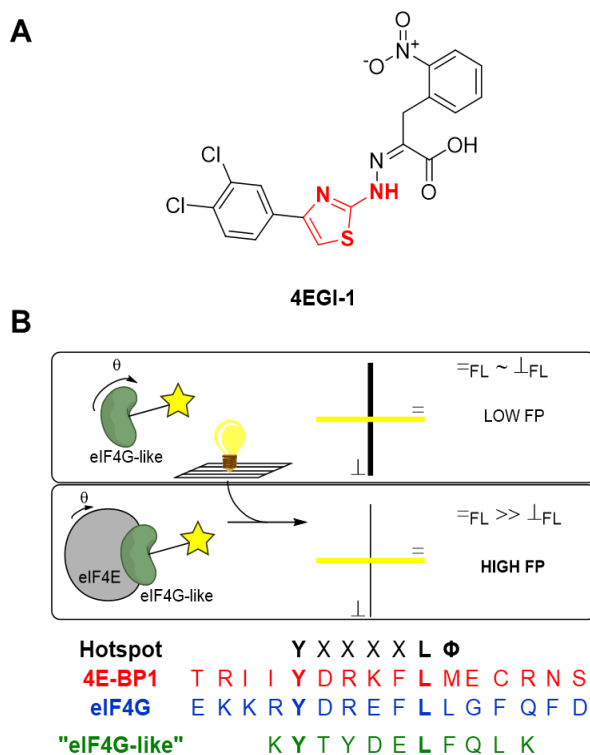


Figure 16. 4EGI-1. A) 4EGI-1 structure, 2-aminothiazole is highlighted in red; B) schematic of the HTS FP assay used by Moerke et al. and peptide probe sequence

technique. As of January 2018, there were approximately 2,700 FP assays reported against nearly 1,700 different protein, enzyme, RNA, and receptor targets. The fundamental principle of FP is the inverse relationship between the polarized fluorescence and its molecular rotation. Polarized

light source excites the fluorescence probe, the emission fluorescence is filtered parallel and perpendicular to the excitation plane, and measured (**Figure 16B**, modified⁴). In FP assays designed for PPI HTS campaigns, this fluorescence probe is generally a fluorophore–labeled peptide composed of the hotspot binding sequence. In absence of a binding event, these fluorophore peptides have high molecular rotation (θ), and therefore, will yield depolarized emission signal (parallel ~ perpendicular polarized fluorescence); in binding to a protein and undergoing a significant gain in the molecular weight, the fluorophore–peptide/protein complex have much lower molecular rotation and will yield increased polarized emission (parallel \gg perpendicular fluorescence).

In the specific design of the FP assay that led to the discovery of 4EGI–1, Moerke et al. did not use the native peptide sequence extracted from neither mammalian eIF4G nor 4E–BP1, but designed a sequence modified from yeast CAF20³, KYTYDELFLQLK, with modest binding affinity of 150nM. The authors did not elaborate further on their sequence choice, but peptide aggregation may have forced the investigators to make subtle amino acid mutations⁵. For weaker PPIs, FP assays may require proteins and/or peptides above soluble and aggregate–free concentrations to observe a robust S/B and suitable Z' factors. For the stronger PPIs, the FP assay may require proteins and/or peptides at a concentration far past the binding affinity, and significantly decrease the likelihood of discovering a hit compound strong enough to disrupt the PPI in the HTS campaign. For instance, the reported affinities of mammalian native 4E–BP1, eIF4GI, and eIF4GII canonical binding motif are very strong, below 50 nM by isothermal calorimetry⁶; an optimal HTS FP assay designed against these interactions would require much less than 50 nM of fluorescently–labeled peptides, or suffer from a drastically reduced chances of discovering a hit compound through screening. 4EGI–1 HTS campaign used a peptide that

yielded binding affinity of 3 μM and had greatly increased their chances of obtaining a hit compound. FP assays are also susceptible to the HTS compound interference through fluorescence quenching and autofluorescence⁷. The extent of chemical interference can be mitigated by designing, optimizing, and running two sequential (or simultaneous) FP assays with two different fluorophores; a hit compound confirmed by the two FP assays is likely to be a true positive. Despite the listed limitations, FP assays remain a powerful and heavily utilized technique in most HTS campaigns due to their low cost and simplicity.

4EGI-1 binding to eIF4E was characterized and confirmed through nuclear magnetic resonance (NMR) experiments. NMR is rarely used in large HTS campaigns due to its low throughput, the extensive amounts of reagents required, and the often-required nuclei labeling of proteins. In fact, NMR confirmation of 4EGI-1 binding required greater than 200 μM of highly soluble and well-behaved mammalian eIF4E; however, mammalian eIF4E is notoriously insoluble and susceptible to aggregation and precipitation, and had to be tagged with a solubility enhancement tag, GB1⁸, for the NMR characterization. Despite the limitations, NMR boasts very high sensitivity, reveals extensive molecular details about the PPI, and is extremely useful for evaluating the potential “ligandability⁹” of the PPI. HTS NMR is a popular technique for fragment-based drug discovery to build the potential agonist/antagonist, and has shown success in building MCL-1 inhibitors^{1, 10-11} and Smac/DIABLO PPI inhibitors. HTS NMR is a powerful alternative to the cases in which the traditional HTS campaigns have failed or as a secondary confirmation assay. GB1-eIF4E titrations to 4EGI-1 showed 25 $\mu\text{M} \pm 11\mu\text{M}$ binding affinity, suggesting that it acted as a 4E-BP mimetic compound, and further *in cellulo* eIF4E pull-down experiments showed a successful dose-dependent inhibition of eIF4G-eIF4E interaction and stimulation of the eIF4E-4E-BP1 interaction.

Despite the initial success of 4EGI-1, rising evidence suggests that the anti-proliferative effects of 4EGI-1 may not solely be due to the inhibition of the eIF4E PPIs. In addition to the inconsistent binding mechanism of action, 4EGI-1 has shown similar IC₅₀ in both *in vitro* assays (25 μM) and cell apoptosis assays (1 – 30 μM) and strengthens the possibility that 4EGI-1 induces non-specific interactions in its mechanism of action. 4EGI-1 treatments also induced phenotypes inconsistent with previous eIF4E knockouts and knockdowns, from inhibiting eIF4E-independent protein translation¹⁴⁻¹⁵ to anti-proliferative activities in multiple myeloma¹⁶⁻¹⁸ and in leukemia. Furthermore, its role as a 4E-BP mimetic was later corrected when 4EGI-1-eIF4E protein complex was crystallized and showed allosteric binding mechanism of action. 4EGI-1 also contain structural motifs that are commonly classified as “pan-assay interference compounds” or PAINS. Specifically, the 2-aminothiazole motif on 4EGI-1 (**Figure 16A**) has documented metabolic reactivity to yield toxic and protein reactive metabolites²⁶. Although a recent study found that the presence of a specific PAINS motif does not accurately dictate the whole molecule as a PAINS²⁷, the current 4EGI-1 studies appear to be insufficient to disprove this possibility and dampens the enthusiasm of 4EGI-1 as a successful chemical probe and potential clinical candidate.

3.2 4E1RCAT DISCOVERY AND VALIDATION

In 2011, Cencic et al.²⁷ reported a HTS campaign that discovered a new eIF4E PPI inhibitor, 4E1RCat (**Figure 17A**) using a time resolved fluorescence resonance energy transfer (TR-FRET) assay (**Figure 17B**). FRET is another popular mix-and-read HTS assay. As of

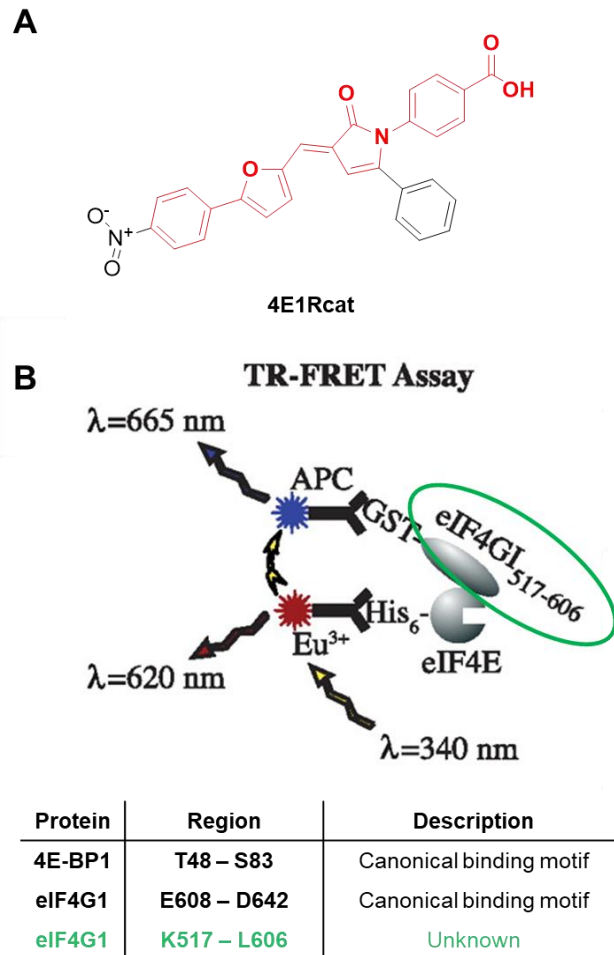


Figure 17. 4E1RCat. A) 4E1RCat structure, promiscuous scaffold highlighted in red; B) schematic of the HTS TR-FRET assay used by Cencic et al1, and the eIF4G1 region used in the screen

January 2018, there were approximately 1,600 FRET assays reported against nearly 1,200 different protein, enzyme, and receptor targets. FRET exploits the transfer of non-radiative energy between a donating fluorophore (donor) to the accepting fluorophore (acceptor) within limited distance (often to less than 10 nm). In HTS FRET, a protein pair is labeled with a donor and an acceptor fluorophore through chemical conjugation or fluorescently-tagged antibodies. Upon interaction, depending on the biophysical orientations of the fluorophore pairs, the excitement of the donor will result in acceptor emission. Its strengths, like FP assays, are its easy implementation, high-throughput, and relative low cost. However, FRET is not without its limitations: 1) multiple combinations of donor/acceptor fluorophore pairs need to be explored for

the protein pair to optimize signal and protein complex stability, 2) the biophysical orientations of the two fluorophores bound to their respective partners on the protein complex must be within 10 nm and may require different protein constructs to move the fluorophore from N-terminus to C-terminus or vice versa. And as with most fluorescence-based assays, FRET is highly susceptible to quenching and autofluorescence by the library compounds and assay buffer/media²⁸. In addition, wide donor emission and acceptor excitation spectra could allow nonspecific background fluorescence and drastically reduce the assay sensitivity and robustness. TR-FRET addresses the interferences by replacing the donor fluorophores with rare earth metals cryptates bound to Europium or Terbium. These improved donor fluorophores have long luminescence half-life (up to 1500 μs ²⁹), allowing a time-delay between the donor excitation and measuring the acceptor emission. The compound/buffer/media interference, and the nonspecific acceptor excitations all have very rapid fluorescence decay and are eliminated by the actual acceptor emission measurement. Furthermore, the rare earth metal cryptates have greater proximity limit, in most cases up to 20 nm, and have greater tolerance for biophysical orientation errors of protein-protein complex.

Cencic et al. chose Eu-W1024-labeled anti-6x-His antibody as the donor fluorophore to recognize His₆-tagged eIF4E and allophycocyanin tagged anti-GST IgG antibody as the acceptor fluorophore to recognize GST-tagged eIF4GI₅₁₇₋₆₀₆ with 50 μs time delay. The assay was designed, optimized, and screened, with reported average Z' factor above 0.6 and S/B above 10. The donor/acceptor pairs for TR-FRET are ever-expanding, and various assay optimizations³⁰ are continuously reported and edited for greater robustness and larger applications.

The eIF4G1 region chosen for this TR-FRET HTS campaign is questionable, as the K517 – L606 motif is not part of the canonical binding motif to eIF4E, and the specific purpose and structure of this region remains unknown (could also be a mistake in the manuscript). Although 4E1RCat claims to be a 4E-BP mimetic compound, the protein-4E1RCat complex remains unsolved; In addition, a large substructure of 4E1RCat has also been shown to inhibit the p300-CBP PPI, E. coli heptosyl transferase WaaC, cholesterol accumulation, the MurG glycosyltransferase, mPGES-1 and PTPMT1³¹⁻³², and could be a very promiscuous ligand. Thus, 4E1RCat, like 4EGI-1, remains an imperfect chemical probe.

3.4 HTS PPI CAT-ELCCA

3.4.1 PPI CAT-ELCCA AND AGGREGATORS

In addition to the previously demonstrated compatibilities of cat-ELCCA with fluorescent molecules and fluorescence quenchers, PPI cat-ELCCA also tolerated up to 10% DMSO for compound dosing. Subsequently, the known aggregators that are littered within screening libraries³² were assayed in PPI cat-ELCCA. These aggregate-forming molecules, quercetin, benzyl benzoate and Congo Red (**Figure 18A**), were tested at 12.5, 25 and 50 μ M; of these, Congo Red was found to inhibit the assay (**Figure 18B**) in a dose-dependent manner. The removal of detergent Tween-20 from the assay buffer eliminated this dose-responsive nature of Congo Red (**Figures 18C, D**). Furthermore, as observed from assaying the linear peptides at high concentrations, Congo Red in absence of Tween-20 exhibited high increase in the chemiluminescence signal. Thus, this spike in the PPI cat-ELCCA signal is associated with aggregators or at compound doses in which the chemical induces protein aggregation and

precipitation. Congo Red is likely a real, yet non-specific inhibitor of the PPI and the assay, as evidenced by its Hill slope < -2 similar to **4EGI-1** and **4E1RCat**.

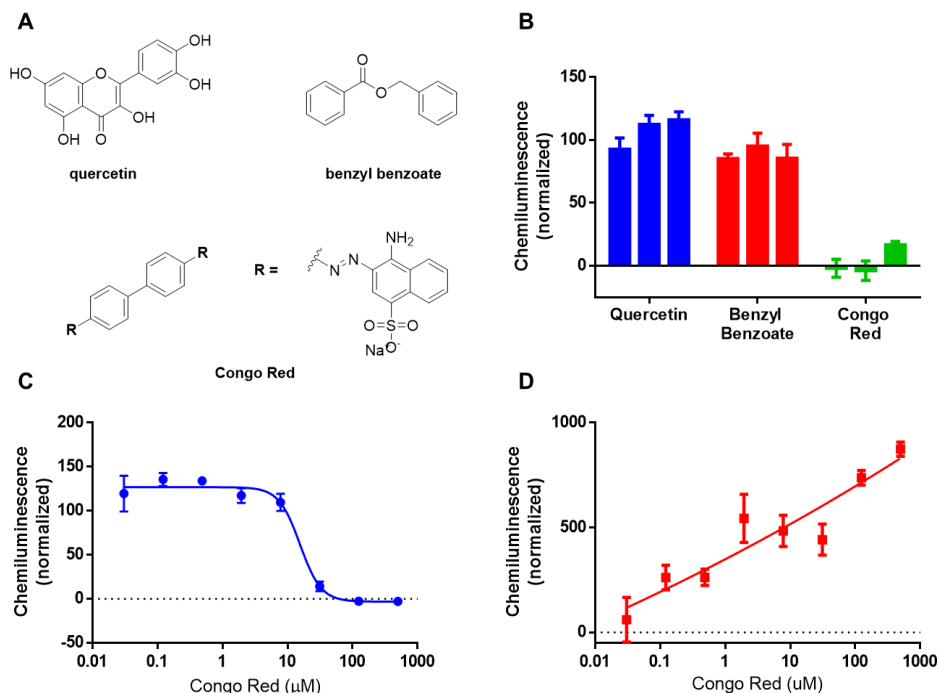


Figure 18. Effect of aggregators on PPI cat-ELCCA. Aggregator characterization of PPI cat-ELCCA. A) Established aggregators, B) Effect of aggregators, C,D) Dose-dependence of Congo Red in the presence and absence of 0.01% Tween-20, respectively. All experiments were conducted in triplicates ($n=3$) and shown as the mean \pm SD.

3.4.2 HTS SCREENING

3.4.2.1 FRAGMENT LIBRARIES

To support the use of PPI cat-ELCCA in high-throughput inhibitor discovery, the assay was miniaturized to screen against the eIF4E-4E-BP1 interaction. Importantly, the assay performed excellently with a measured Z' factor of 0.66, S/B ratio of 23 and signal-to-noise (S/N) ratio of $>10,000$ (**Figure 19A**). Both aspiration-based (Biotek ELX 405) and centrifugation-based (BlueCatBio BlueWashers) plate washers were evaluated during the assay miniaturization; despite the greater washing capacity of the centrifugation-based plate washer – as evidenced by

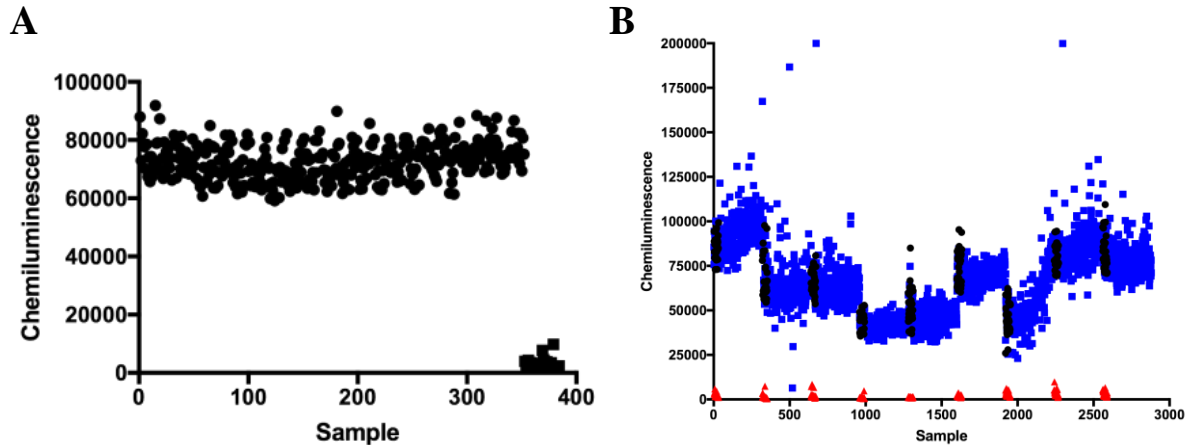


Figure 19. PPI cat-ELCCA HTS Characterization. A) PPI cat-ELCCA exhibits Z' factor greater than 0.65, B) preliminary screening with fragment library compounds

complete elimination of residual liquid in the wells post-wash – the edge wells consistently yielded lower signal output. Biotek ELX 405 washer often suffered from technical difficulties (clogged pins, uneven liquid distribution, and etc.), but these problems were easily addressable. Thus, PPI cat-ELCCA was miniaturized for HTS campaign using the aspiration-based washer. HTS potential is generally determined by the Z' factor, and it is the most important statistical parameter; assays exhibiting Z' factors of ≥ 0.5 are regarded as suitable assays to conduct a HTS campaign. As additional characterization, a small collection of ~3,000 fragment molecules were screened at high concentrations (400 μM –1 mM). The required high dosage using this library is often accompanied by an increase in the compound interference in biochemical assays³³⁻³⁴ and are limited to using low-throughput biophysical methods. Although no hit compounds were identified (**Figure 19B**), the assay performed well with Z' factors ranging between 0.44–0.67. With respect to compound interference, few compounds had yielded luminescence signals higher than the negative control; based on the previous results with Congo Red (aggregator) in the absence of detergent, these compounds likely induced aggregation or had crashed out of solution

due to insolubility. Nonetheless, based on this and the presented preliminary data, PPI cat-ELCCA was employed in further HTS campaign to discover the chemical probes for the eIF4E PPIs.

3.4.2.2 NPE LIBRARIES

PPI cat-ELCCA was used to screen the natural product extract library (**Figure 20**). CCG NPEs are derived from a large collection of cyanobacteria and sponges from all over the globe. In brief, pure strains of microbes are isolated from these sediments through carefully

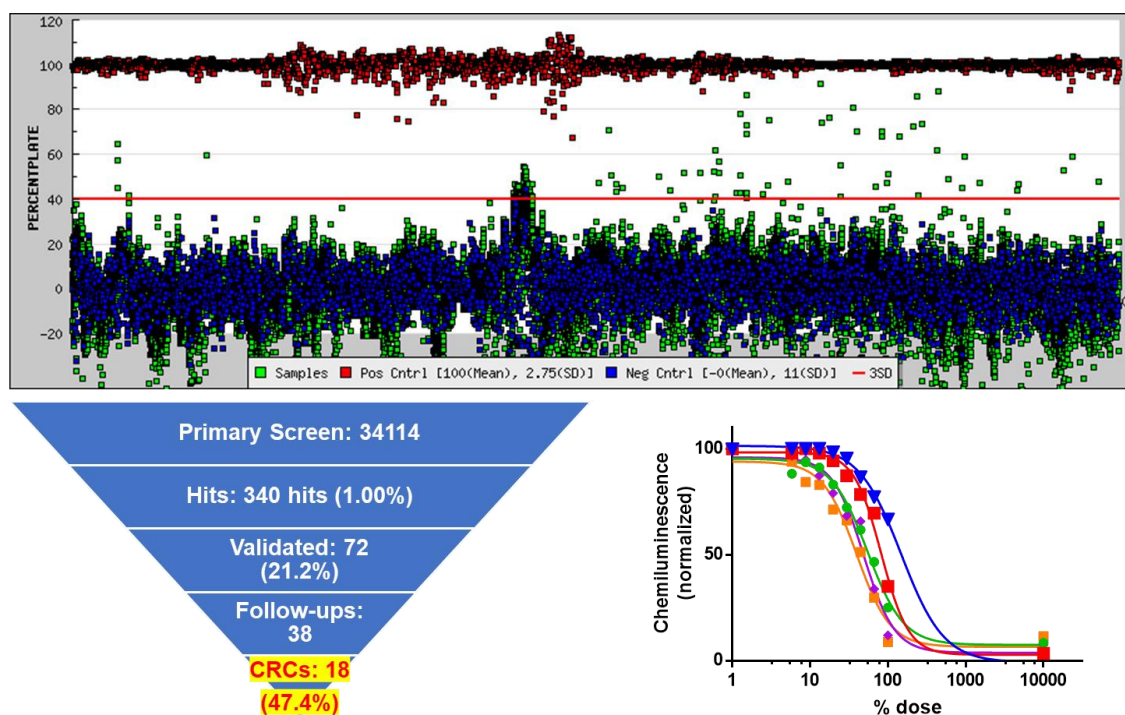


Figure 20. The primary screening of the NPE library. $Z' = 0.62$. HTS statistics of the NPE library using PPI cat-ELCCA, representative CRCs of validated hits normalized to the assay controls. The CRC data was collected in duplicates ($n=2$).

monitored conditions, and new natural product molecules are extracted for analysis in HTS campaigns. The active fraction must then be subjected to iterative fractionation and screening process to narrow down to the active compound, which will then require full chemical characterization and re-testing. Upon successful identification and characterization of the active

compounds, the strains responsible for its production are phylogenetically characterized. CCG NPEs have been utilized successfully to discover novel activities of known natural products^{32, 35}; however, it is underutilized in HTS campaigns due to the high false positive hit rates and the labor-intensive identification of the active compounds³⁶⁻³⁷. The fluorescence and quenching interferences from the NPE library can be somewhat mitigated by using red-shifted dye or fluorophores since the NPEs may interfere significantly more with blue-shifted fluorescence wavelengths³⁵. The potential reactive metabolites could be neutralized through specific chemical conditioning, and pre-fractionation drastically reduces sample complexity for easier identification of the active compound. Employing quantitative HTS and utilizing compound titrations to prioritize identifications of active fractions can dramatically improve lead validation as well¹. Clearly, the NPE library requires a robust, sensitive assay to obtain high confidence screening data in midst of the complex chemical mixtures. PPI cat-ELCCA is an ideal assay that could identify the untapped potential inhibitors of this underutilized library.

The primary campaign identified 340 hits with greater than 50% inhibition (1.00%), and 72 hits were validated (21.2%). To prioritize the fractions for further fractionations, concentration response curves (CRC) were acquired from 38 validated hits; of these, 18 samples (47.4%) appeared dose-responsive with hill slopes ranging from -0.5 to -2.0, suggesting a ligand binding mechanism of action. The 18 samples are pending re-isolation from their respective cultures by the Sherman group. The successful NPE library screening campaign suggests that PPI cat-ELCCA is a powerful tool in screening complex mixtures.

3.4.2.3 ELI LILLY BIOLOGY INTERROGATION COMPOUND LIBRARY

As part of the Eli Lilly Open Innovation Drug Discovery program, the Garner group received their customized Biology Interrogation Compound (BIC) library to screen against the

eIF4E–4E-BP1 interaction using PPI cat-ELCCA (**Figure 21**). The primary campaign against

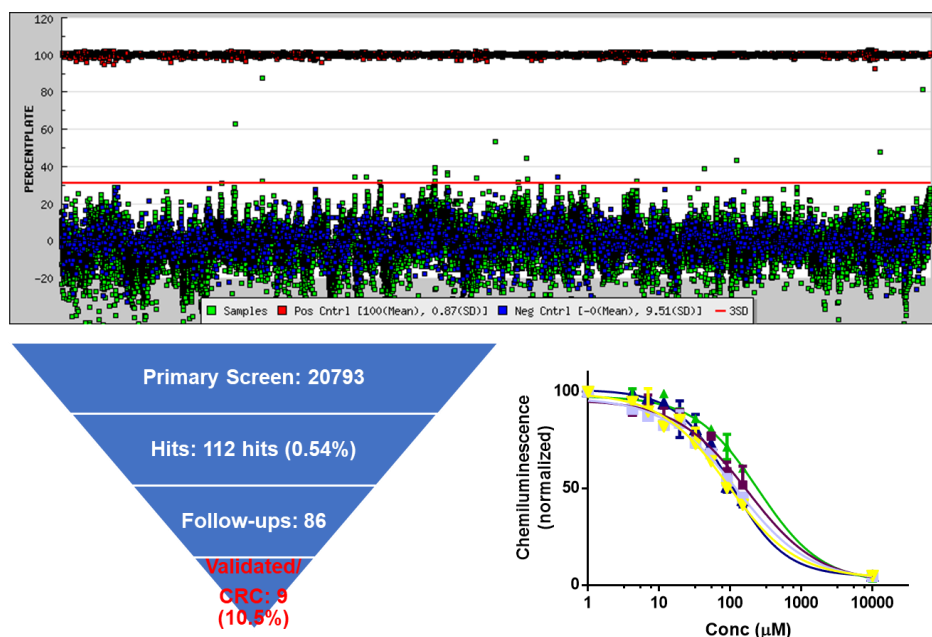


Figure 21. The primary screening of the BIC library. $Z' = 0.7$. HTS statistics of the NPE library, and the representative CRCs of validated hits normalized to the assay controls. The CRCs were collected in duplicates ($n=2$) and shown as the mean \pm SD.

Compound	K_d (μM)	IC_{50} (μM)	n_H
W000116041_P20	5.2 ± 0.2	177.8	-0.9
W000112230_B11	4.5 ± 0.6	162	-0.4
W000112312_E10	12 ± 3	263	-1.0
W000112300_J06	N/A	102	-1.7
W000112312_N14	N/A	35	-0.5
W000112264_O12	N/A	60	-0.74
W000112226_D10	5.1 ± 0.6	123	-0.8
W000112304_I16	13 ± 2	110	-1.1
W000116059_D13	5.1 ± 0.9	100	-0.9

Table 2. Validated hits from the BIC library. The binding affinities were All experiments were conducted in duplicates ($n=2$).

20,793 compounds identified 112 hits with greater than 10% inhibition (0.54%); CRC were obtained for 86 hits for confirmation, and 9 compounds were identified to be dose-responsive

(10.5%). Of these 9 compounds, 6 had elicited direct binding to eIF4E by SPR and are currently being investigated under collaboration with Eli Lilly (**Table 2**).

3.5 CONCLUSION

The HTS campaigns to discover potent small molecule inhibitors targeting the eIF4E interactions have remained elusive. Although both 4EGI-1 and 4E1RCat inhibitors successfully disrupt the eIF4E interactions, their chemical structures resemble PAINS and other known nonspecific binding motifs, and ultimately, are poor candidates for the therapeutic development. The HTS campaign using PPI cat-ELCCA to screen against the eIF4E interactions was advantageous over the previously attempted campaigns using FP and TR-FRET. First, PPI cat-ELCCA screened against the more physiologically relevant full-length proteins that best mimicked the native eIF4E interactions instead of relying on the “hot spot”. Second, the catalytic amplification of PPI cat-ELCCA signal allowed for compound screening against 4 nM protein complex whereas the FP assay required more than 50 nM peptide-protein complex. Third, the low chemical interference of PPI cat-ELCCA allowed for high confidence screening in the novel chemical space of natural product extracts. Despite these incremental gains, ultimately, the small molecule drug discovery targeting the eIF4E interactions remain a work in progress, with extensive compound isolation and characterizations of the NPE hits and further compound explorations from the BIC library hits. However, novel HTS assay like PPI cat-ELCCA could be the paradigm shifting tool needed to succeed where the traditional assays have failed, and to breathe new life into the drug discovery campaigns of difficult, elusive PPI targets.

3.6 HTS PPI CAT-ELCCA PROTOCOL (384-WELL FORMAT)

HTS PPI cat-ELCCA Protocol (384-well format)

Buffer A: 50 mM Phosphate Buffer (pH 7.4), 200 mM NaCl, 0.01% Tween-20, 2 mM DTT

Buffer B: 50 mM Phosphate Buffer (pH 7.4), 200 mM NaCl, 0.05% Tween-20

Buffer C: 50 mM Phosphate Buffer (pH 7.4)

****Pre-wash with and pre-dispense a dummy dispense (~half of the required volume, or less)***

1. Immobilization of biotin-eIF4E (10 μ L of 50 nM in Buffer A)
 - a. ****Prime the tubing well****
 - b. POS Ctrl (usually columns 23-24): add Buffer A (10 μ L)
 - c. NEG Ctrl (usually columns 1-2): add biotin-eIF4E (10 μ L)
 - d. Compound wells (usually columns 3-22): add biotin-eIF4E (10 μ L)
 - e. Cover the wells with plate-sealing tape.
 - f. Spin down on centrifuge (1000xRPM, 1min, 4C)
 - g. Overnight incubation (4 $^{\circ}$ C)
 - h. ****Thoroughly wash and clean the dispensing cassette with Buffer C, and then with water****
2. Removing well contents
 - a. Prime ELX405 with Buffer B & wash with Method #66
 - b. Lay absorbent towel, smack the plates post wash (should see residual liquid leaving stains on the towel)
 - c. Finish washing the rest of the plates in the exact same way prior to the next step
3. PPI incubation of mTet 4E-BP1 (10 μ L of 4nM in Buffer A)
 - a. ****Prime the tubing well****
 - b. Add mTet 4E-BP1 (10 μ L of 4 nM in Buffer A) to all the wells

- c. Dispense the compounds
 - d. Cover the wells with plate–sealing tape
 - e. Spin down on centrifuge (1000xRPM, 1min, 4C)
 - f. Incubate at 4 °C for 45 min
4. Removing well contents
- a. Prime ELX405 with Buffer B & wash with Method #66
 - b. Lay absorbent towel, smack the plates post wash (should see residual liquid leaving stains on the towel)
 - c. Finish washing the rest of the plates in the exact same way prior to the next step
5. Click chemistry with TCO–HRP (10 µL of 1 µM in Buffer A)
- a. **Prime the tubing well**
 - b. Add TCO–HRP (10 µL of 1 µM in Buffer A) to all the wells
 - c. Cover the wells with plate–sealing tape
 - d. Spin down on centrifuge (1000xRPM, 1min, 4C)
 - e. Incubate at RT for 45 min
6. Removing well contents
- a. Prime ELX405 with Buffer B & wash with Method #66
 - b. Lay absorbent towel, smack the plates post wash (should see residual liquid leaving stains on the towel)
 - c. Finish washing the rest of the plates in the exact same way prior to the next step
7. Final wash with Buffer C
- a. Prime ELX405 with Buffer C & wash with Method #66

- b. Lay absorbent towel, smack the plates post wash (should see residual liquid leaving stains on the towel)
 - c. Finish washing the rest of the plates in the exact same way prior to the next step
8. chemiluminescence detection
- a. ****Prime the tubing well****
 - b. Add chemiluminescence substrate (25 μ L of 1:1 mixture of black & white components of the chemiluminescence substrates) to all the wells
 - c. Stack the plates, from bottom up = 1,2,3,4,dummy
9. Readout
- a. Load up the stacker with the plates, and start the data collection
 - i. The protocol takes the focal adjustment from the first plate and keeps that constant throughout the rest of the plates
 - ii. The protocol marks the gain from A2, and sets it to 60% for each plate

3.7 EXPERIMENTAL

Plate washing was performed using a Biotek 405 ELX plate washer. Liquid handling was performed using a Multidrop Combi Reagent Dispenser (Thermo Scientific). All the compounds were dispensed using a Sciclone (Caliper) liquid handler with V&P pintool. The fragment library includes 2,668 fragments of MW 150–300 (Asinex) and 237 natural product–like fragments (AnalytiCon Discovery). Asinex fragments were screened at 1 mM final concentration. AnalytiCon fragments were screened at 400 μ M final concentration. The NPE library compounds were screened at 0.5% DMSO final concentration, or at 200–fold dilution of

the stock. Chemiluminescence signal was detected using a PHERAstar plate reader using LUM plus module (BMG Labtech).

3.8 REFERENCES

1. Moerke, N. J.; Aktas, H.; Chen, H.; Cantel, S.; Reibarkh, M. Y.; Fahmy, A.; Gross, J. D.; Degterev, A.; Yuan, J.; Chorev, M., Small-molecule inhibition of the interaction between the translation initiation factors eIF4E and eIF4G. *Cell* **2007**, *128* (2), 257-267.
2. Hall, M. D.; Yasgar, A.; Peryea, T.; Braisted, J. C.; Jadhav, A.; Simeonov, A.; Coussens, N. P., Fluorescence polarization assays in high-throughput screening and drug discovery: a review. *Methods and applications in fluorescence* **2016**, *4* (2), 022001-022001.
3. Marcotrigiano, J.; Gingras, A.-C.; Sonenberg, N.; Burley, S. K., Cap-dependent translation initiation in eukaryotes is regulated by a molecular mimic of eIF4G. *Molecular cell* **1999**, *3* (6), 707-716.
4. Lea, W. A.; Simeonov, A., Fluorescence Polarization Assays in Small Molecule Screening. *Expert opinion on drug discovery* **2011**, *6* (1), 17-32.
5. Simeonov, A. D. M., Interference with Fluorescence and Absorbance. In *Assay Guidance Manual [Internet]*, Bethesda (MD): Eli Lilly & Company and the National Center for Advancing Translational Sciences: 2015 Dec 7.
6. Zhou, P.; Lugovskoy, A. A.; Wagner, G., A solubility-enhancement tag (SET) for NMR studies of poorly behaving proteins. *Journal of Biomolecular NMR* **2001**, *20* (1), 11-14.
7. Surade, S.; Blundell, Tom L., Structural Biology and Drug Discovery of Difficult Targets: The Limits of Ligandability. *Chemistry & Biology* **2012**, *19* (1), 42-50.
8. Friberg, A.; Vigil, D.; Zhao, B.; Daniels, R. N.; Burke, J. P.; Garcia-Barrantes, P. M.; Camper, D.; Chauder, B. A.; Lee, T.; Olejniczak, E. T.; Fesik, S. W., Discovery of Potent Myeloid Cell Leukemia 1 (Mcl-1) Inhibitors Using Fragment-Based Methods and Structure-Based Design. *Journal of Medicinal Chemistry* **2013**, *56* (1), 15-30.
9. Huang, J.-W.; Zhang, Z.; Wu, B.; Cellitti, J. F.; Zhang, X.; Dahl, R.; Shiao, C.-W.; Welsh, K.; Emdadi, A.; Stebbins, J. L.; Reed, J. C.; Pellicchia, M., Fragment-Based Design of Small Molecule X-Linked Inhibitor of Apoptosis Protein Inhibitors. *Journal of Medicinal Chemistry* **2008**, *51* (22), 7111-7118.
10. Chen, L.; Aktas, B. H.; Wang, Y.; He, X.; Sahoo, R.; Zhang, N.; Denoyelle, S.; Kabha, E.; Yang, H.; Freedman, R. Y.; Supko, J. G.; Chorev, M.; Wagner, G.; Halperin, J. A., Tumor suppression by small molecule inhibitors of translation initiation. *Oncotarget* **2012**, *3* (8), 869-881.

11. Yi, T.; Kabha, E.; Papadopoulos, E.; Wagner, G., 4EGI-1 targets breast cancer stem cells by selective inhibition of translation that persists in CSC maintenance, proliferation and metastasis. *Oncotarget* **2014**, *5* (15), 6028-37.
12. McMahon, R.; Zaborowska, I.; Walsh, D., Noncytotoxic inhibition of viral infection through eIF4F-independent suppression of translation by 4EGI-1. *J Virol* **2011**, *85* (2), 853-64.
13. Redondo, N.; Garcia-Moreno, M.; Sanz, M. A.; Carrasco, L., Translation of viral mRNAs that do not require eIF4E is blocked by the inhibitor 4EGI-1. *Virology* **2013**, *444* (1-2), 171-80.
14. Attar-Schneider, O.; Drucker, L.; Zismanov, V.; Tartakover-Matalon, S.; Lishner, M., Targeting eIF4GI translation initiation factor affords an attractive therapeutic strategy in multiple myeloma. *Cell Signal* **2014**, *26* (9), 1878-87.
15. Descamps, G.; Gomez-Bougie, P.; Tamburini, J.; Green, A.; Bouscary, D.; Maiga, S.; Moreau, P.; Le Gouill, S.; Pellat-Deceunynck, C.; Amiot, M., The cap-translation inhibitor 4EGI-1 induces apoptosis in multiple myeloma through Noxa induction. *Br J Cancer* **2012**, *106* (10), 1660-7.
16. Tamburini, J.; Green, A. S.; Bardet, V.; Chapuis, N.; Park, S.; Willems, L.; Uzunov, M.; Ifrah, N.; Dreyfus, F.; Lacombe, C.; Mayeux, P.; Bouscary, D., Protein synthesis is resistant to rapamycin and constitutes a promising therapeutic target in acute myeloid leukemia. *Blood* **2009**, *114* (8), 1618-27.
17. Tamburini, J.; Green, A. S.; Chapuis, N.; Bardet, V.; Lacombe, C.; Mayeux, P.; Bouscary, D., Targeting translation in acute myeloid leukemia: a new paradigm for therapy? *Cell Cycle* **2009**, *8* (23), 3893-9.
18. Willimott, S.; Beck, D.; Ahearne, M. J.; Adams, V. C.; Wagner, S. D., Cap-translation inhibitor, 4EGI-1, restores sensitivity to ABT-737 apoptosis through cap-dependent and -independent mechanisms in chronic lymphocytic leukemia. *Clin Cancer Res* **2013**, *19* (12), 3212-23.
19. Papadopoulos, E.; Jenni, S.; Kabha, E.; Takrouri, K. J.; Yi, T.; Salvi, N.; Luna, R. E.; Gavathiotis, E.; Mahalingam, P.; Arthanari, H.; Rodriguez-Mias, R.; Yefidoff-Freedman, R.; Aktas, B. H.; Chorev, M.; Halperin, J. A.; Wagner, G., Structure of the eukaryotic translation initiation factor eIF4E in complex with 4EGI-1 reveals an allosteric mechanism for dissociating eIF4G. *Proceedings of the National Academy of Sciences* **2014**, *111* (31), E3187-E3195.
20. Baell, J. B., Feeling Nature's PAINS: Natural Products, Natural Product Drugs, and Pan Assay Interference Compounds (PAINS). *J Nat Prod* **2016**, *79* (3), 616-28.
21. Baell, J. B., Screening-based translation of public research encounters painful problems. *ACS Med Chem Lett* **2015**, *6* (3), 229-34.
22. Baell, J. B.; Holloway, G. A., New substructure filters for removal of pan assay interference compounds (PAINS) from screening libraries and for their exclusion in bioassays. *J Med Chem* **2010**, *53* (7), 2719-40.

23. Baell, J. B.; Nissink, J. W. M., Seven Year Itch: Pan-Assay Interference Compounds (PAINS) in 2017-Utility and Limitations. *ACS Chem Biol* **2018**, *13* (1), 36-44.
24. Dalvie, D. K.; Kalgutkar, A. S.; Khojasteh-Bakht, S. C.; Obach, R. S.; O'Donnell, J. P., Biotransformation Reactions of Five-Membered Aromatic Heterocyclic Rings. *Chemical Research in Toxicology* **2002**, *15* (3), 269-299.
25. Jasial, S.; Hu, Y.; Bajorath, J., How Frequently Are Pan-Assay Interference Compounds Active? Large-Scale Analysis of Screening Data Reveals Diverse Activity Profiles, Low Global Hit Frequency, and Many Consistently Inactive Compounds. *Journal of Medicinal Chemistry* **2017**, *60* (9), 3879-3886.
26. Cencic, R.; Hall, D. R.; Robert, F.; Du, Y.; Min, J.; Li, L.; Qui, M.; Lewis, I.; Kurtkaya, S.; Dingleline, R.; Fu, H.; Kozakov, D.; Vajda, S.; Pelletier, J., Reversing chemoresistance by small molecule inhibition of the translation initiation complex eIF4F. *Proceedings of the National Academy of Sciences of the United States of America* **2011**, *108* (3), 1046-1051.
27. Arkin MR, G. M., Fu H, Inhibition of Protein-Protein Interactions: Non-Cellular Assay Formats. In *Assay Guidance Manual [Internet]*, Bethesda (MD): Eli Lilly & Company and the National Center for Advancing Translational Sciences: 2012 Mar 18.
28. Imbert, P.-E.; Unterreiner, V.; Siebert, D.; Gubler, H.; Parker, C.; Gabriel, D., Recommendations for the Reduction of Compound Artifacts in Time-Resolved Fluorescence Resonance Energy Transfer Assays. *ASSAY and Drug Development Technologies* **2007**, *5* (3), 363-372.
29. Baell, J. B.; Ferrins, L.; Falk, H.; Nikolakopoulos, G., PAINS: Relevance to Tool Compound Discovery and Fragment-Based Screening. *Aust. J. Chem.* **2013**, *66*, 1483.
30. Lorenz, D. A.; Song, J. M.; Garner, A. L., High-Throughput Platform Assay Technology for the Discovery of pre-microRNA-Selective Small Molecule Probes. *Bioconjugate Chemistry* **2015**, *26* (1), 19-23.
31. McGovern, S. L.; Caselli, E.; Grigorieff, N.; Shoichet, B. K., A Common Mechanism Underlying Promiscuous Inhibitors from Virtual and High-Throughput Screening. *Journal of Medicinal Chemistry* **2002**, *45* (8), 1712-1722.
32. Suffness, M.; Douros, J. D., Discovery of antitumor agents from natural sources. *Trends in Pharmacological Sciences* **1981**, *2*, 307-310.
33. Raveh, A.; Schultz, P. J.; Aschermann, L.; Carpenter, C.; Tamayo-Castillo, G.; Cao, S.; Clardy, J.; Neubig, R. R.; Sherman, D. H.; Sjögren, B., Identification of Protein Kinase C Activation as a Novel Mechanism for RGS2 Protein Upregulation through Phenotypic Screening of Natural Product Extracts. *Molecular Pharmacology* **2014**, *86* (4), 406-416.
34. Delekta, P. C.; Raveh, A.; Larsen, M. J.; Schultz, P. J.; Tamayo-Castillo, G.; Sherman, D. H.; Miller, D. J., The Combined Use of Alphavirus Replicons and Pseudoinfectious Particles for

the Discovery of Antivirals Derived from Natural Products. *Journal of Biomolecular Screening* **2015**, *20* (5), 673-680.

35. Rishton, G. M., Natural Products as a Robust Source of New Drugs and Drug Leads: Past Successes and Present Day Issues. *The American Journal of Cardiology* **2008**, *101* (10, Supplement), S43-S49.

36. Turek-Etienne, T. C.; Lei, M.; Terracciano, J. S.; Langsdorf, E. F.; Bryant, R. W.; Hart, R. F.; Horan, A. C., Use of Red-Shifted Dyes in a Fluorescence Polarization AKT Kinase Assay for Detection of Biological Activity in Natural Product Extracts. *Journal of Biomolecular Screening* **2004**, *9* (1), 52-61.

37. Grant, S. K.; Sklar, J. G.; Cummings, R. T., Development of Novel Assays for Proteolytic Enzymes Using Rhodamine-Based Fluorogenic Substrates. *Journal of Biomolecular Screening* **2002**, *7* (6), 531-540.

38. Cheng, K. C.-C.; Cao, S.; Raveh, A.; MacArthur, R.; Dranchak, P.; Chlipala, G.; Okoneski, M. T.; Guha, R.; Eastman, R. T.; Yuan, J.; Schultz, P. J.; Su, X.-z.; Tamayo-Castillo, G.; Matainaho, T.; Clardy, J.; Sherman, D. H.; Inglese, J., Actinoramide A Identified as a Potent Antimalarial from Titration-Based Screening of Marine Natural Product Extracts. *Journal of Natural Products* **2015**, *78* (10), 2411-2422.

39. Inglese, J.; Auld, D. S.; Jadhav, A.; Johnson, R. L.; Simeonov, A.; Yasgar, A.; Zheng, W.; Austin, C. P., Quantitative high-throughput screening: A titration-based approach that efficiently identifies biological activities in large chemical libraries. *Proceedings of the National Academy of Sciences* **2006**, *103* (31), 11473-11478.

CHAPTER 4 DESIGN, DEVELOPMENT, AND CHARACTERIZATIONS OF 4E-BP1 MIMETIC STAPLED PEPTIDES

4.1 DRUG DISCOVERY: PEPTIDES TARGETING PROTEIN-PROTEIN INTERACTIONS²

Peptides have gained significant interest in recent years despite their well-documented intrinsic flaws: poor chemical stability and oral availability, short circulating plasma half-life, solubility, and most prominently, low cell permeability. Extensive medicinal chemistry campaigns have addressed these flaws, from ‘piggy-backing’ onto the protein albumin and peptide macrocyclization to increase their effective half-life³, peptide acylation⁴ and pegylation⁵ (both⁶) to increase solubility to bring their candidates closer to therapeutics. Besides the revolutionary discoveries and applications of insulin⁷, there are more than 60 peptide drugs that the US FDA had approved for treatments, more than 140 peptides in clinical trials, and far greater number in preclinical development (reviewed⁸⁻¹⁰).

Constraining the conformational flexibility of a molecule to mimic the active compound structure reduces the entropic penalty of binding to improve affinity and selectivity¹¹. Peptide macrocyclization, or peptide stapling, utilizes this concept in full and has garnered much attention in the recent decade as an innovative medicinal chemistry technique to increase peptide half-life, inhibitory potency, and cell permeability. The structured motifs isolated for peptide

² As of July 2018, this work is under revision at Journal of American Chemical Society and titled “Probing the Importance of Folding Dynamics in the Design of Stapled Peptide Mimics of the Disordered Proteins 4E-BP1 and eIF4G”. Co-authors include: Gallagher, Erin (**Co-first author**, SPR and CD experiments); Menon, Arya (cell biology including eIF4E complex pulldown experiments); Mishra, Lauren (initial stapled peptide design and synthesis); Chmiel, Alyah (peptide synthesis); Mitchell, Dylan (flow cytometry)

design often retain their secondary structures even when it is converted to a peptide. Peptide stapling pre-forms or pre-positions the crucial amino acids to achieve low-energy barriers to adopt various secondary structures, such as α -helices, β -sheets, and β -hairpins.

4.1.1 PEPTIDES

Peptide mediated disruption of the eIF4E interactions have been in the works for decades¹² since the canonical binding motifs of eIF4G and 4E-BP1 have been shown to bind to eIF4E¹³⁻¹⁴. Investigators have attempted to address the peptides' poor permeability through fusion peptides containing cell penetrating peptides (CPP). Herbert et al. demonstrated that a peptide containing penetratin fused to the canonical eIF4E binding motif led to dose-dependent apoptosis, and that alanine mutations at key residues reduced and eliminated this bioactivity¹⁵. Similarly, Brown et al. attached the CPP tag TAT to their enhanced α -helicity eIF4G1 peptide to show a similar improved apoptotic cell death upon treatment¹⁶. However, both studies showed strong evidence of apoptosis with their negative control CPP and required serum deprivation, which highlighted strong possibilities that the observed apoptosis could be due to nonspecific interactions of the CPPs. Alternative to using the CPPs, Ko et al. conjugated the 4E-BP1 mimetic peptide to an agonist of gonadotropin-releasing hormone (GnRH). This fusion peptide exploited the GnRH receptors that are highly expressed in epithelial ovarian cancer¹⁷ to gain both target specificity and increased peptide permeability. This GnRH fused 4E-BP1 peptide successfully reduced the tumor burden in ovarian cancer mouse model compared to the saline treatment. Effectively, these studies demonstrated the therapeutic relevance of a cell permeable 4E-BP1 or eIF4G mimetics and marked the eIF4E interaction as a possible therapeutic target using the emerging peptide stapling technologies.

4.1.2 ALPHA HELIX STAPLED PEPTIDES

Many pathological PPIs¹⁸ are reliant on α -helix driven interactions, including that of the eIF4E PPIs. The canonical binding motifs of both 4E-BP1 and eIF4G bind and adopt a short α -helical structure. The most well-established stapling strategies are through hydrocarbon stapling, lactamisation¹⁹⁻²¹, Cu(I)-catalyzed azide-alkyne cycloaddition (CuAAC)²²⁻²⁷, or thioether stapling²⁸⁻³¹ (**Figure 22**). In general, these strategies capitalize on the peptide backbone hydrogen-bonding network between the amino acids in i , $i+4$ and i , $i+7$ spacings for 1- and 2-

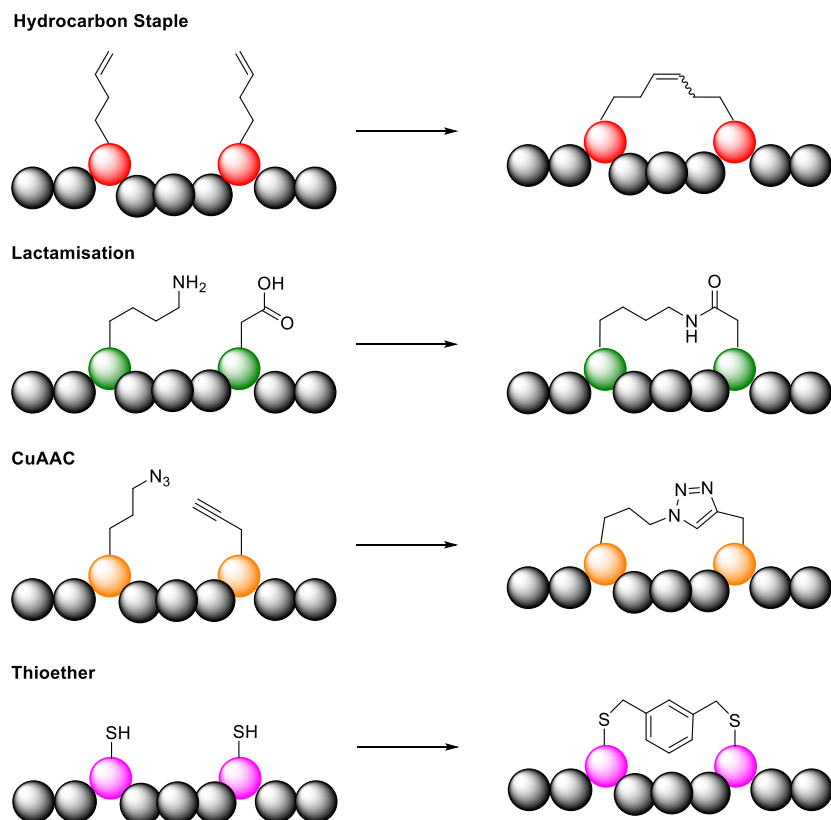


Figure 22. Common α -stabilizing strategies.

helix turns, respectively. Unnatural amino acids are incorporated into these positions during the solid-phase peptide synthesis and are later chemically linked together to create a macrocyclic region that more easily adopts to α -helical structure. Stapled peptides are characterized through 1) a direct binding assay such as SPR to determine the binding kinetics and affinity, 2) a

biophysical assay such as circular dichroism (CD) to determine the helical content, and 3) a competition assay against target PPIs such as FP, TR-FRET, and ELISA to characterize their biochemical inhibition. Fluorescently tagged analogs of the stapled peptides are synthesized and used to characterize the cell permeability through fluorescence activated cell sorting (FACS) and confocal fluorescence microscopy.

The most common stapling strategy is through ring-closing metathesis reaction termed hydrocarbon stapling developed by Blackwell and Grubbs³² using two O-allyl serines spaced $i, i+4$. Hydrocarbon stapling was optimized for α -helix structure stabilization under Schafmeister and Verdine³³, in which α, α -disubstituted amino acids were used in place of O-allyl serines to increase helix propensity. In a ground-breaking study, Walensky et al. developed a series of BID BH3 hydrocarbon stapled peptides for binding proteins in the BCL-2 family³⁴, and showed a drastic increase in cell permeability and *in vivo* stability and efficacy. The stapled BID BH3 peptides had greater affinity than the native sequence to the target BCL-2, induced apoptosis in leukemia cells, and showed potency in leukemia xenografted mice³⁵; since the literature still remains inconclusive on the improvements in cellular uptake from lactamisation or CuAAC³⁶⁻³⁷, the hydrocarbon stapling strategy gained traction as the peptide stapling strategy for therapeutic peptide developments. Since then, the hydrocarbon stapling strategy has been used to target p53-MDM2/MDMX interaction³⁸, HIV-1³⁹, small GTPase RAB25⁴⁰, PKA⁴¹, eIF4E interactions¹, NOTCH transcription factor complex⁴², and EZH2-EED complex⁴³⁻⁴⁴ among others. Inspired by these successes, alternative hydrophobic stapling strategies like perfluoroaryl-Cysteine S_NAr ⁴⁵⁻⁴⁶ and hydrogen-bond surrogates⁴⁷⁻⁵⁰ emerge and continue to expand this exciting field.

It should be noted that the hydrocarbon stapling strategy is still relatively new and in development. The hydrocarbon stapling strategy itself does not guarantee improved binding

affinity⁵¹ or cellular uptake⁵². Whether the disubstituted unnatural amino acids confer significant or any advantages to the helicity, proteolytic stability or binding affinity is under question⁵³ and are currently under investigation. Although evidence suggests that increased cell permeability of stapled peptide may be through an energy-dependent endocytosis pathway⁵⁴⁻⁵⁵, the possibility or the exact method to exploit this pathway for stapled peptide delivery remains unknown and yet undiscovered.

4.1.3 HYDROCARBON STAPLED PEPTIDES TARGETING EIF4E PROTEIN-PROTEIN INTERACTIONS

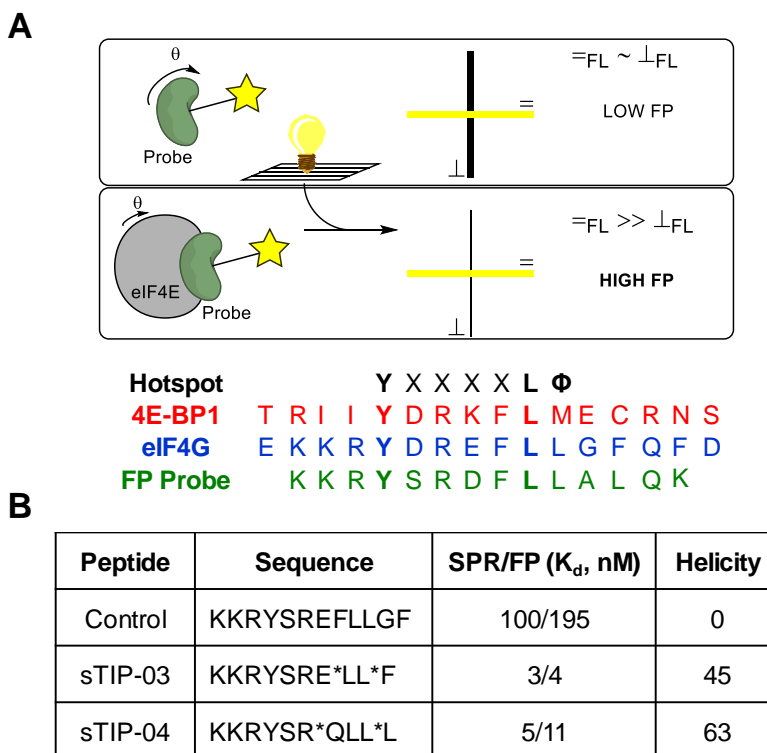


Figure 23. Stapled peptides targeting eIF4E interactions. A) FP design¹. FP probe sequence contained mutations that improved eIF4E binding affinity². B) K_d as reported through SPR and FP, and helicity as reported through CD.

The canonical binding motif of both 4E-BP1 and eIF4G adopt a short α -helix upon binding to eIF4E, and therefore make a great candidate for peptide stapling strategies. In 2012,

Zhou et al. conducted a phage display study to design potent eIF4E binding peptides² and discovered that D5S and G11A mutation had increased the apparent binding affinity of the peptide to eIF4E by 4.6-fold and 2.3-fold, respectively (**Figure 23A**).

Protein crystallization efforts and computational modeling studies showed that D5S mutation increased helicity of the peptide while G11A allowed for more compact packing of the bound peptide to the hydrophobic eIF4E surface. Implementations of two additional disruptive substitutions F8Q and F12L to the D5S G11A mutation sequence improved the apparent binding affinity further to 43 nM, greater than 10-fold increase from that of the linear eIF4G1 sequence (460 nM). With the excitement generated from the success of p53/MDM2 and BCL2–BH3 hydrocarbon stapled peptide inhibitors, Lama et al had pursued rational design of stapled peptides targeting eIF4E interactions¹ based on this potent linear eIF4G1 mutation sequence. Six hydrocarbon stapled peptides were synthesized and characterized, and two peptides – **sTIP-03** and **sTIP-04** – had exhibited binding affinity over the native peptide by approximately 20–fold (**Figure 23B**). Molecular dynamics simulations and the overlaid predicted structures using the solved crystal structure of eIF4E found that these two potent peptides had different mechanisms of enhanced binding, adding another dimension of complexity to the rationale design of stapled peptides. Despite this promising *in vitro* data, the lead candidate **sTIP-03** reduced eIF4E and its biomarker survivin only in absence of fetal calf serum (FCS)⁵⁶⁻⁵⁷, and further patents and studies developing **sTIP-03** and **sTIP-04** as therapeutic agents appear to have stopped.

4.2 RESEARCH DESIGN

As the development of **sTIP-03** and **sTIP-04** had shown, the hydrocarbon stapled (HCS) peptides provide an attractive alternative to small molecule modulators to target and disrupt the eIF4E interactions. Although **sTIP-03** was bioactive only in absence of fetal calf serum (FCS)⁵⁶⁻

⁵⁷, rigorous formulations can (and has) reduced serum binding properties of the HCS peptides and improved their cellular potency⁵⁸. However, a more common practice is to optimize the sequence and the stapling strategy to limit the serum binding properties. Fortunately, eIF4G1 is

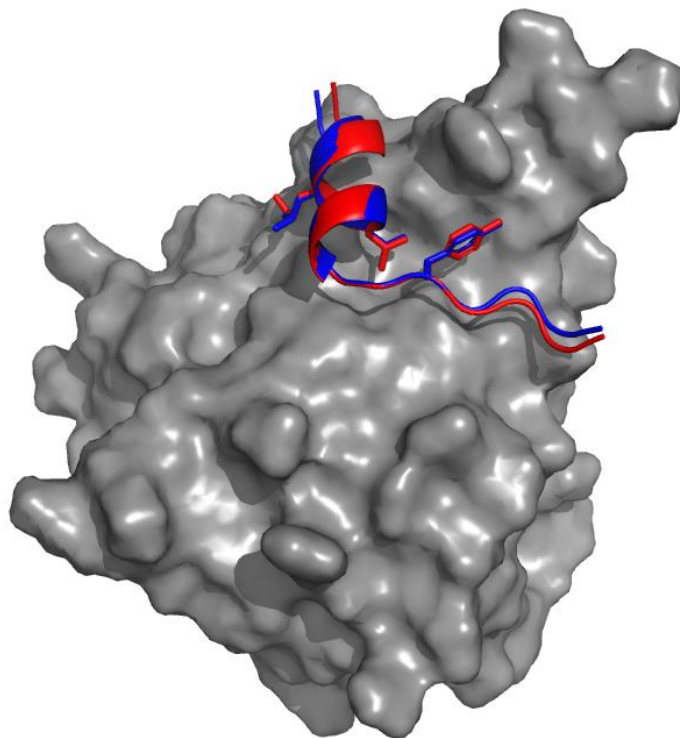


Figure 24. Overlay and amino acid sequences of the eIF4G mimetic sequence (blue, PDB: 5T46) and of the 4E-BP1 mimetic sequence (red, 4UED) bound to eIF4E (gray). Key side-chain residues of the canonical binding motif are displayed.

not the only protein binding to eIF4E and 4E-BPs can provide an epitope to design and characterize HCS peptides on. Studies show that the ectopic expressions of 4E-BP1 in transformed cells lead to suppressed tumorigenicity *in vitro*⁵⁹⁻⁶⁰ and *in vivo*⁶¹, and the aerosol delivery of 4E-BP1 gene inhibited the proliferation of lung cancer cells in *K-ras*^{LA1} model¹⁷. 4E-BP1 peptide modified for cell permeability also induced apoptosis in lung cells¹⁷, and 4E-BP1 peptide fused to gonadotropin-releasing hormone (GnRH) inhibited the growth of GnRH receptor-positive cells without significant cytotoxic effects to the host tissues¹⁷. Based on these mounting evidences, the 4E-BP epitope is a strong foundation to develop therapeutic HCS

peptides on for targeting the CdT-driven cancers. As previously mentioned, 4E-BP1 is an intrinsically disordered protein⁶² that adopts a short α -helical structure upon binding to eIF4E, thereby forming the 4E-BM of the PPI⁶² abiding to the sequence – YX₄L Φ where Y,X,L, and Φ

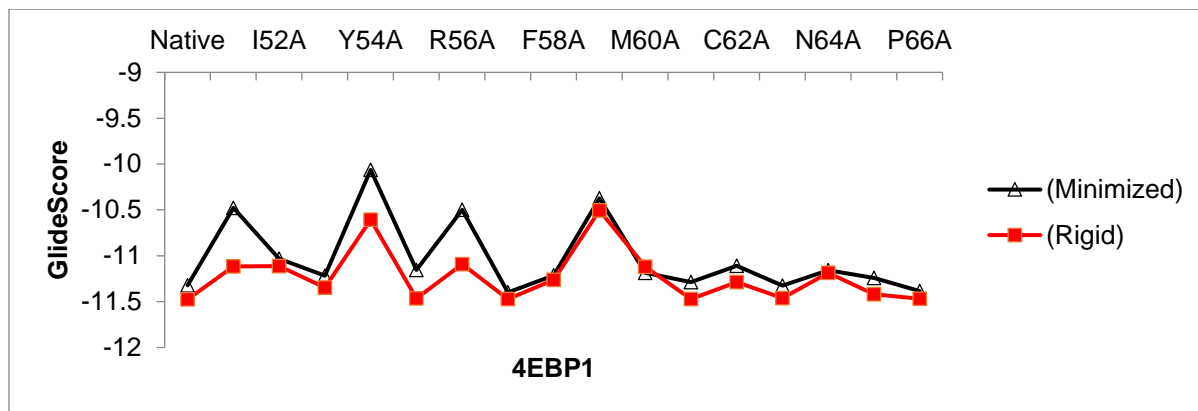


Figure 25. Virtual sequential alanine mutagenesis on 4E-BP1. The docking poses of each 4E-BP1 mutant peptide with eIF4E were analyzed against that of the native 4E-BP1 with eIF4E using Glide, with (Minimized) and without (Rigid) energy minimization prior to Glide scoring. A higher Glide Score indicates an unfavorable mutation, and therefore, a greater contribution to the ligand binding affinity.

denote Tyr, any amino acid, Leu, and hydrophobic residue, respectively⁶²⁻⁶⁴ (**Figure 24**). Like **sTIP-03** and **sTIP-04**, stabilization of the 4E-BP1 canonical binding helical motif would enhance eIF4E binding and yield greater inhibition from the reported benefits of peptide stapling⁶⁵. Virtual sequential alanine mutagenesis (courtesy of Dr. Lauren Mishra) using the X-ray crystal structure of 4E-BP1 peptide–eIF4E complex indicated that an *i, i+4* staple at Lys57/Glu61 positions would leave minimal disturbance to the key interactions (**Figure 25**). Furthermore, a slight difference in residue contribution to the peptide binding affinity were predicted from high (Red, Minimized) and low (black, Rigid) ligand sampling 4E-BP1 peptide model. To further investigate this impact of high and low ligand sampling of the stapled peptides (and in effect, the difference between induced fit binding model and the conformational selection model), the Garner group focused on designing and synthesizing two distinct 4E-BP1 HCS peptides: a high ligand sampling peptide (induced fit) containing mono-substituted (*S*)-2-(4'-

pentenyl)glycines at the stapling sites (mHCS)⁶⁵, and a low ligand sampling (conformational selection) peptide containing more commonly used (*S*)-2-(4'-pentenyl)alanines (HCS) (**Figure 26**). **mHCS 4E-BP1** would be subjected to additional structural reorganization upon binding than **HCS 4E-BP1** from the lack of methyl moiety on the

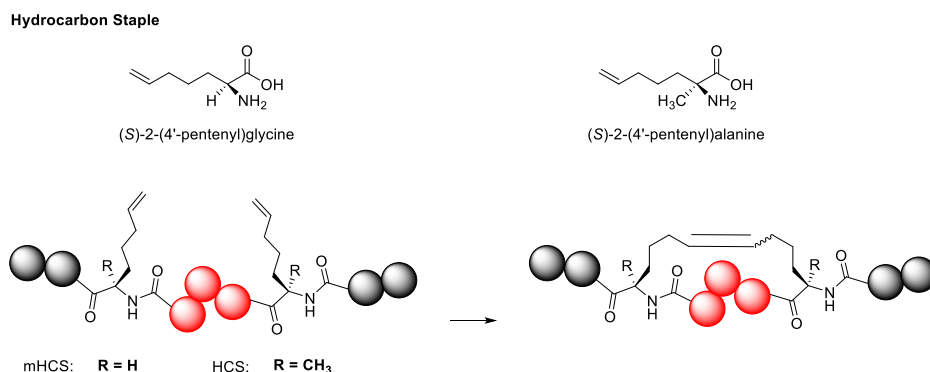


Figure 26. Hydrocarbon stapled peptides. **mHCS** and **HCS** peptides are synthesized with monosubstituted pentenylglycine and disubstituted pentenylalanine, respectively. unnatural amino acid alpha carbon, and potentially mimic the greater plasticity of disordered protein like 4E-BP1. The resulting impact in binding kinetics and inhibitory potency of **mHCS 4E-BP1**, **HCS 4E-BP1**, and various analogs were evaluated.

4.3 HCS STAPLED PEPTIDES

4.3.1 4E-BP1 LINEAR SEQUENCE OPTIMIZATIONS

Despite the strong inhibitory potency of the 4E-BP1 peptide (as evaluated by PPI cat-ELCCA), methionine oxidation and cysteine-induced peptide dimerization posed difficulties in 4E-BP1 peptide synthesis, purification, handling and storage. Prolonged storage of the peptide stocks often resulted in the loss of *in vitro* activity and precipitation upon thawing, all with the accompanying dimerization and/or a gain of +16 or +32 confirmed by LC-MS. Additionally, the 4E-BP1 peptide displayed poor aqueous solubility and was prone to aggregation which led to a significant product loss. 4E-BP1 sequence optimizations were required to identify and evaluate

the methionine and cysteine bio-isosteres and substitutions (**Figure 27**). **4E-BP1** and peptides **1-5** were synthesized and characterized. Peptide **1** was derived from 4E-BP2 protein, a homologous protein in the 4E-BP family that is less characterized than 4E-BP1 and more highly expressed in the brain⁶⁵. As expected, peptide **1** (19 ± 1 nM) reported similar low nanomolar inhibitory potency as **4E-BP1** peptide (31 ± 1 nM) without the concerns of methionine oxidation

Peptide	Sequence	IC ₅₀ (nM)	K _i (nM)
4E-BP1	G ₄₉ T R I I Y D R K F L M E C R N ₆₄	31 ± 4	7
1	G ₄₉ T R I I Y D R K F L L D R R N ₆₄	19 ± 1	9
2	G ₄₉ T R I I Y D R K F L Nle E R R N ₆₄		
3	G ₄₉ T R I I Y D R K F L Nle E K R N ₆₄		
4	G ₄₉ T R I I Y D R K F L Nle E C R N ₆₄	164 ± 1	82
5	R ₅₁ I I I Y D R K F L M E C R ₆₃	7 ± 1	4

B

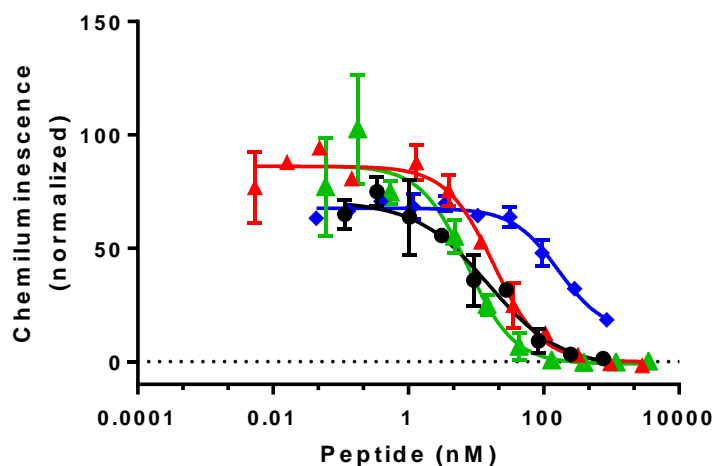


Figure 27. Linear sequence characterization. 4E-BP1 peptide mimetic sequence optimizations and inhibitory potencies. PPI cat-ELCCA dose response curves corresponding of linear peptides **4E-BP1** (black), **1** (red), **4** (blue), and **5** (green). All experiments were conducted in triplicates (n=3) and shown as the mean ± SD.

and peptide dimerization. Although M60L and E61D substitutions from 4E-BP1 to 4E-BP2 sequence carry relatively minor molecular differences, it was encouraging that the C62R was well-tolerated since many cell penetrating peptides are identified by net positively charged

peptides⁶⁶. Unfortunately, synthesis and purifications of **mHCS-2** proved difficult and required alternative sequence optimizations. Peptide **2** incorporated a reported bio-isostere of methionine, norleucine⁶⁷, and the C62R substitution that was well tolerated in peptide **1**. Similarly, peptide **3** incorporated norleucine in place of methionine and C62K substitution based on the sequence of homologous protein 4E-BP3. Prior to the final purifications of peptides **2** and **3**, the Garner group discovered that the full-length 4E-BP1 protein carrying M60A mutation had significant loss in inhibitory potency compared to the WT 4E-BP1 (**Figure 15A, Chapter 2**) and confirmed a similar loss of inhibitory potency with peptide **4**. Peptide **4** suffered greater than 10-fold increase in the apparent IC₅₀ (164 ± 1 nM) in comparison to the **4E-BP1** peptide and peptide **1**. Peptides **2** and **3** experiments were abandoned, and no further attempts were made to substitute the native M60 and C62 residues. Instead, to reduce the nonpolar nature of the peptide and to increase its solubility, G49, T50, and N64 of **4E-BP1** peptide were eliminated to produce peptide **5**. Peptide **5** benefited from easier synthesis, purification, and higher aqueous dissolution (> 1.0 mM) than the other linear peptides discussed; surprisingly, peptide **5** also yielded the highest inhibitory potency of 7 ± 1 nM and became a strong candidate for HCS peptide development. Overall, the modifications to the **4E-BP1** peptide sequence reduced its inhibitory potency, and the identification of bio-isosteres to the native M60 and C62 residues was unsuccessful. In addition to **4E-BP1** peptide, peptide **5** was identified as good candidates for further HCS developments.

4.3.2 RING CLOSING METATHESIS

The stapling procedure was adapted⁶⁸ using Grubbs catalyst generation I and II (**Figure 28A**). It should be noted that the N-terminal Fmoc can be removed upon prolonged exposure to RCM reaction conditions, and potentially nullify further RCM reaction from the increased

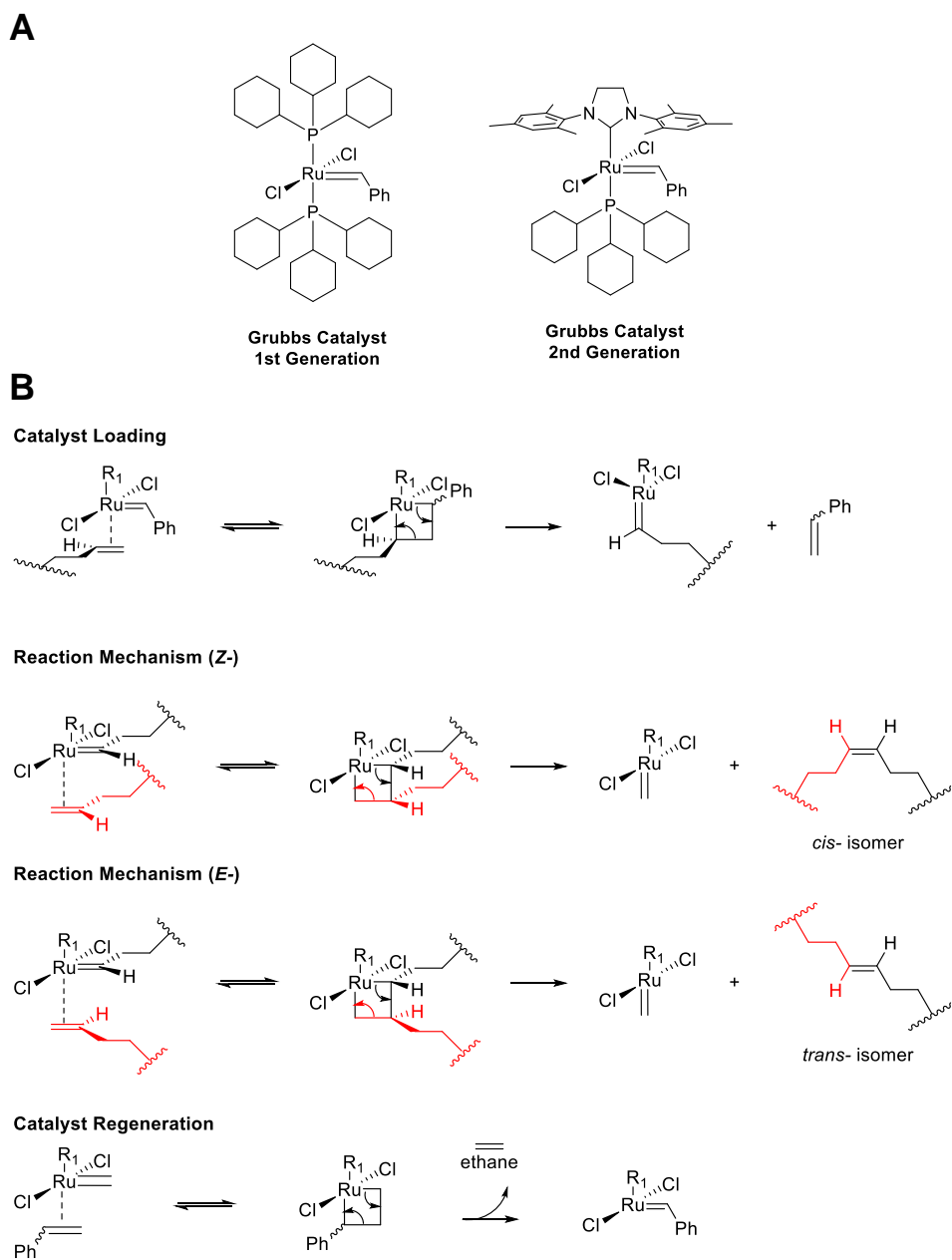


Figure 28. Ring closing metathesis. A) Grubbs Generation I and II catalysts for RCMs. B) RCM mechanism categorized into 3 steps: Catalyst loading, Reaction, and Catalyst Regeneration. The ligand *ortho*- to the ruthenium complex are tricyclohexylphosphine and N-heterocyclic carbenes for generation I and II, respectively.

competition of the free amine to the olefinic substrate binding site on the catalysts. The catalysts are light and moisture sensitive and suffer from a loss of RCM efficiency over time. Investigators use the Grubbs Catalyst generation I^{34, 42, 52, 69-70} and II⁷¹⁻⁷⁴ interchangeably depending on the

required reactivity and the reaction conditions. The reaction mechanism for both generation I and II catalysts are identical (**Figure 28B**), in which the phosphine group dissociates to yield a reactive 14–electron ruthenium complex that binds to the olefinic substrate. The kinetic superiority of generation II catalyst comes from the greater selectivity for binding to the olefinic substrates in the presence of this dissociated tricyclohexylphosphine group⁷⁵. The first olefinic substrate is loaded onto the catalyst, replacing the styrene group. And then, the second olefinic substrate forms a metallo–organic complex with the catalyst loaded with the first olefinic substrate, and the alkene bond cyclizes the two terminal olefins together. The catalyst is regenerated by releasing ethane as a by–product. The reaction mechanism clearly suggests the possibilities of forming a regioisomer mixture in the RCM depending on the olefinic substrate orientation (**Figure 28B**, *cis*– and *trans*– mechanism). In fact, Schaffmeister et al.³³ originally reported two separable HCS peptides with identical molecular mass for *i*, *i*+7 stapled RNase A peptide with distinct CD profiles (18% to 7%), indicating a significant difference in the alpha helix structure. Another study⁷³ reported different ratios of the double bond diastereomeric products upon using Grubbs Generation I catalyst and Generation II/Hoveyda–Grubbs catalyst. Douse et al.⁷⁰ confirmed the presence of *E*– and *Z*– isomers of different activities targeting *Plasmodium falciparum* myosin A (myoA)–myoA tail interacting protein. Verdine et al. also note that the RCM reactions will yield one major olefin isomer along with a minor isomer⁶⁸. The isomer ratio appears to be largely determined by the R1 group orthogonal to the olefinic substrate plane (**Figure 28B**), and to the flexibility and the length of the olefinic substrate⁷⁶. Unsurprisingly, the high plasticity and flexibility of mHCS peptides led to regioisomeric mixtures that was unobserved in the HCS peptides. *For the presented experiments, mHCS peptides were isolated and used as a regioisomeric mixture, and the resulting IC₅₀ was reported*

from this mixture. The further investigations into the isomers' isolation and characterizations are detailed in a later section (**Chapter 4.4**)

4.3.3 MHCS PEPTIDES

Encouraged by the potent inhibition displayed by the **4E-BP1** peptide, peptide **1** and peptide **5**, mHCS analogs of these peptide candidates were made (**Figure 29A**). RCM reactions were carried out using Grubbs Catalyst Generation I following the established protocol⁶⁸. Unfortunately, **mHCS-1** could not be further characterized due to the insufficient purity. All the

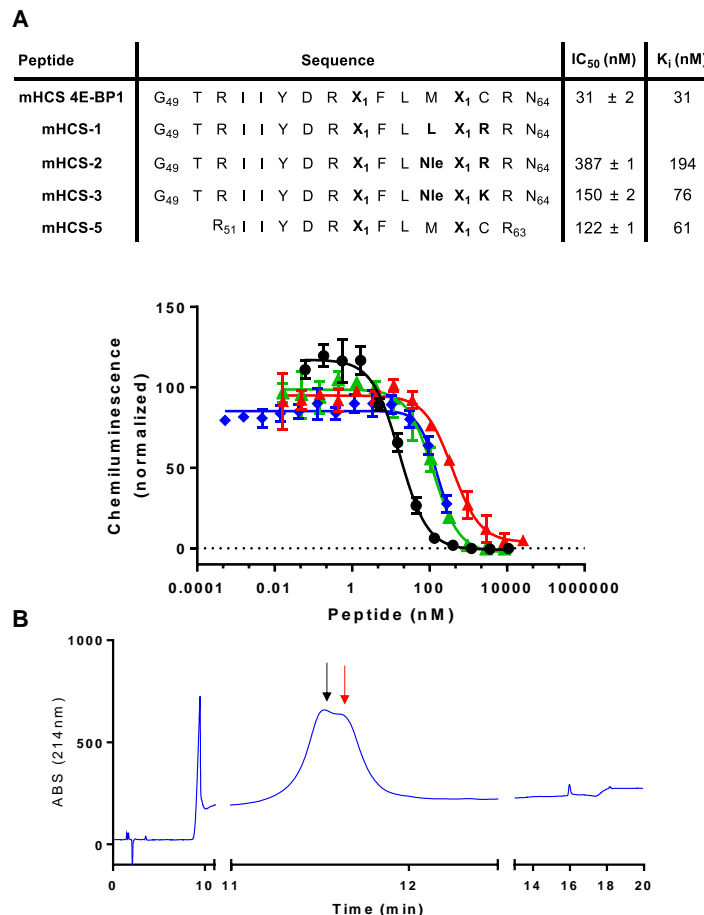


Figure 29. mHCS-4E-BP1. A) mHCS peptides of 4E-BP1, 1 – 3, and 5 and their *in vitro* inhibitory potency. mHCS-1 was not assayed due to the lack of purity. **mHCS 4E-BP1** (black), **mHCS-2** (red), **mHCS-3** (blue), and **mHCS-5** (green). B) analytical HPLC spectra of stock **mHCS 4E-BP1** purity confirmed by LC-MS. The dose-responsive curves were conducted in triplicates (n=3) and shown as the mean ± SD.

mHCS peptides carried a minimum of two closely eluting peaks (**Figure 29B**, rest LC spectra in appendix) with identical molecular mass. The close retention time and the molecular mass suggested that the co-eluting peaks were isomers of the desired mHCS peptides. Despite the known synthesis and isolations of regioisomeric HCS peptides, the finding of isomers in *i*, *i+4* positioned stapled peptides were surprising. While the mHCS peptides were designed specifically to contain the greater ligand sampling to target eIF4E (by having a more flexible hydrocarbon staple lacking the C_α methyl group), the reported regioisomers were only observed using the highly flexible unnatural amino acids positioned at *i*, *i+7* positions with long hydrocarbon linkers (8–9 methylene groups). The co-eluting peaks were inseparable despite the attempted HPLC purification method developments, re-synthesis and iterative purifications. For the initial PPI cat-ELCCA evaluations, the mHCS peptides were isolated, purified, and used after confirming purity through the LC-MS total ion count (TIC) spectra.

The failure to purify and isolate **mHCS-1** despite the repeated synthetic and purification attempts were discouraging given the inhibitory potency of peptide **1**. **mHCS 4E-BP1** was plagued by decreased aqueous solubility and difficult purifications, all without an improvement in its inhibitory potency (IC₅₀ = 31 ± 2 nM) compared to the **4E-BP1** peptide. **mHCS-5** had high aqueous solubility comparable to that of peptide **5** but suffered from a 17-fold loss in IC₅₀ (122 ± 1 nM); this poor translation of inhibitory potency from the linear peptides to the mHCS peptides led to the renewed attempts to evaluate **mHCS-2** and **mHCS-3**. Unfortunately, both **mHCS-2** and **mHCS-3** exhibited poor inhibitory potency in comparison to that of **mHCS 4E-BP1** with IC₅₀ of 387 ± 1 nM and 152 ± 2 nM, respectively. Although the mHCS peptides failed to elicit a significant improvement over their linear peptides in *in vitro* assays like PPI cat-ELCCA, the mHCS peptides could still have greater inhibitory effect in cell treatments due to

changes in cell permeability and peptide stability. **mHCS 4E-BP1** retained the inhibitory potency of **4E-BP1** peptide and was selected for further cellular treatment studies.

4.3.4 HCS PEPTIDES

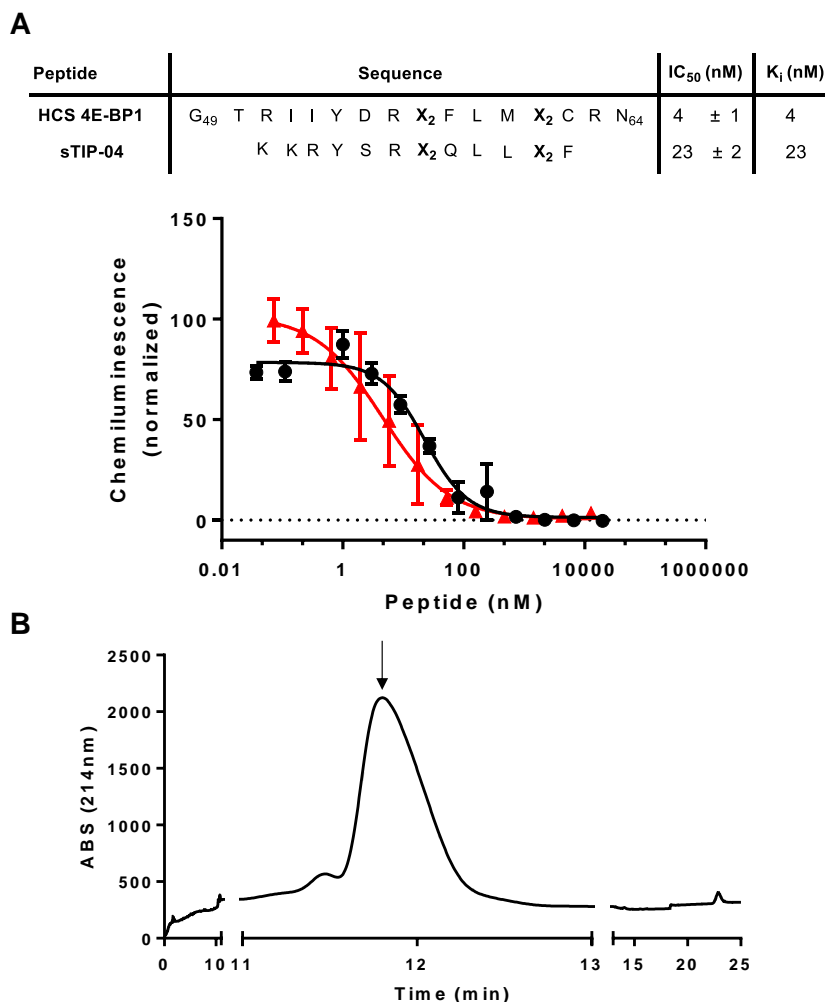


Figure 30. HCS peptides. A) HCS peptides of **4E-BP1**, and **sTIP-04** and the *in vitro* inhibitory potency. **HCS 4E-BP1** (black), **sTIP-04** (red). B) analytical HPLC spectra of stock **HCS 4E-BP1** purity confirmed by LC-MS. The dose-responsive curves were conducted in triplicates (n=3) and shown as the mean ± SD.

Encouraged by the potent inhibition of **4E-BP1** peptide and **mHCS 4E-BP1**, **HCS 4E-BP1** was synthesized and characterized (**Figure 30A**). **HCS-5** was not synthesized due to the observed loss in inhibitory potency of **mHCS-5**. **sTIP-04**, a reported eIF4G1 mimetic stapled

peptide⁷⁷, was also synthesized and characterized as a HCS peptide control. RCM reactions were carried out using Grubbs Catalyst Generation I following the established protocol⁶⁸. Contrary to the purifications of **mHCS 4E-BP1**, both **sTIP-04** and **HCS 4E-BP1** purifications were more facile, without significant HPLC purification method development and iterative purifications. Furthermore, both **sTIP-04** and **HCS 4E-BP1** eluted as one clearly defined peak (**Figure 30B**, the rest are available in appendix) and suggested the presence of just one isomer. **HCS 4E-BP1** was purposely designed to exhibit lesser ligand sampling to target eIF4E (by having a more rigid hydrocarbon staple due to the C_α methyl group); the increased rigidity likely limited ligand sampling during the RCM reaction as well, leading to the formation of the more favored Z-isomer. Unnatural amino acid (*S*)-2-(4'-pentenyl)alanine is the most commonly used to generate the HCS peptides; based on this evidence and on the lack of reports concerning the regioisomer formations of *i*, *i+4* positioned HCS peptides using (*S*)-2-(4'-pentenyl)alanine, regioisomeric mixtures may not be a notable problem in general HCS peptide studies.

In comparison to **mHCS 4E-BP1**, **HCS 4E-BP1** exhibited greater aqueous solubility (comparable to that of **4E-BP1** peptide). More importantly, **HCS 4E-BP1** exhibited greater than 7-fold increase in the inhibitory potency (IC₅₀ = 4 ± 1 nM) compared to the **4E-BP1** peptide. Although more studies are required to validate the nature of high and low ligand sampling in regard to disordered protein like 4E-BP1, the different inhibitory potencies of **mHCS 4E-BP1** and **HCS 4E-BP1** suggests that a low-ligand sampling, rigid α-helix mimetic resembling the bound 4E-BP1-eIF4E complex could be a better inhibitor. Extrapolating on this hypothesis, the difference between **mHCS 4E-BP1** and **HCS 4E-BP1** could suggest that 4E-BP1-eIF4E interaction may be driven by a “lock-and-key” like rather than an “induced-fit” like mechanism, and that the high plasticity of disordered proteins like 4E-BP1 may not be critical to mimic for

designing inhibitors and stapled peptides. Unsurprisingly, **sTIP-04** was also a potent inhibitor of 4E-BP1 – eIF4E interaction ($IC_{50} = 23 \pm 2$ nM) without the easily oxidized methionine and cysteines. However, **sTIP-04** is effective only as an *in vitro* control model due to its serum-binding properties and its limited use in cellular treatments.

4.3.5 CELLULAR TREATMENTS

The cellular efficacies and cellular penetrance of **4E-BP1** peptide, **mHCS 4E-BP1**, and **HCS 4E-BP1** were evaluated in MDA-MB-231 cells. MDA-MB-231 is a triple negative breast cancer cell line exhibiting overexpression of eIF4E and eIF4G in addition to 4E-BP1 hyperphosphorylation⁷⁸, and is a useful model cell line to evaluate the inhibition of eIF4E interactions. The cellular permeability of **4E-BP1**, **mHCS 4E-BP1**, and **HCS 4E-BP1** were evaluated through fluorescence assorted cytometry sorting (FACS)⁷⁸. The fluorescein-conjugated peptides were synthesized and purified; the N-terminal β -alanine residues prior to fluorescein provided a non-degradable linker to prevent TFA-induced degradation of the peptide⁷⁸. The resulting fluorescein tagged **4E-BP1**, **mHCS 4E-BP1**, and **HCS 4E-BP1** (labeled **f4E-BP1**, **fmHCS 4E-BP1**, **fhCS 4E-BP1**, respectively) were difficult to solubilize in aqueous media, easily prone to precipitation, and required dissolution in a solution of 1:2 DMF:H₂O v/v which limited the FACS assay concentration to 1.0 μ M. **f4E-BP1** peptide precipitated within minutes of contacting the cellular media, and therefore could not be analyzed through FACS (data not shown). **fhCS 4E-BP1** was found to readily enter MDA-MB-231 cells and exhibited a higher fluorescence intensity than the fluorescein control cells consistently over the replicates and re-synthesis (**Figure 31A**). Unfortunately, **fmHCS 4E-BP1** showed highly variable cell permeability between the biological replicate experiments and the re-synthesis, and its cell

penetration was determined to be inconclusive. The inconsistencies of **fmHCS 4E-BP1** FACS results may arise from the previously noted presence of regioisomers, and (or) sample dissolution and formulation. Despite the inconclusive cell penetration of **fmHCS 4E-BP1**, cellular efficacy treatments showed similar inhibitory potencies between **mHCS 4E-BP1** and **HCS 4E-BP1** in

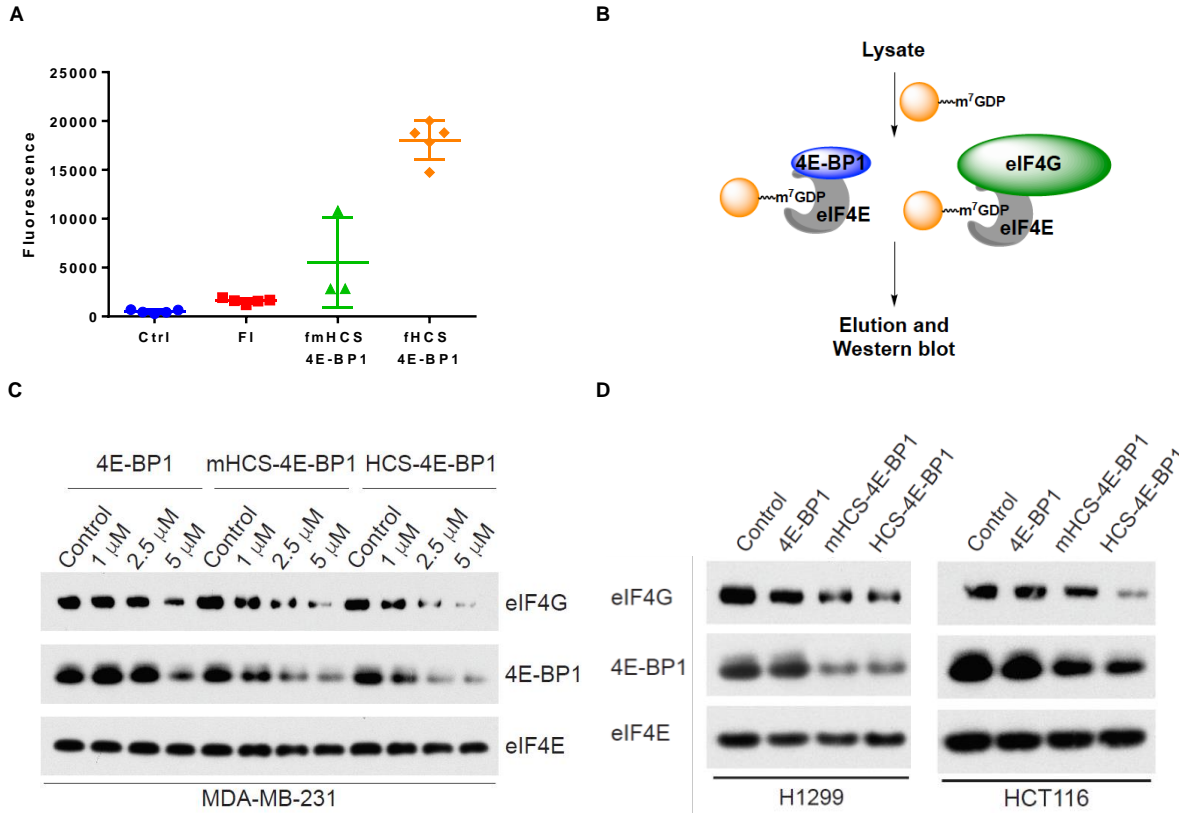


Figure 31. Cellular assays for mHCS and HCS peptides. A) Cellular permeability of FITC-labeled HCS-4E-BP1 as determined via flow cytometry (n = 3) in MDA-MB-231 cells. Cells were treated at 1 μM for 6 h. Ctrl: 1:2 DMF:H₂O v/v, FI: dichlorofluoresceine. B) Cellular inhibitory activities of the linear 4E-BP1 and **HCS-4E-BP1** peptides as determined via m⁷GDP cap affinity chromatography. Inhibition of the eIF4E-4E-BP1 and eIF4E-eIF4G PPIs in C) MDA-MB-231 cells, and (C) HCT116 cells (2.5 μM), and H1299 cells (2.5 μM). In all cases, cells were treated for 6 h and eIF4E was used as a normalization control.

m⁷GDP cap pull-down assay²⁸ (**Figure 31B**). The addition of hydrophobic fluoresceine and 2x β-alanines may have decreased solubility, induced aggregations, and altered net structure of **mHCS 4E-BP1**; alternatively, ChloroAlkane Penetration Assay developed by Kritzer and co-

workers²⁸ could measure the cellular penetrance of **mHCS 4E-BP1** by implementing a relatively minor chemical change to the peptide (a terminal chloro-alkane).

To test the inhibitory effect on eIF4E PPIs, cells were treated with varying concentrations of peptides and the resulting lysates were analyzed using a m⁷GDP cap pull-down assay. **4E-BP1** peptide showed a modest inhibition at the highest concentration tested (5 μM) likely due to its poor cellular uptake⁷⁹ (**Figure 31C**). Both **mHCS 4E-BP1** and **HCS 4E-BP1** exhibited greater inhibition of eIF4E interactions than **4E-BP1** peptide under the identical dosage, but similar efficacies as estimated by the band intensities of eIF4E bound eIF4G1 and 4E-BP1 (**Figure 31C**). Cellular inhibitory effects were analyzed on two additional cell lines that also exhibit hyperactivated CdT: HCT116 colorectal carcinoma cells⁷⁹ and H1299 non-small cell lung cancer cells (**Figure 31D**)⁷⁹. Similar to the results observed in MDA-MB-231 cells, **HCS 4E-BP1** showed promising activity in *both* cell lines, demonstrating its potential as a chemical probe for interrogating the eIF4E PPIs. This is particularly important, as the existing small molecule inhibitors of the eIF4E-eIF4G PPI, 4EGI-1⁷⁹ and 4E1RCat,⁷⁹ contain structural features that classify them as pan-assay interference compounds or PAINS⁷⁹⁻⁸⁰. **mHCS 4E-BP1** exhibited a limited potency in inhibiting the eIF4E interactions in colorectal carcinoma disease model. In lieu of the overall lower inhibitory efficacies, the difficult peptide preparations, and the inconsistent cellular permeability, **mHCS 4E-BP1** was concluded as an unreliable chemical probe for interrogating eIF4E PPIs. **HCS 4E-BP1** presents the first documented cell permeable HCS peptide targeting eIF4E PPIs that remain bio-active in presence of serum, and thus hold potential as a valuable probe targeting the CdT initiation.

4.4 HYDROCARBON STAPLED PEPTIDES: REGIOISOMERS

4.4.1 MHCS CASE STUDY

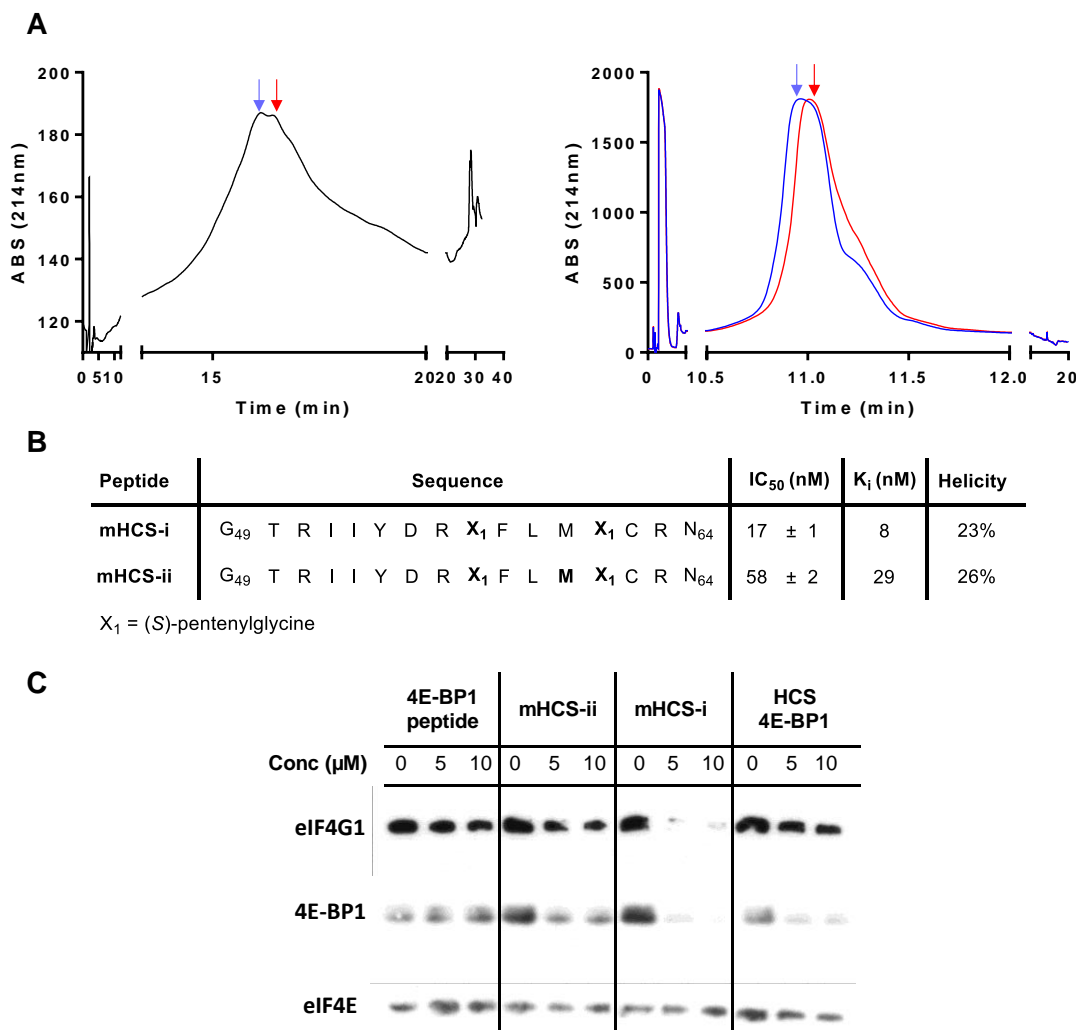


Figure 32. mHCS-4E-BP1 diastereomers. A) the semi-prep HPLC purification (left) and the analytical spectra (right) of **mHCS-i** (blue) and **mHCS-ii** (red) B) *in vitro* characterizations of **mHCS-i** and **mHCS-ii** by PPI cat-ELCCA (n=3) C) Cellular inhibitory activities of the **4E-BP1** peptide, **mHCS-i**, **mHCS-ii**, and **HCS 4E-BP1** as determined via m⁷GDP cap affinity chromatography in MDA-MB-231 cells. In all cases, cells were treated for 6 h and eIF4E was used as a normalization control.

As previously mentioned, all the mHCS peptides contained co-eluting peaks of identical molecular mass, and were hypothesized to be the regioisomers of *i*, *i+4* positioned hydrocarbon stapled peptides. Extensive semi-prep HPLC purification optimizations and repeated attempts to

force synthesis of one isomer over the other remained mostly unsuccessful. However, one such attempt led to two separated **mHCS 4E-BP1** regioisomers containing one early eluting isomer **mHCS-i** and later eluting **mHCS-ii** (Figure 32A). **mHCS-i** exhibited greater than 3-fold reduction in the IC_{50} in comparison to **mHCS-ii** despite the lack of difference in the intrinsic α -helicity as measured by CD (Figure 32B). Most surprisingly, **mHCS-i** exhibited a greater potency in cellular treatment than **mHCS-ii**, **4E-BP1** peptide, and **HCS 4E-BP1**, and had reduced eIF4E associated eIF4G1 and 4E-BP1 levels to completion at 5 μ M (Figure 32C). Encouraged by this result, further biophysical characterizations of **mHCS** regioisomers were

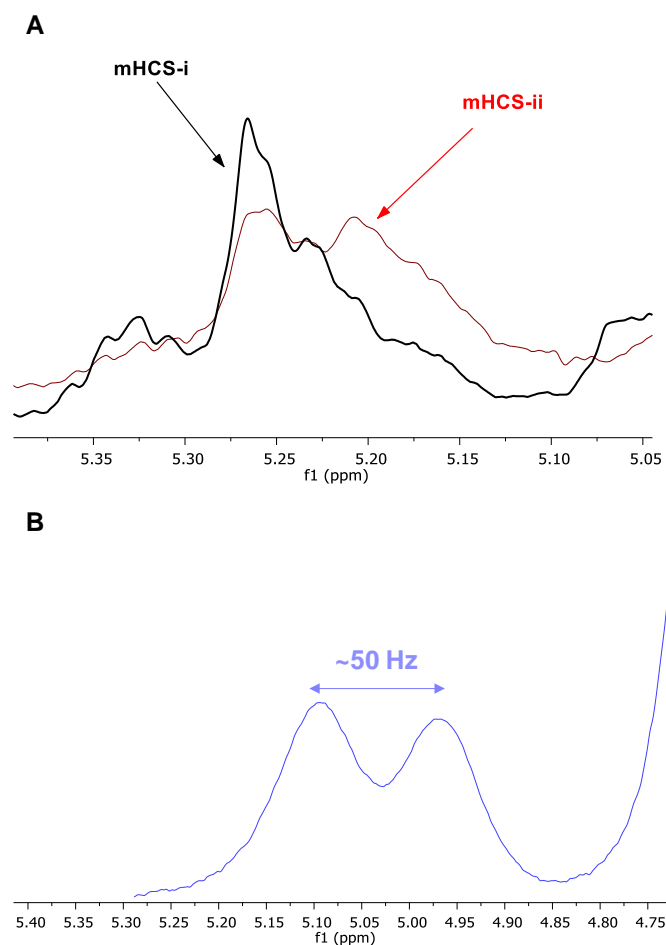


Figure 33. Peptide diastereomer NMR. A) Overlaid 1D NMR spectra of **mHCS-i** (black) and **mHCS-ii** (red). B) 1D NMR spectra of **HCS 4E-BP1** (blue). Significant water contamination and the poor solubility yielded in unresolved low signal olefinic peaks in all cases

pursued through NMR.

The literature shows that the chemical shifts and the coupling constants representative of the E- and Z- isomers^{70, 76, 81-83} are identified by 1D and/or a HOMO-decoupling NMR experiments selective for the adjacent methylene protons. **mHCS-i** and **mHCS-ii** NMR experiments were limited by the poor peptide solubility in water, DMSO, and other organic solvents which yielded low signal, unresolved peaks. And despite the extensive lyophilization and drying, water (δ 4.6) could not be removed thoroughly from the peptide sample and drowned the already low olefinic proton peak between δ 5.4 to δ 5.0. **mHCS-i** and **mHCS-ii** spectra could be overlaid almost perfectly on top of one another, with special exception at the olefinic proton region (**Figure 33A**). Measuring the crude coupling constants between the two dominant

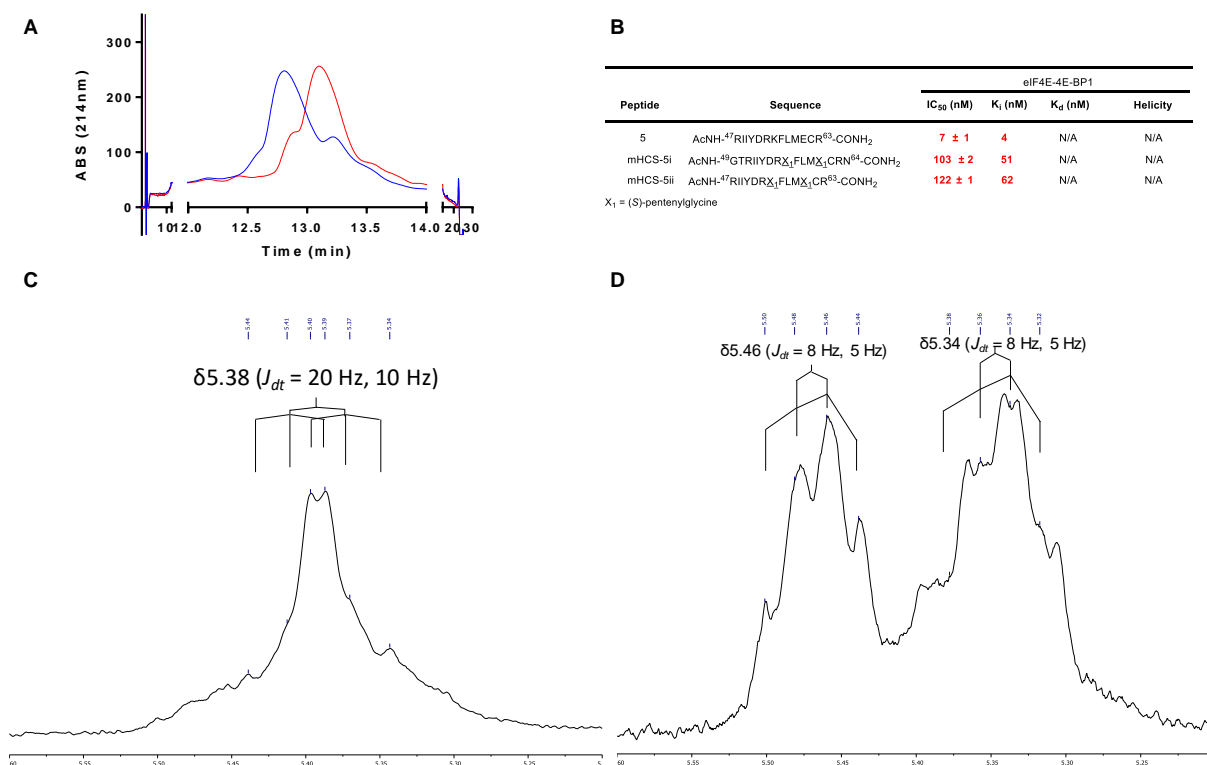


Figure 34. mHCS-5i and mHCS-5ii NMR. A) the analytical spectra of **mHCS-5i** (blue) and **mHCS-5ii** (red) B) *in vitro* characterizations of **mHCS-5i** and **mHCS-5ii** by PPI cat-ELCCA, and SPR (n=3). 1D NMR spectra and analysis of **mHCS-5i** (C) and **mHCS-5ii** (D) with alkene ³J_{HH} values of 20 Hz and 8 Hz, respectively.

peaks⁸²⁻⁸³ of **mHCS-ii** yielded 26 Hz that failed to fit neither *E*- nor *Z*- isomer and required a complex second-order splitting analysis for characterization. **HCS 4E-BP1** also lacked the exceptional aqueous, DMSO, and other solvent solubility to acquire a well resolved olefinic proton region and suffered from a similar water peak interference (**Figure 33B**). As expected, measuring the crude coupling constants between the two dominant peaks⁸²⁻⁸³ of **HCS 4E-BP1** yielded approx. 50 Hz that failed to fit neither *E*- nor *Z*- isomer, and again suggested that a more complex second-order splitting analysis was required for characterization.

Although **mHCS-5** lacked the *in vitro* inhibitory potency and the direct binding affinity, it yielded two isolatable isomers **mHCS-5i** (blue) and **mHCS-5ii** (red) in high purity that **mHCS 4E-BP1** had never achieved (**Figure 34A**). **mHCS-5i** and **mHCS-5ii** inhibitory potencies and direct binding affinities to eIF4E did not produce the stark difference that **mHCS-i** and **mHCS-ii** had exhibited (**Figure 34B**); however, the two isomers dissolved extremely well in deuterated acetic acid for NMR studies. The analysis of these well-resolved, complex second-order coupling multiplex representative of the olefinic protons indicated that **mHCS-5i** and **mHCS-5ii** were *E*- and *Z*- isomers with ³J_{HH} values of 20 Hz and 8 Hz, respectively (**Figure 34C, D**). The **mHCS-5** regioisomer case revealed that the two peptide isomers can be identified through 1D NMR with the high resolution, but these isomers may not necessary elicit different bioactivities. Thus, when the explicit differences are present between the peptide isomers' activities like for **mHCS-i** and **mHCS-ii**, a confirmation or an elimination of the isomers' impact in the difference is critical for further medicinal chemistry campaigns.

In attempts to establish a detailed systematic workflow to identify HCS peptide isomers, **sTIP-04** was used as a model peptide due to its extremely high aqueous solubility (> 5.0 mM) and the unreactive amino acid side chains. Since **sTIP-04** only had one peak in the analytical LC

spectrum, and in general, RCM reactions of *i, i+4* positioned olefinic acids favor *Z*- isomer⁸⁴, **sTIP-04** was hypothesized to be a *Z*- isomer. In order to simplify the complex second-order coupling of the olefin protons, homo-decoupling of the methylene protons during 1D NMR acquisition was attempted. First, double-quantum filtered COSY (dqfCOSY) experiment was performed on **sTIP-04** to identify the chemical shift regions in which the methylene protons coupling to the olefinic protons resided which was confirmed between δ 2.0 – 1.8 (**Figure 35A**). And then, a 1D homo-decoupling selective for the methylene protons at a chemical shift region of δ 2.0 – 1.8 (**Figure 35B**) showed a coupling value of 11 Hz between the two olefinic protons and confirmed that **sTIP-04** is indeed a *Z*- isomer. Unfortunately, neither **mHCS 4E-BP1** nor

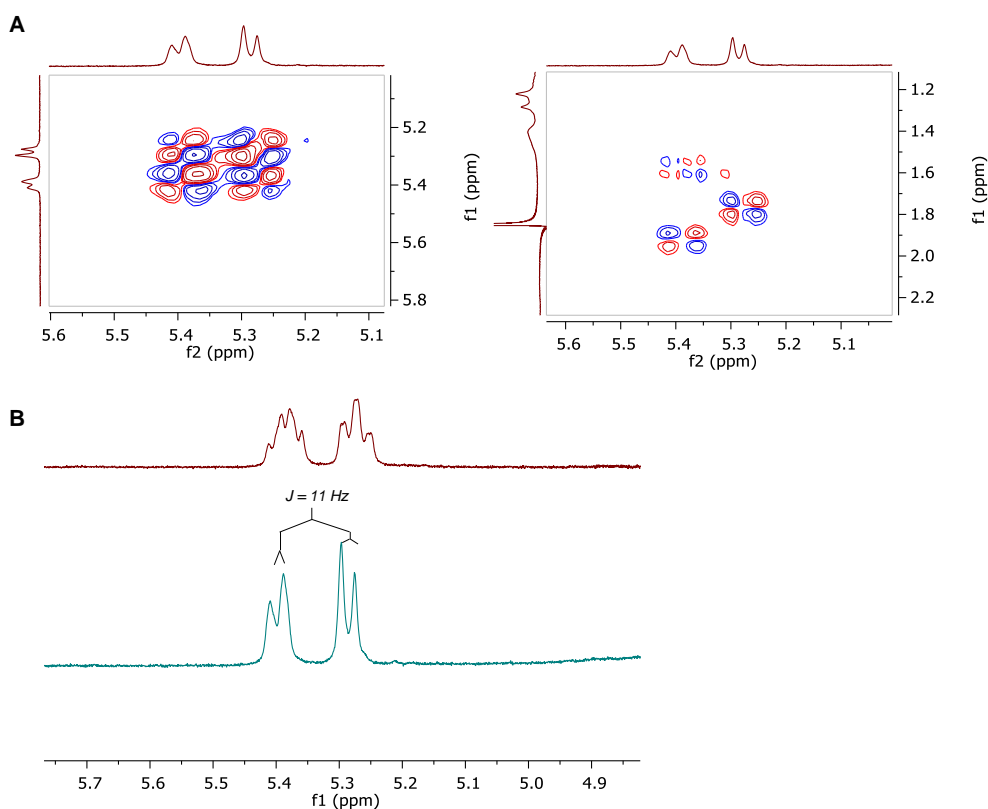


Figure 35. **sTIP-04** NMR. A) dqfCOSY 2D NMR of **sTIP-04**. The cross-peaks representative of the olefinic protons (δ 5.4 – 5.2) and of the coupling methylene protons (δ 1.95 – 1.8) were identified. B) Stacked **sTIP-04** 1D NMR (red) and homo-decoupling of the protons at a chemical shift of 2.0 – 1.8 ppm (blue) during the acquisition. The resulting coupling constant of 11 Hz suggest that **sTIP-04** is a *Z*- isomer.

HCS 4E–BP1 could be dissolved in sufficient concentration to achieve the high signal required for dqfCOSY and the representative crosspeaks of the methylene protons were drowned in the experimental noise. Since **HCS 4E–BP1** used identical olefinic unnatural amino acid as **sTIP–04** and was validated to contain just one peptide peak by HPLC, **HCS 4E–BP1** was hypothesized to be a *Z*– isomer and further experiments were not pursued to confirm the isomer. **mHCS 4E–BP1** was re–synthesized and the two diastereomeric peptides were isolated as a slight mixture for more extensive NMR studies. The peptides were designated **mHCS–i** and **mHCS–ii** based on the earlier and later elution retention time, respectively. Since dqfCOSY experiments required higher solubility than neither **mHCS–i** nor **mHCS–ii** could achieve, TOCSY was used to determine the approximate chemical shift region that the olefin coupling methylene protons resided in. **mHCS–ii** TOCSY indicated that the vinyl protons residing in the chemical shift region between δ 5.4 and δ 5.2 were coupling to the methylene protons H_a and H_b in δ 2.1 – δ 1.6, and δ 1.4 and δ 1.1, respectively (**Figure 36A**). However, the 1D homo-decoupling selective for the methylene protons at the chemical shift region of δ 2.1 – 1.6 failed to simplify the second–order coupling of the olefinic protons between δ 5.4 and δ 5.2 and the molecular structural determinations of **mHCS–i** and **mHCS–ii** were inconclusive (**Figure 36B**). Further attempts to identify and characterize **mHCS–i** and **mHCS–ii** were halted due to the difficulties in the sample preparation from the rapid methionine oxidation and peptide dimerization in the NMR acquisition condition (RT, ~36 h).

As a final attempt to simplify the **mHCS–i** and **mHCS–ii** synthesis and purification for cellular treatment studies, RCM reaction was performed using Grubbs Generation I and Generation II catalysts to synthesize **mHCS–G1** and **mHCS–G2**, respectively. Similar to the different ratios of the diastereomeric products upon using Grubbs Generation I catalyst and

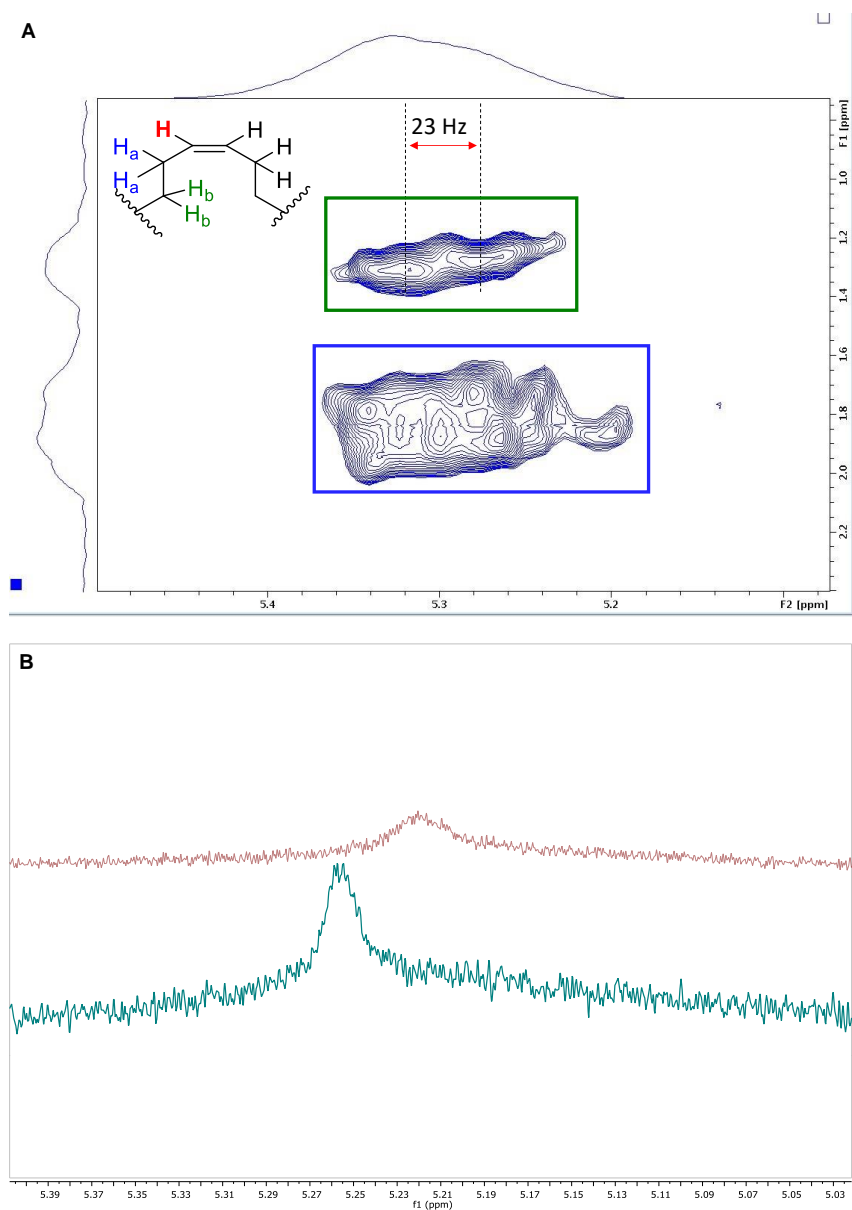


Figure 36. mHCS-ii NMR. A) TOCSY 2D NMR of **mHCS-ii**. The cross-peaks representative of the vinyl proton (δ 5.4 – δ 5.2) coupling methylene protons H_a (δ 2.1 – δ 1.6) and H_b (δ 1.4 – δ 1.1) were identified. B) Stacked **mHCS-ii** 1D NMR (red) and homo-decoupling of the protons at a chemical shift of 2.1– 1.6 ppm (blue) during the acquisition

Generation II/Hoveyda–Grubbs catalyst⁷³, the kinetic advantage of Generation II catalyst over the Generation I catalyst could shift the reaction equilibrium towards one isomer over the other and reproduce the previously observed *in vitro* properties of **mHCS-i** and **mHCS-ii**. Surprisingly, **mHCS-G1** was a mixture containing approx. equal amounts of the two co-eluting peaks while **mHCS-G2** yielded a mixture favoring the isomer with the later retention time

(Figure 37A). Contradictory to the previous results of **mHCS-i** and **mHCS-ii**, **mHCS-G2** that contained the late eluting peptide as the dominant isomer (similar to **mHCS-ii**) exhibited enhanced inhibitory potency (IC_{50} 14 ± 3 nM) and direct binding to eIF4E (K_d 19.1 ± 0.1 nM) over that of **mHCS-G1** (IC_{50} and K_d of 31 ± 5 nM and 28.2 ± 0.1 nM, respectively) (Figure 37B). Ultimately, the campaign to isolate and characterize the possible two isomers of **mHCS 4E-BP1** was terminated when **mHCS-G1** and **mHCS-G2** failed to reproduce the drastic difference in inhibiting the eIF4E interactions in cellular treatments (Figure 37C). The reported **mHCS 4E-BP1** studies (PPI cat-ELCCA, SPR, CD, cellular treatments, FACS) were completed using the regioisomeric mixtures unless otherwise noted.

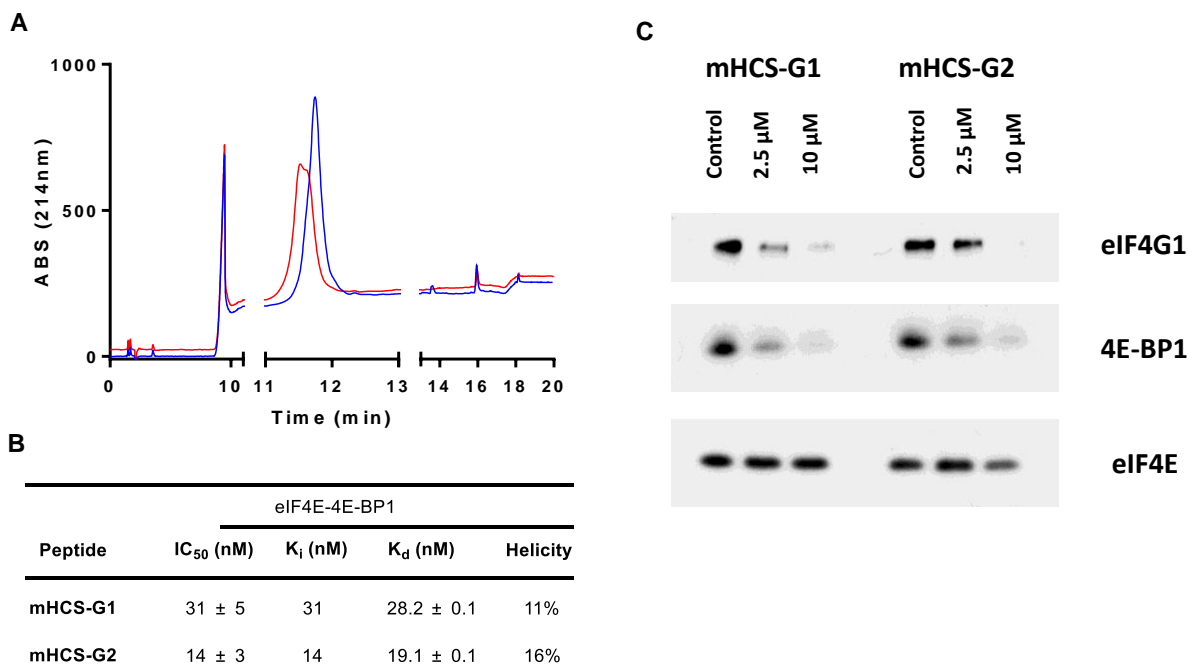


Figure 37. Investigation of Grubbs' catalysts. A) the analytical spectra of **mHCS-G1** (red) and **mHCS-G2** (blue), B) *in vitro* characterizations of **mHCS-G1** and **mHCS-G2** by PPI cat-ELCCA, SPR, and CD ($n=3$), C) Cellular inhibitory activities of **mHCS-G1** and **mHCS-G2** as determined via m^7 GDP cap affinity chromatography. Inhibition of the eIF4E-4E-BP1 and eIF4E-eIF4G PPIs in MDA-MB-231 cells. In all cases, cells were treated for 6 h and eIF4E was used as a normalization control.

4.4.3 SURFACE PLASMON RESONANCE AND CIRCULAR DICHROISM

A subset of notable peptides and isomers were selected for further biophysical characterizations through SPR and CD (**Table 3**, courtesy of Erin Gallagher). A detailed characterization of the peptide binding kinetics and their inherent α -helix structure could corroborate the critical differences between peptides representing induced fit binding model (**mHCS 4E-BP1**) and of conformational selection model (**HCS 4E-BP1**) in the disordered protein – ordered protein interactions. There is an on-going discussion on whether the interaction between an intrinsically disordered protein like 4E-BP1 and an ordered protein like eIF4E is mainly dictated by the increases in k_a ⁸⁵ similar to those observed between ordered proteins or by

Peptide	Sequence	k_a ($M^{-1} S^{-1}$)	k_d (S^{-1})	K_d (nM)	%Helicity (TFE)
4E-BP1	G ₄₉ T R I I Y D R K F L M E C R N ₆₄	$8.2 \pm 3 \times 10^5$	$2.1 \pm 0.4 \times 10^{-2}$	26 ± 6	16 ± 2 (37)
mHCS 4E-BP1	G ₄₉ T R I I Y D R X ₁ F L M X ₁ C R N ₆₄	$4.69 \pm 0.02 \times 10^5$	$1.127 \pm 0.002 \times 10^{-2}$	24.0 ± 0.1	11 ± 1 (38)
mHCS-G2	G ₄₉ T R I I Y D R X ₁ F L M X ₁ C R N ₆₄	$5.78 \pm 0.03 \times 10^5$	$8.60 \pm 0.02 \times 10^{-3}$	14.9 ± 0.1	16 ± 2 (51)
HCS 4E-BP1	G ₄₉ T R I I Y D R X ₂ F L M X ₂ C R N ₆₄	$1.5 \pm 0.2 \times 10^6$	$5 \pm 4 \times 10^{-3}$	4 ± 3	44 ± 7 (83)
5	R ₅₁ I I Y D R K F L M E C R ₆₃		N/A		16 (48)
mHCS-5i	R ₅₁ I I Y D R X ₁ F L M X ₁ C R ₆₃	$7.73 \pm 0.02 \times 10^4$	$6.66 \pm 0.01 \times 10^{-3}$	86.2 ± 0.3	6 ± 1 (31)
mHCS-5ii	R ₅₁ I I Y D R X ₁ F L M X ₁ C R ₆₃	$7.32 \pm 0.01 \times 10^4$	$5.276 \pm 0.008 \times 10^{-3}$	72.0 ± 0.2	7 ± 1 (31)

X₁ = (S)-pentenylglycine X₂ = (S)-pentenylalanine

Table 3. Peptides selected for further biophysical characterizations. Protocols for SPR and CD are detailed in appendix. **mHCS-5i** and **mHCS-5ii** were re-synthesized for SPR and CD experiments and were assigned label by the order of elution by LC. All the experiments were conducted in triplicates (n=3) and shown as the mean \pm SD.

the decreases in k_d ⁸⁵. Interestingly, **HCS 4E-BP1** displayed both an increase in k_a and a decrease in k_d from **4E-BP1** peptide suggesting a binding mechanism through a combination of conformational selection and an induced fit with fast folding upon binding. On the other hand, **mHCS 4E-BP1** suffered from a 2.3-fold reduction in k_a and a similar increase in k_d to maintain a comparative binding affinity to **4E-BP1** peptide, indicating that the greater ligand sampling had hindered the initial association of the disordered peptide to its target but allowed for a

stronger retention of the interaction. **HCS 4E-BP1** also had significant helical structure (approx. 4-fold) than **mHCS 4E-BP1** and confirmed that the conformational selection model had indeed benefited from increased helical structure. In general, the changes in peptide helicity correlated positively with the changes in binding affinity and inhibitory potency as observed from peptide **5** and **mHCS-5i** and **mHCS-5ii**, and **4E-BP1** peptide and **HCS 4E-BP1**.

Although the molecular analysis of **mHCS-G1** and **mHCS-G2** isomers were unsuccessful, both SPR and CD results indicate that the peptides were indeed different. **mHCS-G2** had comparable increase in k_d as **HCS 4E-BP1** and greater helicity than **mHCS 4E-BP1** and suggest that it may have similar molecular structure to **HCS 4E-BP1**. Despite the strong case that **mHCS 4E-BP1** and **mHCS-G2** are regioisomers, the difference in their bioactivities are minute and inconsistent. Similar analogs **mHCS-5i** and **mHCS-5ii** failed to exhibit differences in their bioactivities. Thus, although the regio-isomerizations of the mHCS peptides could indeed be a real phenomenon in **mHCS-G1** and **mHCS-G2**, and **mHCS-5i** and **mHCS-5ii**, the total isolation and characterizations of the two isomers may be unnecessary and labor intensive with little net benefits in the probe development.

4.5 CONCLUSION

The presented investigation into the impact of high and low ligand sampling – and in effect, the difference between induced fit binding model and the conformational selection model – using **mHCS 4E-BP1** and **HCS 4E-BP1**, respectively, indicate that the disordered 4E-BP1 – eIF4E interaction may largely follow the low ligand sampling conformational selection model. The greater structural plasticity of **mHCS 4E-BP1** resulted in comparable α -helicity structural composition, direct binding affinity, and inhibitory potency to **4E-BP1** peptide. Conversely, **HCS 4E-BP1** resulted in greater α -helicity structural composition, direct binding affinity, and

inhibitory potency than both **mHCS 4E-BP1** and **4E-BP1** peptide. The intrinsically disordered protein (IDP) dependent interactions like that of 4E-BP1 – eIF4E are widespread in biology and are involved in many important biological processes, and this investigation suggests that mimicking the plasticity of the interaction may be unnecessary in their biotherapeutics design.

The greater flexibility of the hydrocarbon linkers on mHCS peptides complicated the robust RCM reaction by producing a regioisomeric peptide mixtures. Their mere presence necessitates the (often) difficult HPLC purifications and molecular characterizations. And while the bioactivities of the regioisomeric peptides may be similar as in the cases of **mHCS-5i** and **mHCS-5ii**, or different as in the case of **mHCS-i** and **mHCS-ii**, the inconsistent generation of isomer mixture should caution further stapled peptide designs using (*S*)-2-(4'-pentenyl)glycine. Based on the findings of HCS peptides targeting the eIF4E interactions, the Garner group remains focused on identification and applications of other stapling strategies using lactam and disulfide formations to improve the cellular activity and permeability of 4E-BP1 peptides.

4.6 EXPERIMENTAL

4.6.1 GENERAL MATERIALS AND METHODS

General chemistry methods. RP-HPLC was performed using binary gradients of solvents A and B, where A is 0.1% HCO₂H in water and B is 0.1% HCO₂H in acetonitrile or 0.1% HCO₂H in methanol. Analytical RP-HPLC was performed using an Agilent 1260 Infinity HPLC equipped with a ZORBAX Eclipse SB-C18 column (4.6 × 150 mm; 5 μm) at a flow rate of 1 mL/min, with detection at 214 and 254 nm. Preparative RP-HPLC was performed using an Agilent 1260 Infinity HPLC equipped with a PrepHT SB-C18 column (21.2 × 150 mm; 5 μm) at a flow rate of 12.6 mL/min, with detection at 214 and 254 nm. In all cases, fractions were analyzed off-line

using Agilent Q–TOF HPLC–MS. Peptide stock concentrations were determined using amino acid analysis.

General assay and biology methods. SPR was performed using a SensiQ Pioneer instrument and a HisCap chip (three–dimensional hydrogel surface) with 3 channels in series. BL21DE3 *E. coli* were used for protein expression. CD spectra were recorded on a Jasco I–1500 CD–Spectropolarimeter. IC₅₀ values were determined using PPI cat–ELCCA as reported⁸⁵. Chemiluminescence data was collected on a BioTek Cytation3. Gels were imaged on a ProteinSimple Fluorchem M Gel Imager. MDA–MB–231 and H1299 cells were a kind gift from Dr. Nouri Neamati. HCT116 cells were a kind gift from Dr. Judy Sebolt–Leopold. MDA–MB–231 cells were grown in RPMI–1640 media supplemented with 10% FBS (Atlanta Biologicals), 2 mM glutamine and 1% penicillin–streptomycin. H1299 cells were grown in RPMI–1640 media supplemented with 10% FBS and 2 mM glutamine. HCT116 cells were grown in McCoy’s 5A media supplemented with 10% FBS and 2 mM glutamine. All cell lines were authenticated by STR profiling.

Data analysis. All data was analyzed using GraphPad Prism version 6.01 for Windows 10 (GraphPad Software, www.graphpad.com).

Materials. Fmoc–protected amino acids and Rink amide MBHA resin were purchased from P3 Biosystems and used as received. Fmoc–(S)–2–(4–pentenyl)glycine–OH and Fmoc–(S)–2–(4–pentenyl)alanine–OH were purchased from ArkPharm and used as received. Horseradish peroxidase (HRP), streptavidin–coated 384–well plates (white, high binding capacity; cat

#15505), and SuperSignal West Pico Chemiluminescent substrate kit for PPI cat-ELCCA were purchased from Pierce. eIF4E (9742), 4E-BP1 (9644) and eIF4G (2858) antibodies were purchased from Cell Signaling Technology.

General peptide synthesis methods. 4E-BP1 and eIF4G stapled peptides were synthesized on a 0.2-mmol scale in a 20-mL fritted syringe using MBHA Rink amide resin (0.2 – 0.4 mmol/g loading). In brief, the resin was swelled for 20 min at 25 °C in 1:1 DMF:DCM. Fmoc groups were removed following the addition of a 20% piperidine/DMF solution (10 mL) and gentle agitation for a total of 20 min at 25°C. After each Fmoc deprotection and amino acid couplings, the resin was thoroughly washed with NMP, CH₂Cl₂, and DMF. Amino acid couplings were performed by addition of amino acid (1 mmol) pre-activated with HBTU (0.9 mmol), *N,N*-diisopropylethylamine (2 mmol) in NMP (5 mL), and agitated for 2 – 3 h at 25 °C. The peptide was stapled on resin by bubbling nitrogen gas in DCE solution of Grubbs I or Grubbs II catalyst at 6 mM for at least two hours⁶⁸. The reaction was monitored through 10 – 20 mg resin test cleaves on the LC-MS. The procedure was repeated until the substrate had completely depleted in the LC-MS, usually for a total of three replicates. After stapling, the *N*-terminus was acetylated or modified with fluorescein isothiocyanate (FITC) (separated by 2 β-alanine residues), and the peptide was cleaved from the resin using TFA/thioanisole/water/triisopropylsilane (90:4:4:2) for 4 h at 25 °C. The resulting solution was added to glacial ether (~200 mL) for peptide precipitation. The precipitates were then collected, dissolved, and purified via RP-HPLC. Fractions containing the desired peptide were confirmed by LC-MS, lyophilized, re-dissolved in 1:1 acetic acid:water, and lyophilized again. The non-fluoresceine labeled peptides were dissolved in de-gassed H₂O. Fluoresceine

labeled peptides were dissolved in de-gassed 1:2 DMF:H₂O v/v solution. All peptide stock solutions were centrifugal filtered (PVDF) prior to use. **mHCS-i**, **mHCS-ii**, **HCS 4E-BP1**, **mHCS-5i**, and **mHCS-5ii** NMR spectra were recorded on Varian 500MHz and Bruker DRX 600 MHz instrument.

4.6.2 CELLULAR TREATMENTS

Preparation of m⁷GDP resin. m⁷GDP resin synthesis was adapted from that reported⁸⁶. m⁷GDP sodium salt (2.3 mg; Sigma) was dissolved in water (500 µL), and a solution of sodium periodate (1.1 mg) in sodium acetate buffer (100 µL; 0.1M, pH 6) was added. The resulting mixture was agitated at room temperature for 30 min protected from light. Adipic acid dihydrazide agarose (1 mL packed; Sigma) was washed with water (1× 20 mL) followed by sodium acetate buffer (1× 20mL), and then re-suspended in sodium acetate buffer (2 mL). To this slurry was added with aniline (10 µL) and the oxidized m⁷GDP solution. The resin mixture was then shaken at room temperature for 45 min before adding sodium cyanoborohydride (5 mg) and agitated overnight at 4 °C. The resin was washed with NaCl (1M; 5× 5 mL), equilibrated in buffer A (5 mL; 50 mM HEPES, pH 7, 200 mM KCl), and stored at 4 °C.

m⁷G cap affinity assay. The cap pull-down assay was carried out as previously described⁸⁷. Briefly, MDA-MB-231, HCT116, and H1299 cells were grown in 6-cm dishes and treated with peptides for 6 h. Cells were then lysed in cap pull-down buffer (50 mM HEPES-KOH (pH 7.5), 150 mM KCl, 1 mM EDTA, 2 mM DTT and 0.1% Tween 20) containing protease inhibitors. Cell lysate was centrifuged at 15,000 rpm for 25 min. The supernatant was subsequently incubated for 2 h at 4 °C with m⁷GDP-agarose resin. Beads were washed 3× with the cap pull-

down buffer, 1× with TBS and 1× with water. Proteins were eluted by boiling in 2× LDS sample buffer for 10 min at 70 °C, resolved on a 4–12% Bis–Tris gel, and transferred to PVDF membrane in Towbin’s Buffer. The membrane was blocked in 5% milk for 1 h at 25 °C, and then incubated with a primary antibody (overnight at 4 °C) and secondary antibody (1 h at 25 °C). Proteins were visualized by autoradiography. In all cases, the eIF4E level was used for normalization.

Flow cytometry. MDA–MB–231 cells were grown in 6–well plates and treated with peptides at 1.0 µM for 6 h. Cells were harvested with trypsin and washed once with ice–cold 1× PBS. The cells were then re–suspended in 300 µl of ice–cold 1× PBS, and 1 µl of 50 µg/mL propidium iodide (Sigma) was added and incubated for 10 min. Cells were then filtered before acquiring data using a Cytoflex flow cytometer (Beckman). Median cell fluorescence of propidium iodide negative cells was determined using FlowJo (v10).

4.7 CHAPTER IV REFERENCES

1. Lama, D.; Quah, S. T.; Verma, C. S.; Lakshminarayanan, R.; Beuerman, R. W.; Lane, D. P.; Brown, C. J., Rational Optimization of Conformational Effects Induced By Hydrocarbon Staples in Peptides and their Binding Interfaces. **2013**, *3*, 3451.
2. Zhou, W.; Quah, S. T.; Verma, C. S.; Liu, Y.; Lane, D. P.; Brown, C. J., Improved eIF4E Binding Peptides by Phage Display Guided Design: Plasticity of Interacting Surfaces Yield Collective Effects. *PLOS ONE* **2012**, *7* (10), e47235.
3. Dennis, M. S.; Zhang, M.; Meng, Y. G.; Kadkhodayan, M.; Kirchhofer, D.; Combs, D.; Damico, L. A., Albumin Binding as a General Strategy for Improving the Pharmacokinetics of Proteins. *Journal of Biological Chemistry* **2002**, *277* (38), 35035-35043.
4. Knudsen, L. B., Liraglutide: the therapeutic promise from animal models. *International Journal of Clinical Practice* **2010**, *64*, 4-11.
5. Delgado, C.; Francis, G. E.; Fisher, D., The uses and properties of PEG-linked proteins. *Critical Reviews in Therapeutic Drug Carrier Systems* **1992**, *9* (3-4), 249-304.

6. Zorzi, A.; Middendorp, S. J.; Wilbs, J.; Deyle, K.; Heinis, C., Acylated heptapeptide binds albumin with high affinity and application as tag furnishes long-acting peptides. *Nature Communications* **2017**, *8*, 16092.
7. Bliss, M., *Discovery of Insulin*. 1982.
8. Henninot, A.; Collins, J. C.; Nuss, J. M., The Current State of Peptide Drug Discovery: Back to the Future? *Journal of Medicinal Chemistry* **2017**.
9. Fosgerau, K.; Hoffmann, T., Peptide therapeutics: current status and future directions. *Drug Discovery Today* **2015**, *20* (1), 122-128.
10. Kaspar, A. A.; Reichert, J. M., Future directions for peptide therapeutics development. *Drug Discov Today* **2013**, *18* (17-18), 807-17.
11. Di, L., Strategic approaches to optimizing peptide ADME properties. *AAPS J.* **2015**, *17*, 134.
12. Aktas, B. H.; Halperin, J. A.; Wagner, G.; Chorev, M., Chapter 12 - Inhibition of Translation Initiation as a Novel Paradigm for Cancer Therapy. In *Annual Reports in Medicinal Chemistry*, Macor, J. E., Ed. Academic Press: 2011; Vol. 46, pp 189-210.
13. Matsuo, H.; Li, H.; McGuire, A. M.; Fletcher, C. M.; Gingras, A.-C.; Sonenberg, N.; Wagner, G., Structure of translation factor eIF4E bound to m7GDP and interaction with 4E-binding protein. *Nature Structural Biology* **1997**, *4*, 717.
14. Marcotrigiano, J.; Gingras, A.-C.; Sonenberg, N.; Burley, S. K., Cap-dependent translation initiation in eukaryotes is regulated by a molecular mimic of eIF4G. *Molecular cell* **1999**, *3* (6), 707-716.
15. Herbert, T. P.; Fåhræus, R.; Prescott, A.; Lane, D. P.; Proud, C. G., Rapid induction of apoptosis mediated by peptides that bind initiation factor eIF4E. *Current Biology* **2000**, *10* (13), 793-796.
16. Brown, C. J.; Lim, J. J.; Leonard, T.; Lim, H. C. A.; Chia, C. S. B.; Verma, C. S.; Lane, D. P., Stabilizing the eIF4G1 α -Helix Increases Its Binding Affinity with eIF4E: Implications for Peptidomimetic Design Strategies. *Journal of Molecular Biology* **2011**, *405* (3), 736-753.
17. Ko, S. Y.; Guo, H.; Barengo, N.; Naora, H., Inhibition of Ovarian Cancer Growth by a Tumor-Targeting Peptide That Binds Eukaryotic Translation Initiation Factor 4E. *Clinical Cancer Research* **2009**, *15* (13), 4336-4347.
18. Guharoy, M.; Chakrabarti, P., Secondary structure based analysis and classification of biological interfaces: identification of binding motifs in protein–protein interactions. *Bioinformatics* **2007**, *23* (15), 1909-1918.

19. Shepherd, N. E.; Hoang, H. N.; Abbenante, G.; Fairlie, D. P., Single Turn Peptide Alpha Helices with Exceptional Stability in Water. *Journal of the American Chemical Society* **2005**, *127* (9), 2974-2983.
20. Harrison, R. S.; Shepherd, N. E.; Hoang, H. N.; Ruiz-Gómez, G.; Hill, T. A.; Driver, R. W.; Desai, V. S.; Young, P. R.; Abbenante, G.; Fairlie, D. P., Downsizing human, bacterial, and viral proteins to short water-stable alpha helices that maintain biological potency. *Proc. Natl. Acad. Sci. U.S.A.* **2010**, *107*, 11686.
21. Harrison, R. S.; Ruiz-Gómez, G.; Hill, T. A.; Chow, S. Y.; Shepherd, N. E.; Lohman, R.-J.; Abbenante, G.; Hoang, H. N.; Fairlie, D. P., Novel Helix-Constrained Nociceptin Derivatives Are Potent Agonists and Antagonists of ERK Phosphorylation and Thermal Analgesia in Mice. *Journal of Medicinal Chemistry* **2010**, *53* (23), 8400-8408.
22. Moses, J. E.; Moorhouse, A. D., The growing applications of click chemistry. *Chemical Society Reviews* **2007**, *36* (8), 1249-1262.
23. Presolski, S. I.; Hong, V. P.; Finn, M. G., Copper-catalyzed azide-alkyne click chemistry for bioconjugation. *Curr. Protoc. Chem. Biol.* **2011**, *3*, 153.
24. Cantel, S.; Isaad, A. L. C.; Scrima, M.; Levy, J. J.; DiMarchi, R. D.; Rovero, P.; Halperin, J. A.; D'Ursi, A. M.; Papini, A. M.; Chorev, M., Synthesis and conformational analysis of a cyclic peptide obtained via i to i+4 intramolecular side-chain to side-chain azide - Alkyne 1,3-dipolar cycloaddition. *J. Org. Chem.* **2008**, *73*, 5663.
25. Scrima, M.; Chevalier - Isaad, A. L.; Rovero, P.; Papini, A. M.; Chorev, M.; D'Ursi, A. M., CuI - Catalyzed Azide-Alkyne Intramolecular i - to - (i+4) Side - Chain - to - Side - Chain Cyclization Promotes the Formation of Helix - Like Secondary Structures. *European Journal of Organic Chemistry* **2010**, *2010* (3), 446-457.
26. Kawamoto, S. A.; Coleska, A.; Ran, X.; Yi, H.; Yang, C. Y.; Wang, S. M., Design of triazole-stapled BCL9 alpha-helical peptides to target the beta-catenin/B-cell CLL/lymphoma 9 (BCL9) protein-protein interaction. *J. Med. Chem.* **2012**, *55*, 1137.
27. Wu, Y.; Villa, F.; Maman, J.; Lau, Y. H.; Dobnikar, L.; Simon, A. C.; Labib, K.; Spring, D. R.; Pellegrini, L., Targeting the Genome - Stability Hub Ctf4 by Stapled - Peptide Design. *Angewandte Chemie International Edition* **2017**, *56* (42), 12866-12872.
28. Peraro, L.; Zou, Z.; Makwana, K. M.; Cummings, A. E.; Ball, H. L.; Yu, H.; Lin, Y.-S.; Levine, B.; Kritzer, J. A., Diversity-Oriented Stapling Yields Intrinsically Cell-Penetrant Inducers of Autophagy. *Journal of the American Chemical Society* **2017**, *139* (23), 7792-7802.
29. Brunel, F. M.; Dawson, P. E., Synthesis of constrained helical peptides by thioether ligation: application to analogs of gp41. *Chemical Communications* **2005**, (20), 2552-2554.

30. Peter, T.; Joris, B.; C., P. W.; H., M. R., Rapid and Quantitative Cyclization of Multiple Peptide Loops onto Synthetic Scaffolds for Structural Mimicry of Protein Surfaces. *ChemBioChem* **2005**, *6* (5), 821-824.
31. Jo, H.; Meinhardt, N.; Wu, Y.; Kulkarni, S.; Hu, X.; Low, K. E.; Davies, P. L.; DeGrado, W. F.; Greenbaum, D. C., Development of α -Helical Calpain Probes by Mimicking a Natural Protein-Protein Interaction. *Journal of the American Chemical Society* **2012**, *134* (42), 17704-17713.
32. Blackwell, H. E.; Grubbs, R. H., Highly Efficient Synthesis of Covalently Cross-Linked Peptide Helices by Ring-Closing Metathesis. *Angew. Chem., Int. Ed. Engl.* **1998**, *37*, 3281.
33. Schafmeister, C. E.; Po, J.; Verdine, G. L., An All-Hydrocarbon Cross-Linking System for Enhancing the Helicity and Metabolic Stability of Peptides. *Journal of the American Chemical Society* **2000**, *122* (24), 5891-5892.
34. Walensky, L. D.; Kung, A. L.; Escher, I.; Malia, T. J.; Barbuto, S.; Wright, R. D.; Wagner, G.; Verdine, G. L.; Korsmeyer, S. J., Activation of Apoptosis in Vivo by a Hydrocarbon-Stapled BH3 Helix. *Science* **2004**, *305* (5689), 1466-1470.
35. Verdine, G. L.; Walensky, L. D., The Challenge of Drugging Undruggable Targets in Cancer: Lessons Learned from Targeting BCL-2 Family Members. *Clin. Cancer. Res.* **2007**, *13*, 7264.
36. Lau, Y. H.; de Andrade, P.; Wu, Y.; Spring, D. R., Peptide stapling techniques based on different macrocyclisation chemistries. *Chemical Society Reviews* **2015**, *44* (1), 91-102.
37. Tian, Y.; Jiang, Y.; Li, J.; Wang, D.; Zhao, H.; Li, Z., Effect of Stapling Architecture on Physicochemical Properties and Cell Permeability of Stapled α - Helical Peptides: A Comparative Study. *ChemBioChem* **2017**, *18* (21), 2087-2093.
38. Chang, Y. S.; Graves, B.; Guerlavais, V.; Tovar, C.; Packman, K.; To, K.-H.; Olson, K. A.; Kesavan, K.; Gangurde, P.; Mukherjee, A.; Baker, T.; Darlak, K.; Elkin, C.; Filipovic, Z.; Qureshi, F. Z.; Cai, H.; Berry, P.; Feyfant, E.; Shi, X. E.; Horstick, J.; Annis, D. A.; Manning, A. M.; Fotouhi, N.; Nash, H.; Vassilev, L. T.; Sawyer, T. K., Stapled α -helical peptide drug development: A potent dual inhibitor of MDM2 and MDMX for p53-dependent cancer therapy. *Proceedings of the National Academy of Sciences* **2013**, *110* (36), E3445-E3454.
39. Bhattacharya, S.; Zhang, H.; Debnath, A. K.; Cowburn, D., Solution Structure of a Hydrocarbon Stapled Peptide Inhibitor in Complex with Monomeric C-terminal Domain of HIV-1 Capsid. *J. Biol. Chem.* **2008**, *283*, 16274.
40. Mitra, S.; Montgomery, J. E.; Kolar, M. J.; Li, G.; Jeong, K. J.; Peng, B.; Verdine, G. L.; Mills, G. B.; Moellering, R. E., Stapled peptide inhibitors of RAB25 target context-specific phenotypes in cancer. *Nature Communications* **2017**, *8* (1), s41467-017.
41. Wang, Y.; Ho, T. G.; Bertinetti, D.; Neddermann, M.; Franz, E.; Mo, G. C. H.; Schendowich, L. P.; Sukhu, A.; Spelts, R. C.; Zhang, J.; Herberg, F. W.; Kennedy, E. J.,

- Isoform-selective disruption of AKAP-localized PKA using hydrocarbon stapled peptides. *ACS Chem. Biol.* **2014**, *9*, 635.
42. Moellering, R. E.; Cornejo, M.; Davis, T. N.; Bianco, C. D.; Aster, J. C.; Blacklow, S. C.; Kung, A. L.; Gilliland, D. G.; Verdine, G. L.; Bradner, J. E., Direct inhibition of the NOTCH transcription factor complex. *Nature* **2009**, *462* (7270), 182-188.
43. Kim, W.; Bird, G. H.; Neff, T.; Guo, G.; Kerenyi, M. A.; Walensky, L. D.; Orkin, S. H., Targeted disruption of the EZH2–EED complex inhibits EZH2-dependent cancer. **2013**, *9*, 643.
44. Tan, J. z.; Yan, Y.; Wang, X. x.; Jiang, Y.; Xu, H. E., EZH2: biology, disease, and structure-based drug discovery. *Acta Pharmacol. Sin.* **2014**, *35*, 161.
45. Spokoyny, A. M.; Zou, Y.; Ling, J. J.; Yu, H.; Lin, Y.-S.; Pentelute, B. L., A Perfluoroaryl-Cysteine SNAr Chemistry Approach to Unprotected Peptide Stapling. *Journal of the American Chemical Society* **2013**, *135* (16), 5946-5949.
46. Fadzen, C. M.; Wolfe, J. M.; Cho, C.-F.; Chiocca, E. A.; Lawler, S. E.; Pentelute, B. L., Perfluoroarene–Based Peptide Macrocycles to Enhance Penetration Across the Blood–Brain Barrier. *Journal of the American Chemical Society* **2017**, *139* (44), 15628-15631.
47. Patgiri, A.; Jochim, A. L.; Arora, P. S., A Hydrogen Bond Surrogate Approach for Stabilization of Short Peptide Sequences in α -Helical Conformation. *Accounts of Chemical Research* **2008**, *41* (10), 1289-1300.
48. Henchey, L. K.; Kushal, S.; Dubey, R.; Chapman, R. N.; Olenyuk, B. Z.; Arora, P. S., Inhibition of Hypoxia Inducible Factor 1—Transcription Coactivator Interaction by a Hydrogen Bond Surrogate α -Helix. *Journal of the American Chemical Society* **2010**, *132* (3), 941-943.
49. Henchey, L. K.; Porter, J. R.; Ghosh, I.; Arora, P. S., High specificity in protein recognition by hydrogen-bond-surrogate alpha-helices: selective inhibition of the p53/MDM2 complex. *ChemBioChem* **2010**, *11*, 2104.
50. Patgiri, A.; Yadav, K. K.; Arora, P. S.; Bar-Sagi, D., An orthosteric inhibitor of the Ras-Sos interaction. *Nat. Chem. Biol.* **2011**, *7*, 585.
51. Brown, C. J.; Quah, S. T.; Jong, J.; Goh, A. M.; Chiam, P. C.; Khoo, K. H.; Choong, M. L.; Lee, M. A.; Yurlova, L.; Zolghadr, K.; Joseph, T. L.; Verma, C. S.; Lane, D. P., Stapled peptides with improved potency and specificity that activate p53. *ACS Chem. Biol.* **2013**, *8*, 506.
52. Bernal, F.; Tyler, A. F.; Korsmeyer, S. J.; Walensky, L. D.; Verdine, G. L., Reactivation of the p53 Tumor Suppressor Pathway by a Stapled p53 Peptide. *J. Am. Chem. Soc.* **2007**, *129*, 2456.
53. Yeo, D. J.; Warriner, S. L.; Wilson, A. J., Monosubstituted alkenyl amino acids for peptide "stapling". *Chemical Communications* **2013**, *49* (80), 9131-9133.

54. Walensky, L. D.; Pitter, K.; Morash, J.; Oh, K. J.; Barbuto, S.; Fisher, J.; Smith, E.; Verdine, G. L.; Korsmeyer, S. J., A Stapled BID BH3 Helix Directly Binds and Activates BAX. *Mol. Cell* **2006**, *24*, 199.
55. Chu, Q.; Moellering, R. E.; Hilinski, G. J.; Kim, Y. W.; Grossmann, T. N.; Yeh, J. T. H.; Verdine, G. L., Towards understanding cell penetration by stapled peptides. *Med. Chem. Commun.* **2015**, *6*, 111.
56. BROWN, C. J.-C., Singapore 2, 13863, SG), LANE, David Philip (#20-10 Connexis, Singapore 2, 13863, SG), QUAH, Soo Tng (#20-10 Connexis, Singapore 2, 13863, SG), LAMA, Dilraj (#20-10 Connexis, Singapore 2, 13863, SG), VERMA, Chandra Shekhar (#20-10 Connexis, Singapore 2, 13863, SG) STAPLING eIF4E INTERACTING PEPTIDES. 2014.
57. Michael, J. B.; Tracey, H. C., Plasma / Serum Protein Binding Determinations. *Current Drug Metabolism* **2008**, *9* (9), 854-859.
58. Thean, D.; Ebo, J. S.; Luxton, T.; Lee, X. E. C.; Yuen, T. Y.; Ferrer, F. J.; Johannes, C. W.; Lane, D. P.; Brown, C. J., Enhancing Specific Disruption of Intracellular Protein Complexes by Hydrocarbon Stapled Peptides Using Lipid Based Delivery. *Scientific Reports* **2017**, *7*, 1763.
59. Jiang, H.; Coleman, J.; Miskimins, R.; Miskimins, W. K., Expression of constitutively active 4EBP-1 enhances p27Kip1 expression and inhibits proliferation of MCF7 breast cancer cells. *Cancer Cell International* **2003**, *3* (1), 2.
60. Polunovsky, V. A.; Gingras, A.-C.; Sonenberg, N.; Peterson, M.; Tan, A.; Rubins, J. B.; Manivel, J. C.; Bitterman, P. B., Translational Control of the Antiapoptotic Function of Ras. *Journal of Biological Chemistry* **2000**, *275* (32), 24776-24780.
61. Jacobson, B. A.; Alter, M. D.; Kratzke, M. G.; Frizelle, S. P.; Zhang, Y.; Peterson, M. S.; Avdulov, S.; Mohorn, R. P.; Whitson, B. A.; Bitterman, P. B.; Polunovsky, V. A.; Kratzke, R. A., Repression of Cap-Dependent Translation Attenuates the Transformed Phenotype in Non-Small Cell Lung Cancer Both *In vitro* and *In vivo*. *Cancer Research* **2006**, *66* (8), 4256-4262.
62. Grüner, S.; Peter, D.; Weber, R.; Wohlbold, L.; Chung, M.-Y.; Weichenrieder, O.; Valkov, E.; Igreja, C.; Izaurralde, E., The Structures of eIF4E-eIF4G Complexes Reveal an Extended Interface to Regulate Translation Initiation. *Molecular Cell* **64** (3), 467-479.
63. Mader, S.; Lee, H.; Pause, A.; Sonenberg, N., The translation initiation factor eIF-4E binds to a common motif shared by the translation factor eIF-4[gamma] and the translational repressors 4E-binding proteins. *Mol. Cell. Biol.* **1995**, *15*, 4990-4997.
64. Marcotrigiano, J.; Gingras, A.-C.; Sonenberg, N.; Burley, S. K., Cocystal Structure of the Messenger RNA 5' Cap-Binding Protein (eIF4E) Bound to 7-methyl-GDP. *Cell* **1997**, *89* (6), 951-961.
65. Tsukiyama-Kohara, K.; Vidal, S. M.; Gingras, A.-C.; Glover, T. W.; Hanash, S. M.; Heng, H.; Sonenberg, N., Tissue Distribution, Genomic Structure, and Chromosome Mapping of

Mouse and Human Eukaryotic Initiation Factor 4E-Binding Proteins 1 and 2. *Genomics* **1996**, *38* (3), 353-363.

66. Bechara, C.; Sagan, S., Cell-penetrating peptides: 20 years later, where do we stand? *FEBS Lett.* **2013**, *587*, 1693.

67. Nim, S.; Jeon, J.; Corbi-Verge, C.; Seo, M.-H.; Ivarsson, Y.; Moffat, J.; Tarasova, N.; Kim, P. M., Pooled screening for antiproliferative inhibitors of protein-protein interactions. *Nature Chemical Biology* **2016**, *12*, 275.

68. Kim, Y. W.; Grossmann, T. N.; Verdine, G. L., Synthesis of all-hydrocarbon stapled α -helical peptides by ring-closing olefin metathesis. *Nat. Protoc.* **2011**, *6*, 761.

69. Bird, G. H.; Irimia, A.; Ofek, G.; Kwong, P. D.; Wilson, I. A.; Walensky, L. D., Stapled HIV-1 peptides recapitulate antigenic structures and engage broadly neutralizing antibodies. *Nat. Struct. Mol. Biol.* **2014**, *21*, 1058.

70. Douse, C. H.; Maas, S. J.; Thomas, J. C.; Garnett, J. A.; Sun, Y.; Cota, E.; Tate, E. W., Crystal Structures of Stapled and Hydrogen Bond Surrogate Peptides Targeting a Fully Buried Protein–Helix Interaction. *ACS Chemical Biology* **2014**, *9* (10), 2204-2209.

71. Wels, B.; Kruijtzter, J. A. W.; Garner, K.; Nijenhuis, W. A. J.; Gispen, W. H.; Adan, R. A. H.; Liskamp, R. M. J., Synthesis of a novel potent cyclic peptide MC4-ligand by ring-closing metathesis. *Bioorganic & Medicinal Chemistry* **2005**, *13* (13), 4221-4227.

72. McGrath, S.; Tortorici, M.; Drouin, L.; Solanki, S.; Vidler, L.; Westwood, I.; Gimeson, P.; Montfort, R. V.; Hoelder, S., Structure - Enabled Discovery of a Stapled Peptide Inhibitor to Target the Oncogenic Transcriptional Repressor TLE1. *Chemistry - A European Journal* **2017**, *23* (40), 9577-9584.

73. Shim, S. Y.; Kim, Y. W.; Verdine, G. L., A New $i, i + 3$ Peptide Stapling System for α - Helix Stabilization. *Chemical Biology & Drug Design* **2013**, *82* (6), 635-642.

74. Rezaei Araghi, R.; Ryan, J. A.; Letai, A.; Keating, A. E., Rapid Optimization of Mcl-1 Inhibitors using Stapled Peptide Libraries Including Non-Natural Side Chains. *ACS Chemical Biology* **2016**, *11* (5), 1238-1244.

75. Sanford, M. S.; Ulman, M.; Grubbs, R. H., New Insights into the Mechanism of Ruthenium-Catalyzed Olefin Metathesis Reactions. *Journal of the American Chemical Society* **2001**, *123* (4), 749-750.

76. Bhattacharya, S.; Zhang, H.; Cowburn, D.; Debnath, A. K., Novel structures of self-associating stapled peptides. *Biopolymers* **2012**, *97* (5), 253-264.

77. Lama, D.; Quah, S. T.; Verma, C. S.; Lakshminarayanan, R.; Beuerman, R. W.; Lane, D. P.; Brown, C. J., Rational optimization of conformational effects induced by hydrocarbon staples in peptides and their binding interfaces. *Sci. Rep.* **2013**, *3*, 3451.

78. Jullian, M.; Hernandez, A.; Maurras, A.; Puget, K.; Amblard, M.; Martinez, J.; Subra, G., N-terminus FITC labeling of peptides on solid support: the truth behind the spacer. *Tetrahedron Letters* **2009**, *50* (3), 260-263.
79. Baell, J. B.; Holloway, G. A., New Substructure Filters for Removal of Pan Assay Interference Compounds (PAINS) from Screening Libraries and for Their Exclusion in Bioassays. *J. Med. Chem.* **2010**, *53*, 2719.
80. Baell, J. B.; Ferrins, L.; Falk, H.; Nikolakopoulos, G., PAINS: Relevance to Tool Compound Discovery and Fragment-Based Screening. *Aust. J. Chem.* **2013**, *66*, 1483.
81. Bhattacharya, S.; Zhang, H.; Debnath, A. K.; Cowburn, D., Solution Structure of a Hydrocarbon Stapled Peptide Inhibitor in Complex with Monomeric C-terminal Domain of HIV-1 Capsid. *The Journal of Biological Chemistry* **2008**, *283* (24), 16274-16278.
82. McWhinnie, F. S.; Sepp, K.; Wilson, C.; Kunath, T.; Hupp, T. R.; Baker, T. S.; Houston, D. R.; Hulme, A. N., Mono - Substituted Hydrocarbon Diastereomer Combinations Reveal Stapled Peptides with High Structural Fidelity. *Chemistry - A European Journal* **2018**, *24* (9), 2094-2097.
83. Platt, R. J.; Han, T. S.; Green, B. R.; Smith, M. D.; Skalicky, J.; Gruszczynski, P.; White, H. S.; Olivera, B.; Bulaj, G.; Gajewiak, J., Stapling mimics noncovalent interactions of γ -carboxyglutamates in conantokins, peptidic antagonists of N-methyl-D-aspartic acid receptors. *J. Biol. Chem.* **2012**, *287*, 20727.
84. Jayakody, T.; Marwari, S.; Lakshminarayanan, R.; Tan, F. C. K.; Johannes, C. W.; Dymock, B. W.; Poulsen, A.; Herr, D. R.; Dawe, G. S., Hydrocarbon stapled B chain analogues of relaxin-3 retain biological activity. *Peptides* **2016**, *84*, 44-57.
85. Song, J. M.; Menon, A.; Mitchell, D. C.; Johnson, O. T.; Garner, A. L., High-Throughput Chemical Probing of Full-Length Protein-Protein Interactions. *ACS Combinatorial Science* **2017**, *19* (12), 763-769.
86. Edery, I.; Altmann, M.; Sonenberg, N., High-level synthesis in Escherichia coli of functional cap-binding eukaryotic initiation factor eIF-4E and affinity purification using a simplified cap-analog resin. *Gene* **1988**, *74* (2), 517-525.
87. Yanagiya, A.; Suyama, E.; Adachi, H.; Svitkin, Yuri V.; Aza-Blanc, P.; Imataka, H.; Mikami, S.; Martineau, Y.; Ronai, Z. e. A.; Sonenberg, N., Translational Homeostasis via the mRNA Cap-Binding Protein, eIF4E. *Molecular Cell* **2012**, *46* (6), 847-858.

CHAPTER 5 FUTURE DIRECTIONS

eIF4F is a critical regulatory nexus that is often hyperactivated in cancerous cells to stimulate the translation of a specific subset of mRNA that drive transformation. While the normal nonmalignant cells can tolerate a broad range of eIF4F activity, malignant cells require a constitutively active eIF4F complex to maintain their pathological state. In fact, a normalization rather than a complete inhibition of the eIF4F complex activity was sufficient to induce apoptosis in cancer cells¹ while leaving untransformed cells alive. A successful agent targeting the eIF4F complex could require significantly lower dosage, reduce the overall toxicity, and be selective for the protein translation addicted cancerous cells; it could be the true blade to the Achilles heel of cancer².

PPI cat-ELCCA was successfully used to conduct a screening campaign against the eIF4E–4E-BP1 interaction. The future direction for this versatile assay is to expand and apply it towards other target PPIs such as the eIF4G1–eIF4A interaction, the other critical interaction involved in the CdT initiation. The expression and purification of HT eIF4G1 can be transferred from HEK293T cells to Sf9 insect cells for higher yield, and eIF4G1 expressed from Sf9 cells have shown appropriate binding activities to target proteins³⁻⁵. *In vitro* expression and purification of eIF4A is well-documented⁶, and should require minor optimizations in identifying the active termini position of the HT to obtain the active HT eIF4A.

Admittedly, PPI cat-ELCCA is more labor intensive than other common HTS assays (FP, TR-FRET) even with the aid of liquid washers and dispensers. The next step for HTS campaigns

using PPI cat-ELCCA (and other cat-ELCCAs) is more extensive assay automations. A significant bulk of the labor can be automated with the technological advancements of the liquid handling instrumentation like Biomek Dual FX^P and its modular installations of washers, incubators, and dispensers. In addition, miniaturization using automated liquid and plate handlers can reduce or even remove potential operator error and allow for more consistent results over time. Currently, PPI cat-ELCCA is scripted for near-complete liquid and plate handling on the Biomek Dual FX^P instrumentation at UM CCG; the evaluations of automated PPI cat-ELCCA will be insightful for further assay automation developed from the cat-ELCCA platform.

The eIF4E interaction HTS campaigns yielded few validated NPE fractions and compounds exhibiting dose-dependent activities, which are currently being reproduced and procured for further validations. The complete characterization of active molecule(s) from the NPE and BIC libraries are on-going. First, the microbes are being re-cultured for re-isolation of the active NPE fractions. Following the re-isolation, the active fraction must then be subjected to iterative fractionation and screening processes to narrow down to the active compound(s), which will then require full chemical characterization and re-testing. The bioactive compound(s) will then be investigated for binding affinity to target eIF4E protein by SPR and assayed for eIF4E interaction disruption *in cellulo* by m7GDP-agarose pulldown experiments. Pending confirmations from both SPR and *in cellulo* analysis, medicinal chemistry campaign and SAR studies will be conducted in parallel to solving the compound-protein complex structure. Clearly, this is more time and resource consuming than a typical follow-up studies of hits identified from the commercially available compound libraries; however, the NPE libraries contain vastly more complex chemical identities that may indeed be necessary to target complex PPIs and be worth the initial investment. Furthermore, commercially available libraries have already been screened

against which led to discoveries of 4E1RCat⁷ and 4EGI-1⁸; thus, screening against new chemical libraries was essential for this HTS campaign.

Similarly, custom BIC libraries from Eli Lilly offered a rare access to the unexplored chemical space by both of the prior HTS campaigns against eIF4E interactions. Over 50% of the validated dose-responsive compounds showed direct binding to eIF4E, and the remaining compounds may disrupt the PPI in a novel mechanism (e.g. binding to 4E-BP1) that requires further investigation. A few of the hit compounds have met the criterion as set by OIDD, and efforts to obtain their chemical structures are on-going. Since the hits are representative compounds of the chemical scaffolds extensively researched by Eli Lilly, further collaborative investigations may lead to fast-tracked medicinal chemistry campaigns in which additional analogues are supplied through OIDD and screened using PPI cat-ELCCA and SPR. Ultimately, a successful collaboration with Eli Lilly will accelerate the discovery and confirmations of novel inhibitors of the CdT initiation.

The Garner group discovered that the HCS peptides mimicking 4E-BM of 4E-BP1 showed increased binding affinity over the linear 4E-BP1 peptide and inhibited the eIF4E interactions in presence of FBS *in cellulo*. The synthesis and characterizations of **mHCS 4E-BP1** were riddled with challenges, and in the advent of **HCS 4E-BP1** having superior activity with significantly easier sample preparations, **mHCS 4E-BP1** research is no longer being pursued by the Garner group. Contrary to the hypothesis that significant librational motions of the peptide on the binding interface may be beneficial⁹, **mHCS 4E-BP1** studies concluded that implementing greater flexibility to the staple and decreasing the overall helicity of the **mHCS 4E-BP1** does not increase the binding affinity. Although the emergence of **mHCS 4E-BP1** isomers may of interest from a chemistry perspective – to explore and develop other Grubbs catalysts for RCM that

promote one isomer formation over the other –its practical application in stapled peptides are limited; most *i, i+4* HCS peptides do not suffer from isomerization, and the higher flexibility of longer olefinic substrates of *i, i+8* HCS peptides can achieve similar helicity by using two separate *i, i+4* staples.

The Garner group is currently characterizing the bioactivities of stapling strategies with minor differences like those between *cis*- and *trans*- isomers, specifically concerning the lactam stapled 4E-BP1 mimetics. By reversing the staple positions of the free carboxylate- and the free amino- functionalized unnatural amino acids of the lactam bond, two regioisomeric lactam stapled peptides are created. Preliminary *in cellulo* studies indicate that these regioisomers have different bioactivities and secondary structures. Alternatively, the *cis*- and *trans*- stapling strategies can be mimicked using thioether linkers and bis-cysteine peptides to investigate whether the hydrocarbon stapled regioisomers yields different bioactivities.

In general, the optimizations of 4E-BP1 sequence for stapled peptide designs are still on-going. Bioisostere substitutions of C62 and M60 in 4E-BP1 sequence could increase peptide stability in solution and eliminate or reduce sulfur oxidation. And although M60 substitutions have shown drastic loss in binding activity, C62 may be substituted with difluoro-functionalized unnatural amino acids¹⁰⁻¹¹; despite the reported role of difluoro- analogues in decreasing the peptide helix propensities¹²⁻¹³, HCS strategy should limit this loss and improve the peptide stability and activity. **HCS 4E-BP1** and **4E-BP1** peptide both have relatively poor solubility in water (< 1 mM), and further sequence optimizations using natural and unnatural amino acids as well as peptide truncations are currently on-going to increase the peptide solubilities.

The two-pronged approach in targeting the CdT initiation encloses the described efforts to discover novel small molecule and HCS peptides to disrupt the eIF4E interactions and to

normalize the CdT initiation. Although the two approaches are distinct and separated, their potential outcomes will hopefully find a union in future studies. The eIF4E binding hit molecules can be cross-screened against eIF4E–eIF4G1 interaction to gain insight into whether the hit compounds bind competitively to the canonical binding motif or allosterically towards the cap-binding site. Hot spot modulators of eIF4E can open the path to the identification of scaffolds that can disrupt eIF4F complexes; furthermore, the chemical scaffold could be leveraged as potential unnatural side-chain designs for the future stapled peptides. On the other hand, the allosteric modulators can be linked onto the 4E-BP1 stapled peptides to further enhance the probe binding affinity and potency, or to introduce cell permeability to the otherwise impermeable allosteric modulators. In summary, this work highlights the innovative approach in targeting the CdT initiation through the disruption and normalization of eIF4F complex through novel PPI screening assay to evaluate small molecule inhibitors and stapled peptides.

5.1 REFERENCES

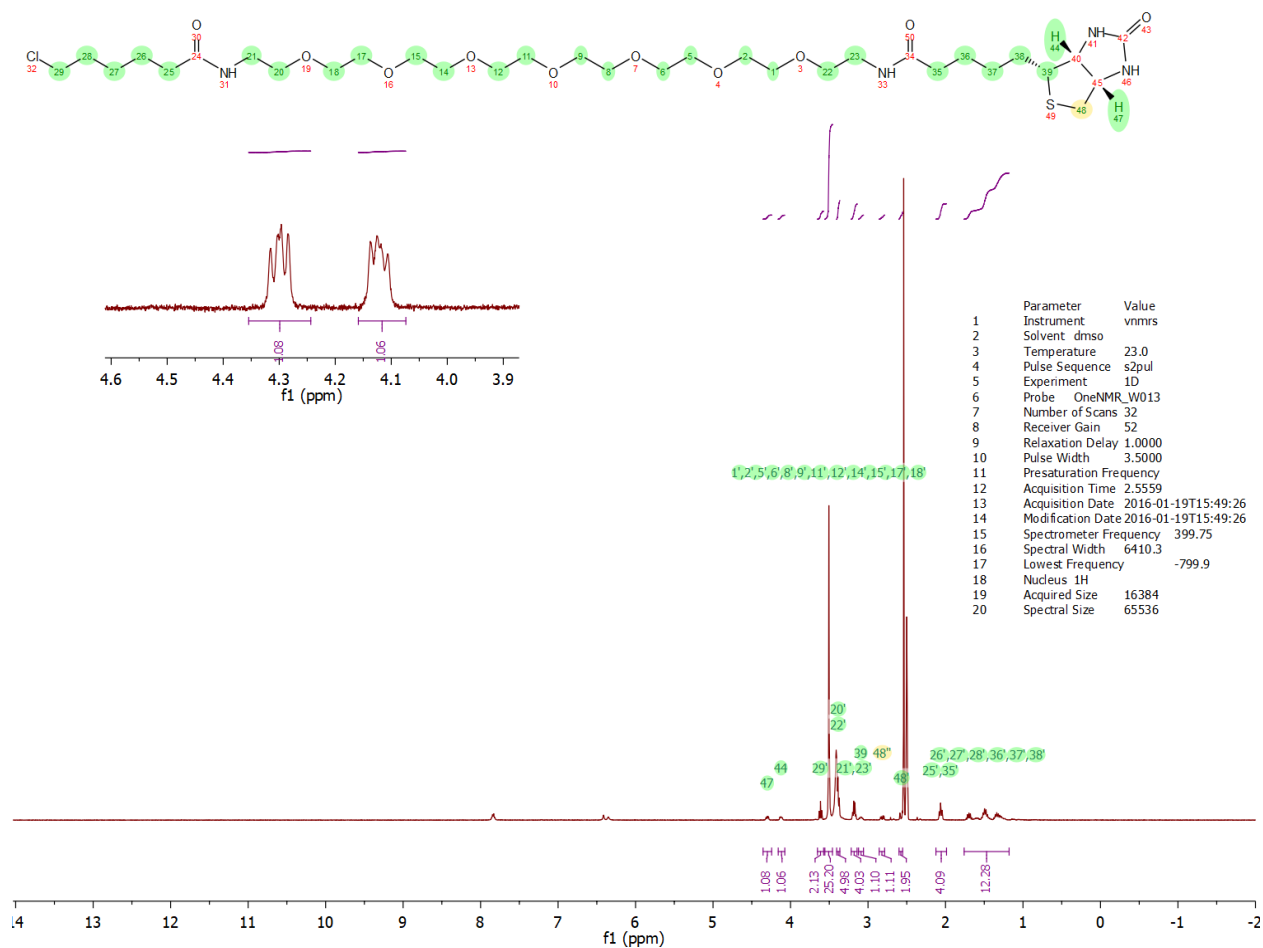
1. Li, B. D. L.; Gruner, J. S.; Abreo, F.; Johnson, L. W.; Yu, H.; Nawas, S.; McDonald, J. C.; DeBenedetti, A., Prospective Study of Eukaryotic Initiation Factor 4E Protein Elevation and Breast Cancer Outcome. *Annals of Surgery* **2002**, *235* (5), 732-739.
2. Bitterman, P. B.; Polunovsky, V. A., Attacking a Nexus of the Oncogenic Circuitry by Reversing Aberrant eIF4F-Mediated Translation. *Molecular Cancer Therapeutics* **2012**, *11* (5), 1051-1061.
3. He, H.; von der Haar, T.; Singh, C. R.; Ii, M.; Li, B.; Hinnebusch, A. G.; McCarthy, J. E. G.; Asano, K., The Yeast Eukaryotic Initiation Factor 4G (eIF4G) HEAT Domain Interacts with eIF1 and eIF5 and Is Involved in Stringent AUG Selection. *Molecular and Cellular Biology* **2003**, *23* (15), 5431-5445.
4. von der Haar, T.; Ball, P. D.; McCarthy, J. E. G., Stabilization of Eukaryotic Initiation Factor 4E Binding to the mRNA 5'-Cap by Domains of eIF4G. *Journal of Biological Chemistry* **2000**, *275* (39), 30551-30555.

5. Ptushkina, M.; von der Haar, T.; Vasilescu, S.; Frank, R.; Birkenhäger, R.; McCarthy, J. E. G., Cooperative modulation by eIF4G of eIF4E-binding to the mRNA 5' cap in yeast involves a site partially shared by p20. *The EMBO Journal* **1998**, *17* (16), 4798-4808.
6. Özeş, A. R.; Feoktistova, K.; Avanzino, B. C.; Fraser, C. S., Duplex Unwinding and ATPase Activities of the DEAD-Box Helicase eIF4A Are Coupled by eIF4G and eIF4B. *Journal of Molecular Biology* **2011**, *412* (4), 674-687.
7. Cencic, R.; Hall, D. R.; Robert, F.; Du, Y.; Min, J.; Li, L.; Qui, M.; Lewis, I.; Kurtkaya, S.; Dingledine, R.; Fu, H.; Kozakov, D.; Vajda, S.; Pelletier, J., Reversing chemoresistance by small molecule inhibition of the translation initiation complex eIF4F. *Proceedings of the National Academy of Sciences of the United States of America* **2011**, *108* (3), 1046-1051.
8. Moerke, N. J.; Aktas, H.; Chen, H.; Cantel, S.; Reibarkh, M. Y.; Fahmy, A.; Gross, J. D.; Degtarev, A.; Yuan, J.; Chorev, M., Small-molecule inhibition of the interaction between the translation initiation factors eIF4E and eIF4G. *Cell* **2007**, *128* (2), 257-267.
9. Zhou, W.; Quah, S. T.; Verma, C. S.; Liu, Y.; Lane, D. P.; Brown, C. J., Improved eIF4E Binding Peptides by Phage Display Guided Design: Plasticity of Interacting Surfaces Yield Collective Effects. *PLOS ONE* **2012**, *7* (10), e47235.
10. Narjes, F.; Koehler, K. F.; Koch, U.; Gerlach, B.; Colarusso, S.; Steinkühler, C.; Brunetti, M.; Altamura, S.; De Francesco, R.; Matassa, V. G., A designed P1 cysteine mimetic for covalent and non-covalent inhibitors of HCV NS3 protease. *Bioorganic & Medicinal Chemistry Letters* **2002**, *12* (4), 701-704.
11. Meanwell, N. A., Synopsis of Some Recent Tactical Application of Bioisosteres in Drug Design. *Journal of Medicinal Chemistry* **2011**, *54* (8), 2529-2591.
12. Gerling, U. I. M.; Salwiczek, M.; Cadicamo, C. D.; Erdbrink, H.; Czekelius, C.; Grage, S. L.; Wadhvani, P.; Ulrich, A. S.; Behrends, M.; Haufe, G.; Koksche, B., Fluorinated amino acids in amyloid formation: a symphony of size, hydrophobicity and [small alpha]-helix propensity. *Chemical Science* **2014**, *5* (2), 819-830.
13. Chiu, H.-P.; Suzuki, Y.; Gullickson, D.; Ahmad, R.; Kokona, B.; Fairman, R.; Cheng, R. P., Helix Propensity of Highly Fluorinated Amino Acids. *Journal of the American Chemical Society* **2006**, *128* (49), 15556-15557.

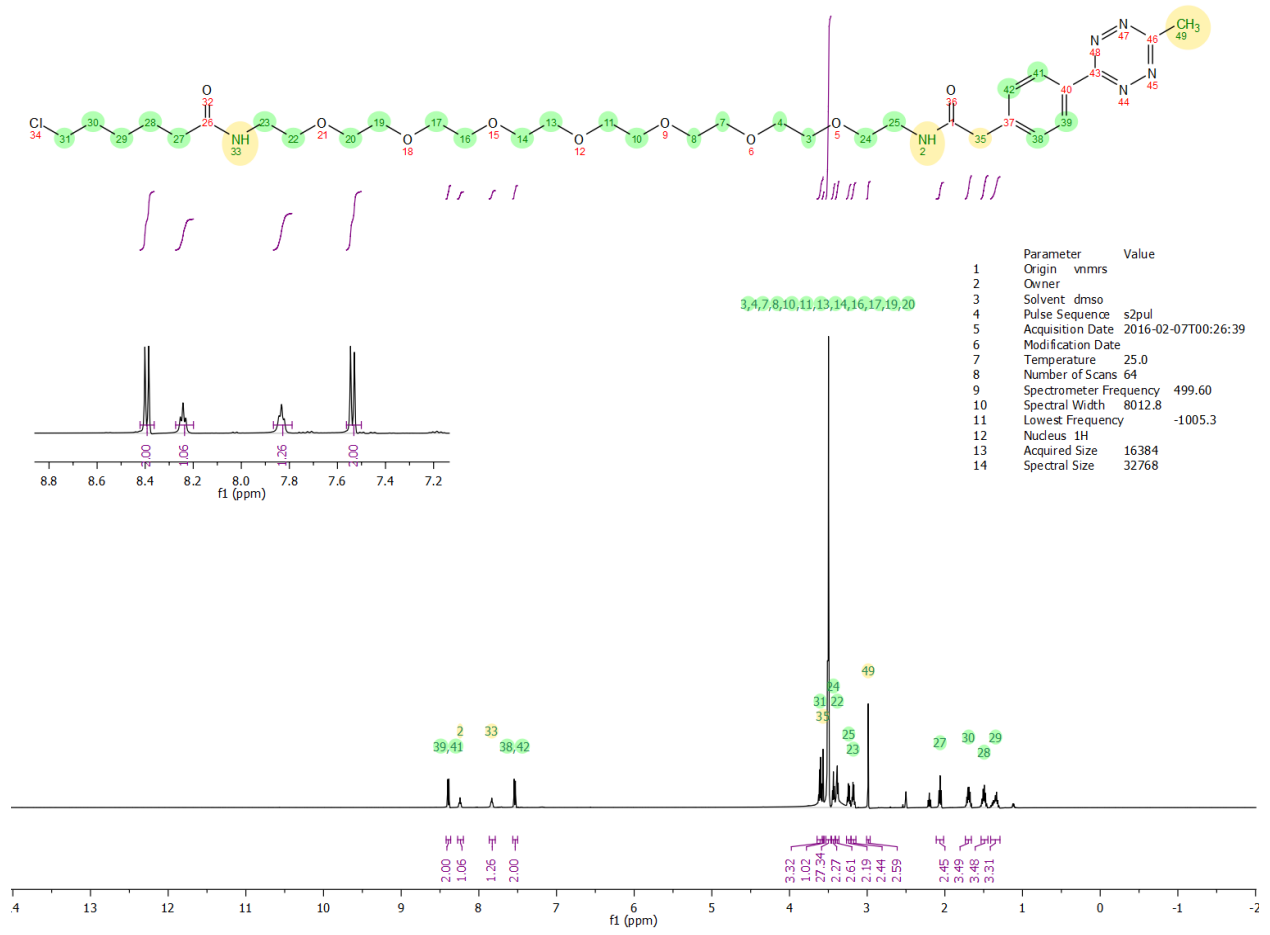
APPENDIX

NMR Spectra

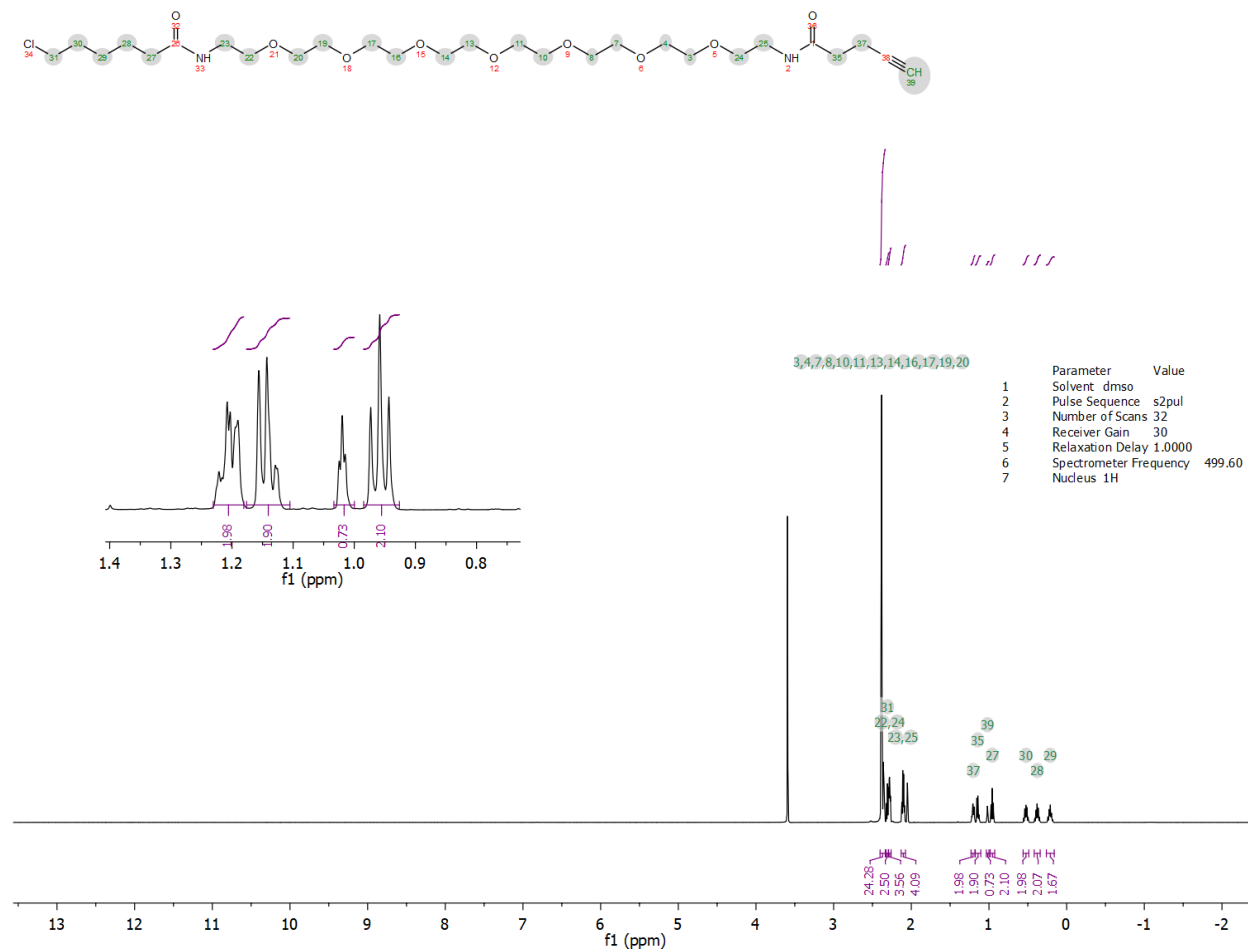
BIOTIN-PEG7-HT LIGAND



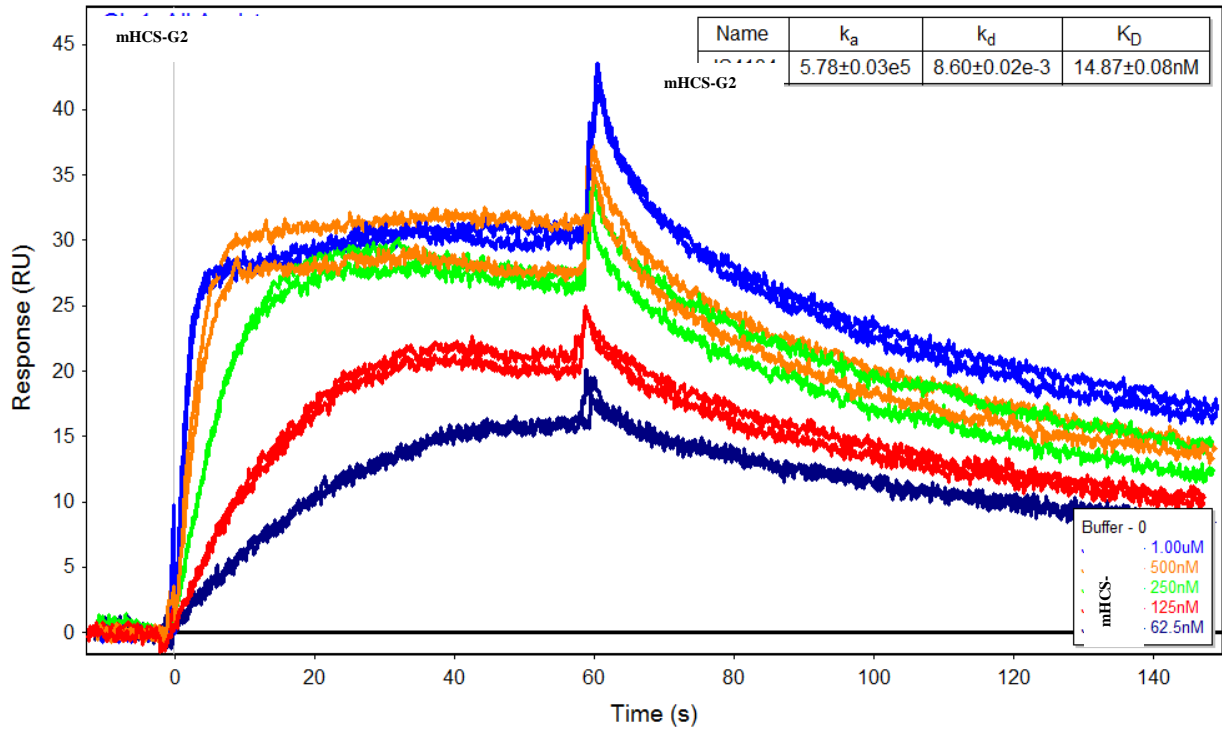
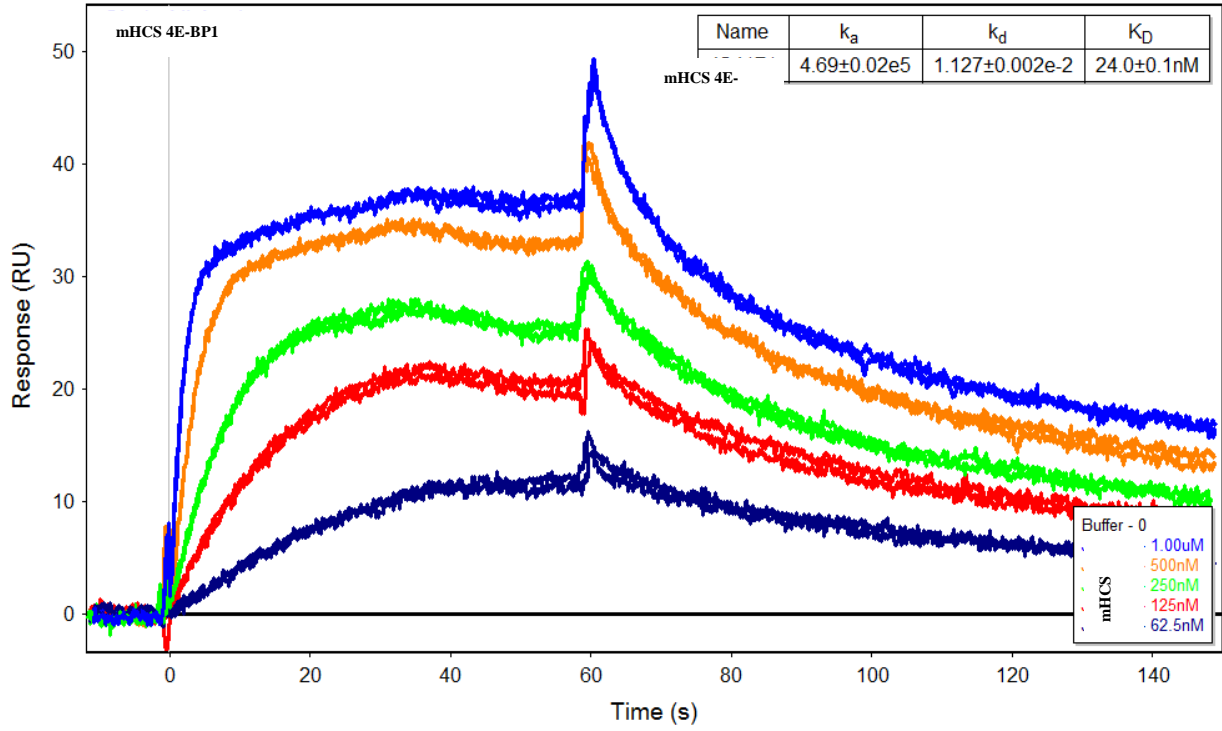
MTET-PEG7-HT LIGAND

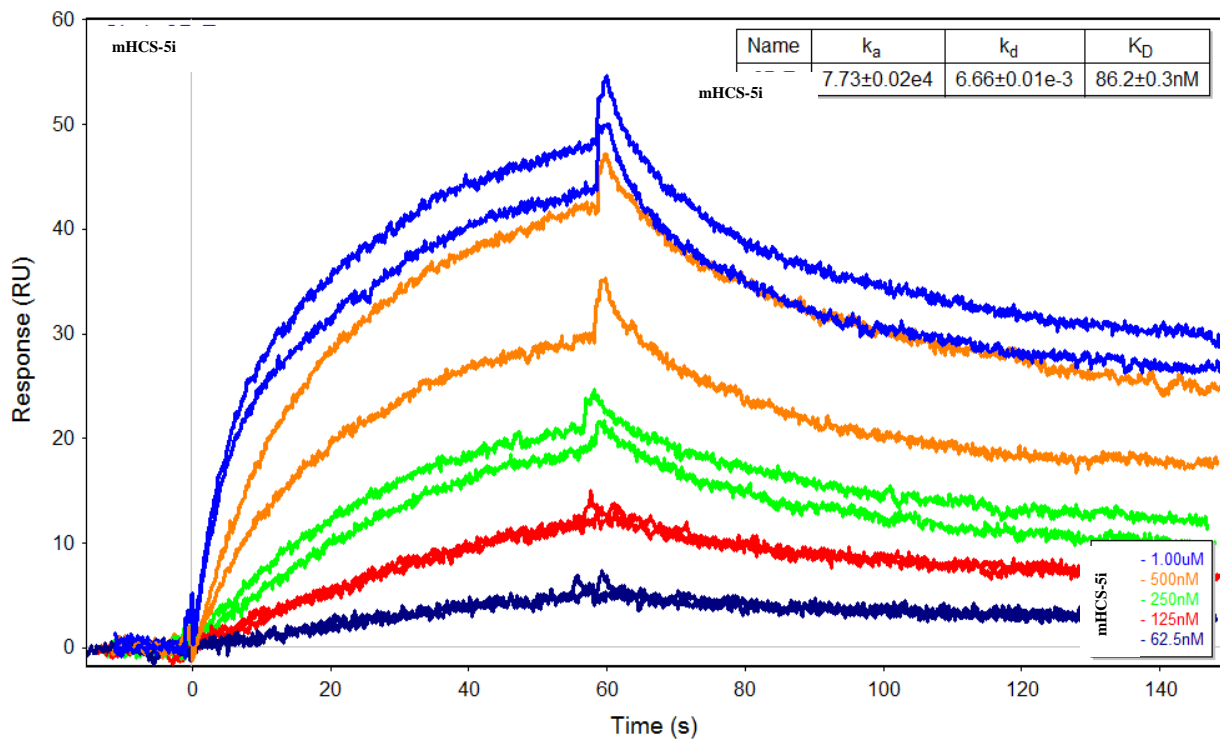
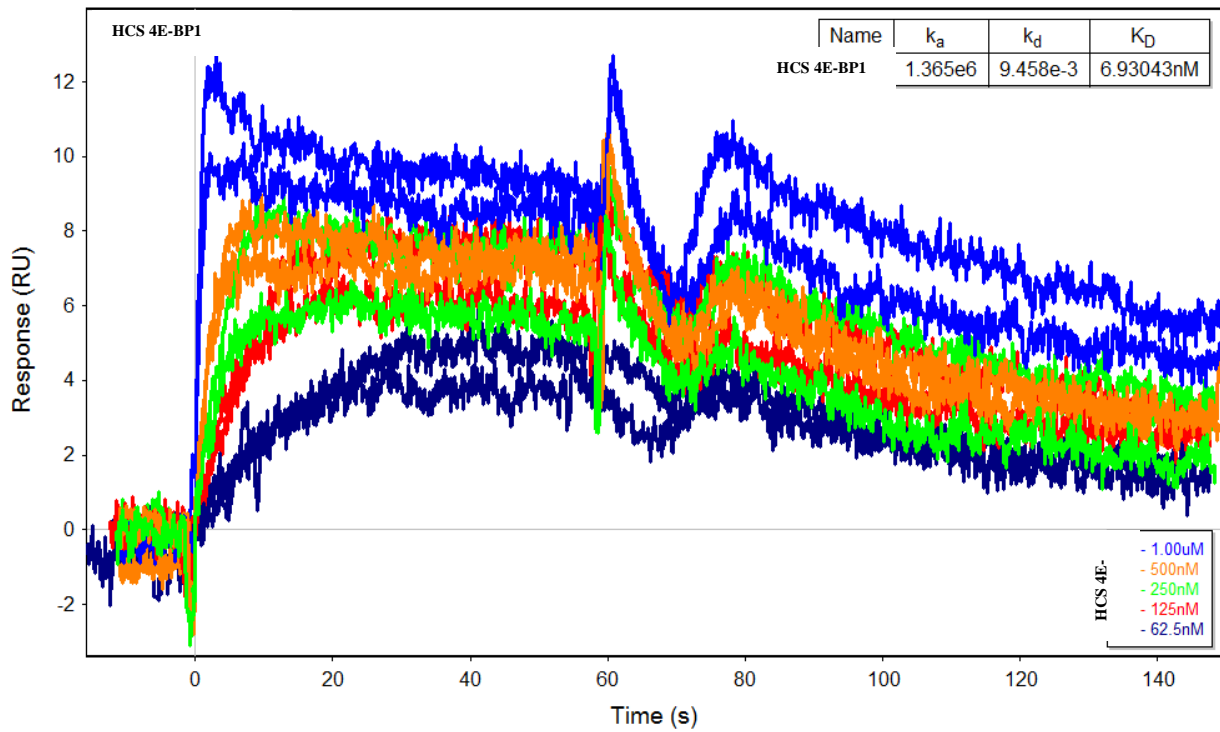


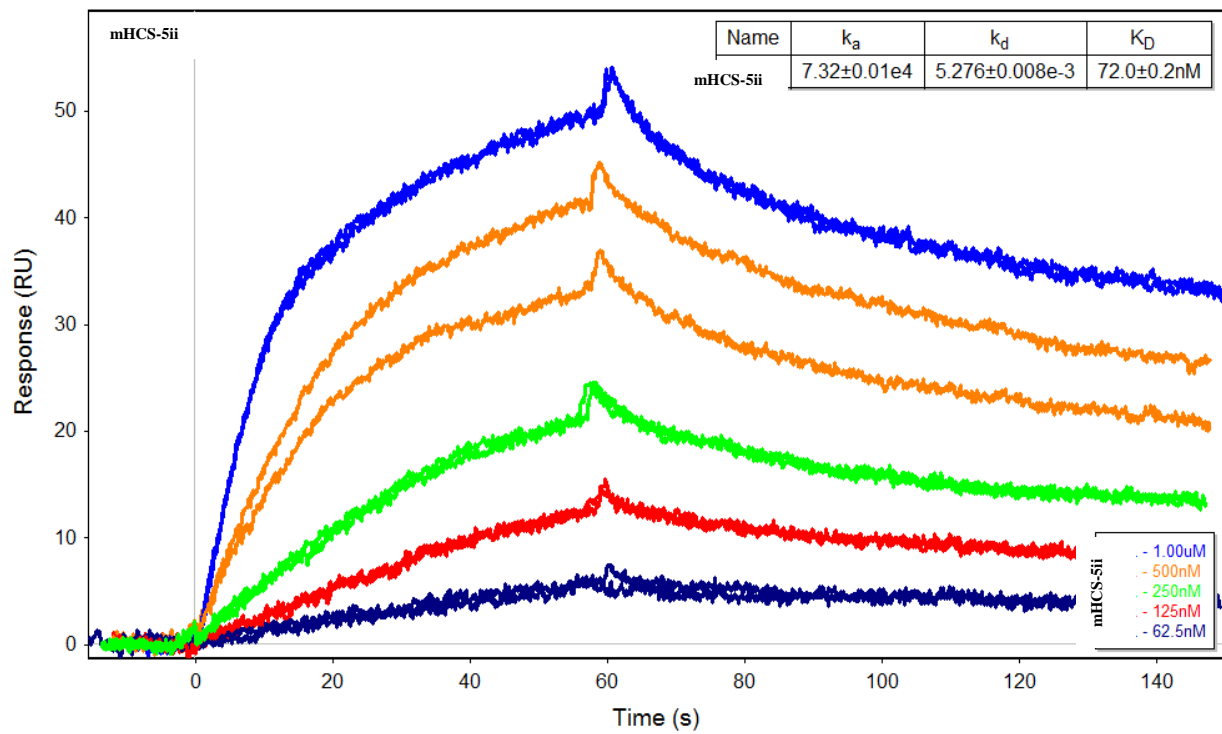
ALKYNE-PEG7-HT LIGAND



SPR SENSOGRAMS

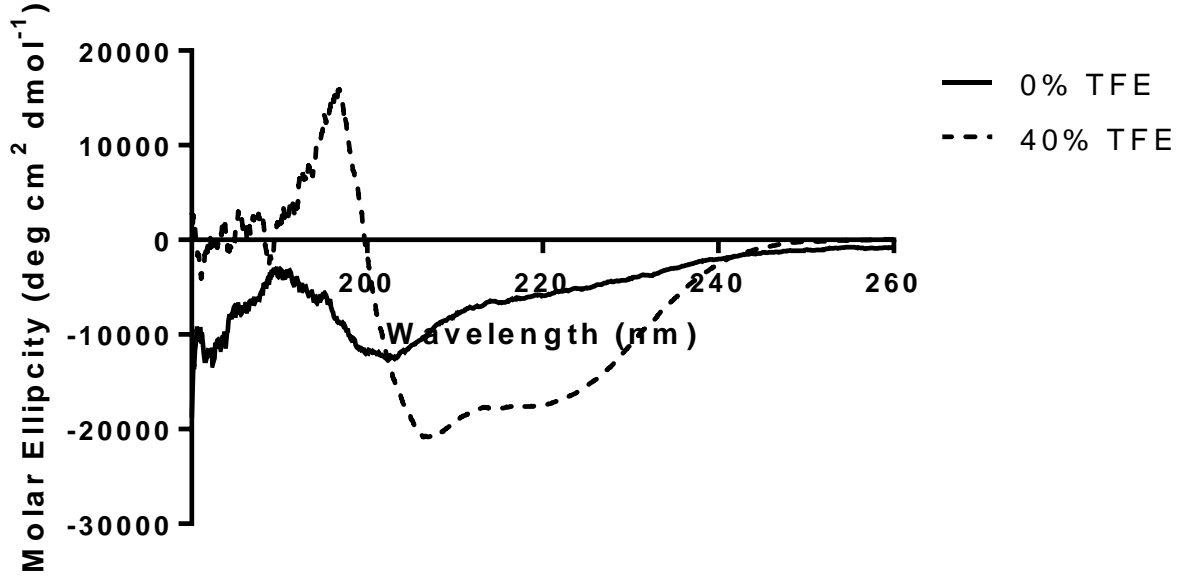




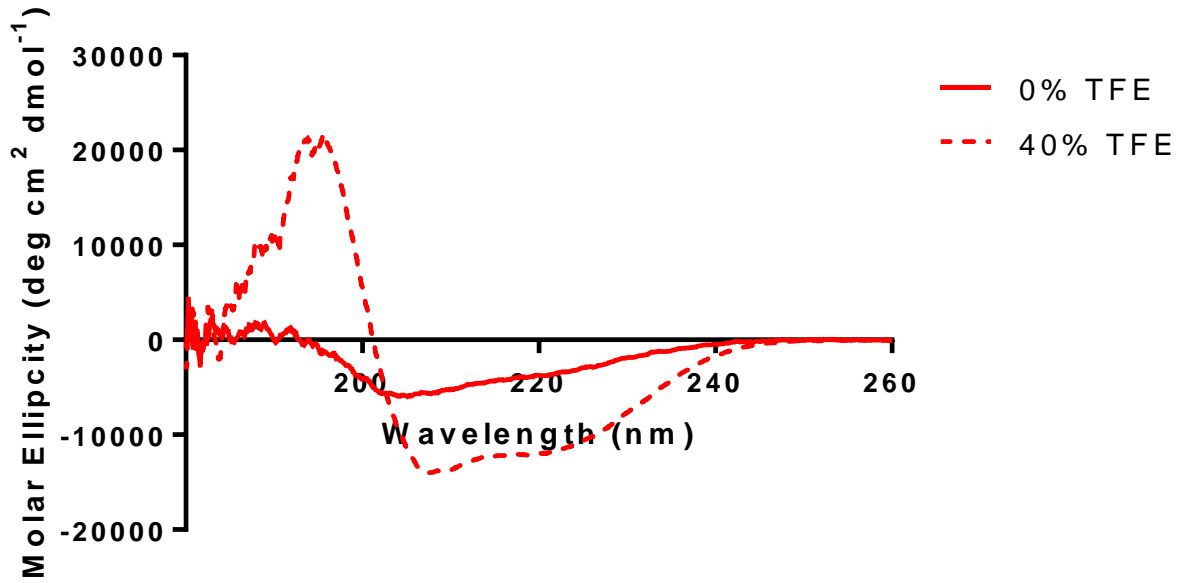


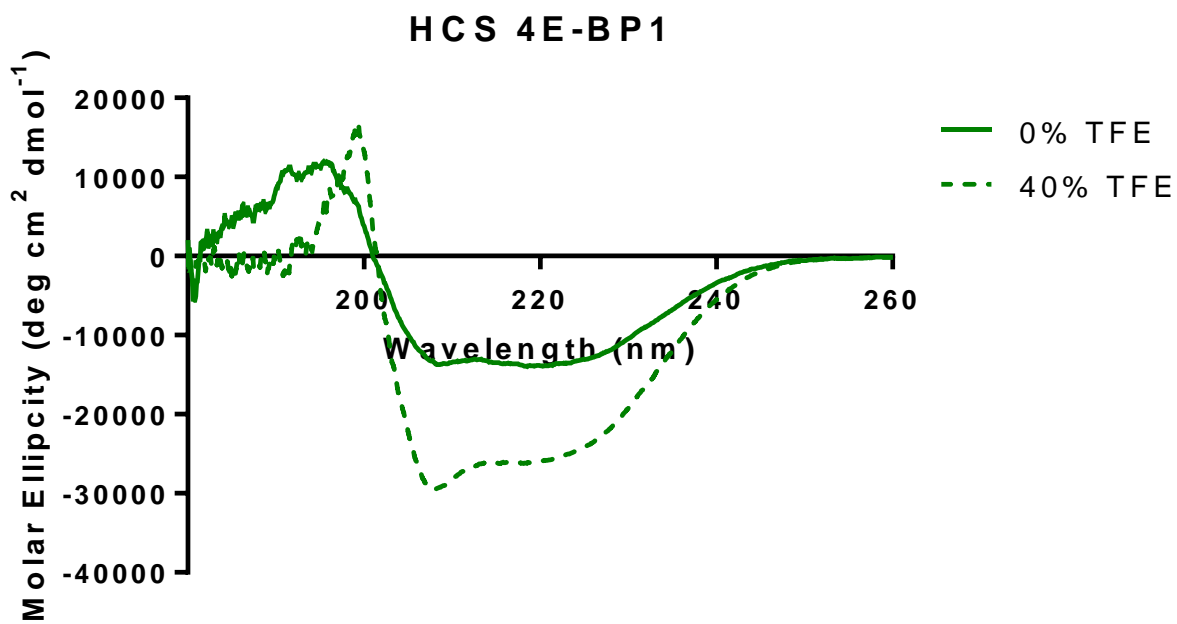
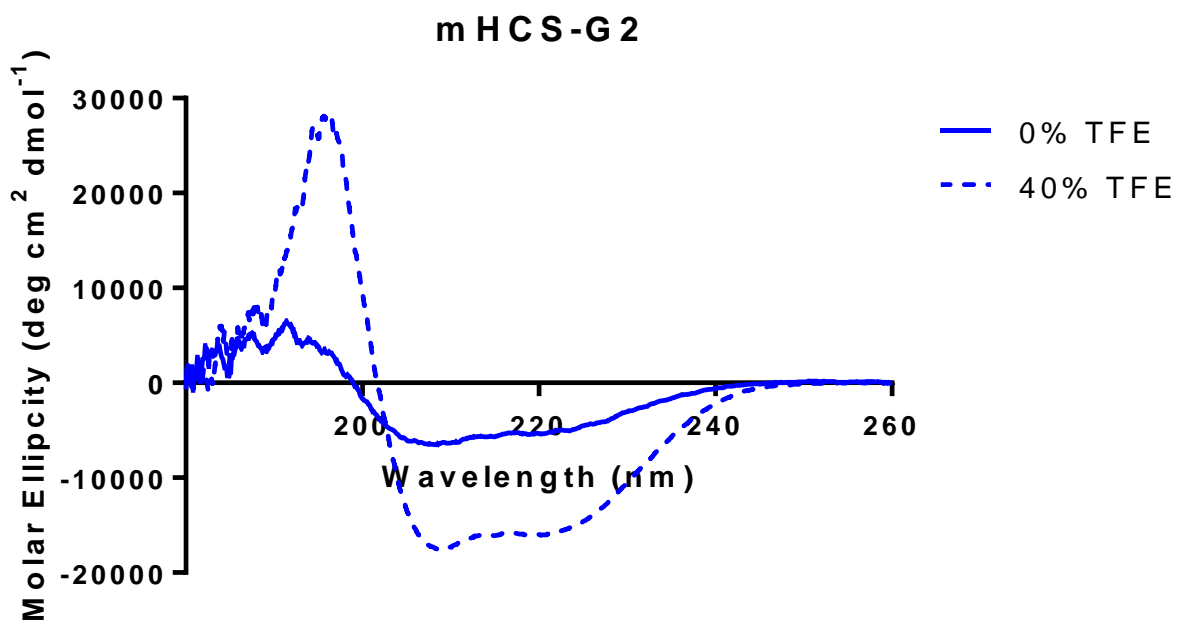
CIRCULAR DICHROISM SPECTRAS

4E-BP1

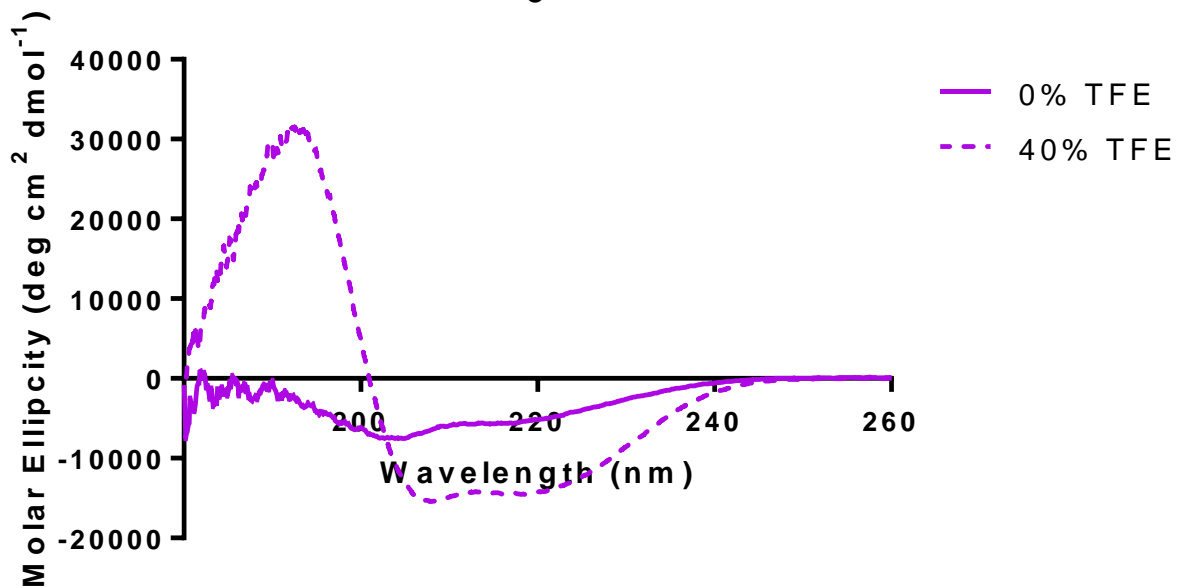


mHCS 4E-BP1





5



mHCS-5i

